

Apatite Thermochronology of the
Bole-Nangodi Shear Zone (northern
Ghana): Insights into the Thermal
History of Equatorial Atlantic Rifting

Thesis submitted in accordance with the requirements of the University of
Adelaide for an Honours Degree in Geology

Nicholas Stewart Fernie

November 2016



THE UNIVERSITY
of ADELAIDE

APATITE THERMOCHRONOLOGY OF THE BOLE-NANGODI SHEAR ZONE (NORTHERN GHANA): INSIGHTS INTO THE THERMAL HISTORY OF EQUATORIAL ATLANTIC RIFTING

RUNNING TITLE

Apatite Thermochronology of the Bole-Nangodi Shear Zone

ABSTRACT

The Bole-Nangodi (BN) shear zone is located in northern Ghana and is thought to represent the continental extension of an equatorial Atlantic transform fault. This study applies low temperature thermochronology to constrain the thermal history of the BN shear zone with relation to Gondwana break-up during the Mesozoic. Apatite Fission track data obtained from the Ghanese Paleo-proterozoic basement along the primary NE-SW structural trend of the BN shear zone suggests a complex two phase cooling history. (1) Heating of the crust in the late Triassic – early Jurassic, related with the emplacement of the Central Atlantic Magmatic Province (CAMP), (2) Cooling associated with rift shoulder exhumation during early Cretaceous rifting of Africa from Brazil.

Cooling ages obtained across the structural architecture furthermore constrain differential exposure of the thermal history, preserving older (CAMP) signatures to the south and younger (rifting) signatures to the north of the BN shear zone respectively. This indicates that the BN shear zone has been reactivated during the Cretaceous as a result of the build-up of strain being generated by the Central and South Atlantic rift margins.

The results obtained in this work indicate the extent to which CAMP related heat flow has affected the upper crust within the West African Craton can at least be constrained to northern Ghana. Furthermore, Cretaceous intra-continental strike-slip faulting of the West African continental crust was likely induced along Paleo-proterozoic shear zones acting as zones of weakened crust where deformation and rifting were localised and may have ultimately controlled the orientation of fracture zones within the Equatorial Atlantic.

KEYWORDS

Cretaceous, exhumation, Gondwana, West African Craton, Ghana, AFT, shear zone, thermochronology, thermal history.

TABLE OF CONTENTS

Apatite Thermochronology of the Bole-Nangodi Shear zone (northern Ghana): Insights into the thermal history of Equatorial Atlantic Rifting	i
Running title	i
Abstract.....	i
Keywords.....	i
List of Figures and Tables	3
1. Introduction	7
2. Geological Setting	10
3. Methods	14
3.1 Apatite Fission Track thermochronology	14
3.2 Apatite U-Pb Dating	15
3.3 Laboratory Processing	15
3.4 Apatite Fission Track and AU-Pb Analysis	15
3.5 Data Presentation and Modelling	18
4. Results	19
4.1 Sample locations.....	19
4.2 Apatite Fission Track Age Results	22
4.2.1 Group 1	22
4.2.2 Group 2.....	24
4.2.3 Group 3.....	26
4.2.4 Group 4.....	27
4.2.5 Pooled Study Area.....	30
4.3 Apatite Fission Track Thermal History Modelling	31
4.3.1 Group 1 (Oldest AFT ages, southeast of the BN shear zone) :	31
4.3.2 Group 2 (Two age components, along strike of the BN shear zone):	31
4.3.3 Group 3 (Young AFT ages, northwest and southwest of the BN shear zone):	32
4.3.4 Group 4 (Youngest AFT ages located in the central BN shear zone):	32
4.3.5 Pooled thermal history model:.....	34
4.4 Apatite U-Pb Results	35
5. Discussion.....	40
5.1 Confined Track Length vs Age comparison.....	40
5.2 Low-temperature (~120-60°C) thermal events.....	44
5.3 Late Triassic to Early Jurassic	44
5.4 Early to middle Cretaceous Cooling.....	45

5.5 Late Cretaceous – Cenozoic Cooling	48
5.6 Differential exhumation with respect to the Bole-Nangodi Shear Zone	50
5.7 U-Pb Data	55
6. Conclusions	55
7. Acknowledgments	56
8. References	56
9. Appendix A: Data Table.....	63
10. Appendix B: Extended Method	84

LIST OF FIGURES AND TABLES

Figure 1 – Globe image with indication of the study area in Ghana (box framed) and showing the approximate locations of CAMP, the Paraná – Etendeka LIP, the Benue Trough (Buiter and Torsvik 2014), Ghana, the Bole-Nangodi shear zones and the Romanche and St Paul’s Transform Zones (Basile et al., 2005; Block et al., 2015). Modified from plate rotation files from Gplates software (Seton et al., 2012) 9

Figure 2 – Schematic geological map of the study area located in northern Ghana. Showing sample locations (Modified after Block *et al.* 2016)..... 11

Figure 3 - Map of the study area showing sample locations as coloured circles, lithology’s and AFT results. CA – Central Age, P1 – Peak 1 Age, P2 – Peak 2 Age, MTL – Mean Track Length and Θ^1 – MTL Standard Deviation. Modified after Block *et al.* 2016 21

Figure 4 - Radial plots of calculated AFT cooling ages for each sample location associated with sample Group 1 (A-C). D: Represents a pooled radial plot of Group 1 samples. Central age values were calculated using RadialPlotter and for dispersions >25% and $P(\chi^2)$ less than 0.05 age peak discrimination was performed using the RadialPlotter software (Vermeesch 2009). Percentage of data associated with each peak is bracketed adjacent to the age of each peak. [C] on the X- Axis represents the amount of ^{238}U in ppm. The left Y-Axis represents 2 standard deviations from the central age. Right ‘curved’ Y-Axis shows increasing age in Ma. The values along the X-axis show single-grain age uncertainties. Frequency plots depict track length distributions and are annotated with the number of measured confined track lengths (CTNs), Mean track length (MTL), Standard Deviation (StdDev) and Standard Error (StdErr)..... 23

Figure 5 - Radial plots of calculated AFT cooling ages for each sample location associated with sample Group 2 (A-D). E: Represents a pooled radial plot of Group 2 samples. Central age values were calculated using RadialPlotter and for dispersions >25% and $P(\chi^2)$ less than 0.05 age peak discrimination was performed using the RadialPlotter software (Vermeesch 2009). Percentage of data associated with each peak is bracketed adjacent to the age of each peak. [C] on the X- Axis represents the amount of ^{238}U in ppm. The left Y-Axis represents 2 standard deviations from the central age. Right ‘curved’ Y-Axis shows increasing age in Ma. The values along the X-axis show single-grain age uncertainties. Frequency plots depict track length distributions and are annotated with the number of measured confined track lengths (CTNs), Mean track length (MTL), Standard Deviation (StdDev) and Standard Error (StdErr)..... 25

Figure 6 - Radial plots of calculated AFT cooling ages for each sample location associated with sample Group 3 (A-H). I: Represents a pooled radial plot of Group 3 samples. Central age values were calculated using RadialPlotter and for dispersions >25% and $P(\chi^2)$ less than 0.05 age peak discrimination was performed using the RadialPlotter software (Vermeesch 2009). Percentage of data associated with each peak is bracketed adjacent to the age of each peak. [C] on the X- Axis represents the amount of ^{238}U in ppm. The left Y-Axis represents 2 standard deviations from the central age. Right ‘curved’ Y-Axis shows increasing age in Ma. The values along the X-axis show single-grain age uncertainties. Frequency plots depict track length distributions and are annotated with the number of measured confined track lengths (CTNs), Mean track length (MTL), Standard Deviation (StdDev) and Standard Error (StdErr)..... 27

Figure 7 - Radial plots of calculated AFT cooling ages for each sample location associated with sample Group 3 (A-H). I: Represents a pooled radial plot of Group 3

samples. Central age values were calculated using RadialPlotter and for dispersions >25% and $P(\chi^2)$ less than 0.05 age peak discrimination was performed using the RadialPlotter software (Vermeesch 2009). Percentage of data associated with each peak is bracketed adjacent to the age of each peak. [C] on the X- Axis represents the amount of ^{238}U in ppm. The left Y-Axis represents 2 standard deviations from the central age. Right ‘curved’ Y-Axis shows increasing age in Ma. The values along the X-axis show single-grain age uncertainties. Frequency plots depict track length distributions and are annotated with the number of measured confined track lengths (CTNs), Mean track length (MTL), Standard Deviation (StdDev) and Standard Error (StdErr). 29

Figure 8 - Radial plots of calculated AFT cooling ages for all samples within the study region. Central age values are by calculated RadialPlotter and for dispersions >25% age peak discrimination was performed using the RadialPlotter software (Vermeesch 2009). Percentage of data associated with each peak is bracketed adjacent to the age of each peak. [C] on the X- Axis represents the amount of ^{238}U in ppm. The left Y-Axis represents 2 standard deviations from central age (Ma). Right ‘curved’ Y-Axis shows increasing age in Ma. ^{238}U ppm values greater than 75ppm are displayed as purple circles. 30

Figure 9 - Thermal History models (tT) for all samples based on AFT and MTL data, developed using QTQt software (Gallagher 2012). Hot to Cold colours represent the probability as displayed on the right Y-Axis. The left Y-Axis represents temperature ($^{\circ}\text{C}$). The X-Axis represents Time (Ma). Modelling is poorly resolved prior to 200Ma for A, B and C and 140Ma for D as noted by cold colours. A: Model derived from samples, BN-252 and BN-446. B: Model derived from samples BN-016. C: Model derived from samples BN-223, BN-241, BN-043, BN-172, BN-278, BN-396 and BN-598. D: Model derived from samples BN-155, and BN-127. Purple lines represent the 90% confidence interval for the model. The black line represents the average or ‘expected’ model. 33

Figure 10 - Thermal History model (tT) of all (13) samples, pooled together. See caption for Figure 9. 34

Figure 11 - Results of U-Pb dating of apatite from 18 samples plotted on Tera Wasserburg Concordia diagrams for each sample with ^{207}Pb corrected weighted mean ^{206}Pb - ^{238}U plots as insets. Organised according to Formation/suite as listed in Table 4. Red ellipses represent the uncertainty in isotopic ratios for each single grain spot analysis. Dashed ellipses illustrate apatite grains that had analytical problems and/or obvious discordance and were not utilized in the final calculations. Each plot is annotated with Weighted Average values, Upper and Lower intercept ages and associated MSWDs. Red boxes over sample name represent those samples utilised to calculate the common Pb correction in samples from the same formation/suite. 39

Figure 12 – *Above*: Pooled Cartesian plot showing the relationship between Age (Ma) on the X-axis, Confined track lengths (μm) on the Y-axis and ^{238}U concentrations displayed as a colour gradient. *Below Left*: Frequency plots showing the Confined track length (μm) relationship between Peak 1 ages and Peak 2 ages (see caption for Figure 11). *Below Right*: - Radial plot of calculated AFT cooling ages for six discriminated samples within the study region. Central age values are by calculated RadialPlotter and for dispersions >25% age peak discrimination was performed using the RadialPlotter software (Vermeesch 2009). Percentage of data associated with each peak is bracketed adjacent to the age of each peak. [C] on the X- Axis represents the amount of ^{238}U in ppm. The left Y-Axis represents 2 standard deviations from central age (Ma). Right

‘curved’ Y-Axis shows increasing age in Ma. ^{238}U ppm values greater than 75ppm are displayed as purple circles. 42

Figure 13 - *Left*: Cartesian plots showing the relationship between Age (Ma) on the X-axis, Confined track lengths (μm) on the Y-axis and ^{238}U concentrations displayed as a colour gradient. *Right*: Frequency plots showing the Confined track length (μm) relationship between Peak 1 ages and Peak 2 ages. Central ages and associated pooled confined track length information is given in the black text fields. Peak 1 ages and associated confined track length data are displayed in the blue text fields. Peak 2 ages and associated confined track length data are displayed in the red text fields. For each annotated text field - CTNs = number of confined track lengths, MTL = Mean track length, StdDev = Standard Deviation and SE = Standard Error..... 43

Figure 14 – Time sequence showing the evolution of Gondwana break-up between 200Ma and 110Ma in context with late Triassic to mid Cretaceous AFT ages presented in this study. Modified from plate reconstruction models by (Seton et al., 2012). 47

Figure 15 - Time sequence showing the evolution of Gondwana break-up between 100Ma and 60Ma in context with the middle to late Cretaceous AFT ages presented in this study. Modified from plate reconstruction models by (Seton et al., 2012). 49

Figure 16 – Gridded ‘heat map’ for the study area defined by AFT central ages. Hot and Cold colours represent young and old AFT ages respectively. Faults are indicated and coloured according to relative deformation events (absolute timings of D4, D5 and ‘Late Fault’ activity are not known). Modified from Block *et al.*, (2016). A to A’ Cross section is visualised in Figure 15..... 51

Figure 17 - *Above*: Pooled radial plots of separate sample groups as described in the results section of this thesis, coloured following the gridded map in Figure 14. Cold colours represent older AFT central ages and hot colours represent younger AFT central ages. *Below*: SW-NE cartoon cross section from A to A’ pictured in Figure 14 with indication of current sample locations. The colour gradient represents sample ages as described in the legend. Solid lines represent the location of tectonic fabrics according to the regional map modified from Block *et al.*, (2016) and coloured according to relative age as described in the legend. Dashed lines represent the inferred late Cretaceous pre-erosional surface as interpreted by this study..... 52

Table 1 - Analytical details for the LA-ICP-MS as used for AFT and AUPb double dating 17

Table 2 - Sample locations and lithology details. U-Pb formation ages, formation/suite and lithologies are from Block *et al.*, (2015) Block *et al.*, (2016) de Kock *et al.*, (2012) and Baratoux *et al.*, (2011). Migm = migmatite..... 19

Table 3 - AFT dating results organised according to groupings. p_s = density of spontaneous tracks (10^5 tracks/cm²). N_s = number of counted spontaneous tracks. n = number of counted grains. ^{238}U = mean ^{238}U Uranium concentration in ppm. P1 = Peak one age results (Ma). P2 = Peak two age results (Ma). n_l = Number of measured confined track lengths. MTL = Confined Track Mean Track Lengths in μm . Green rows = Group 1 samples, Purple rows = Group 2 samples, Blue rows = Group 3 samples and Red rows = Group 4 samples..... 22

Table 4 – Apatite U-Pb results for all samples arranged according to Formation/suite. Published U-Pb formation ages, formation/suites and lithologies are from Block *et al.*, (2015) Block *et al.*, (2016) de Kock *et al.*, (2012) & Baratoux *et al.*, (2011). Migm =

migmatite. Samples in bold represent the samples which were used to calculate the common Pb contributions for samples from the same rock suite..... 35
Table 5 - Confined track lengths results of six samples and six samples pooled. Central, P1 and P2 ages are given in Ma. Central, P1 and P2 Mean Track Lengths (MTL) are given in μm and 1σ represents one standard deviation from the MTL 41

1. INTRODUCTION

The Ivory Coast-Ghana (ICG) continental margin represents the eastern prolongation of the Romanche Transform zone in the equatorial Atlantic Ocean (Clift et al., 1997) and is marked by a significant basement ridge (Clift 1999). Geo- and thermochronology studies reveal that the ICG basement ridge formed during the Cretaceous in response to rifting between western Africa and Brazil (in the framework of Gondwana break-up) during the opening of the Equatorial Atlantic Ocean (Bouillin et al., 1997; Guiraud and Maurin 1992; Bigot-cormier et al., 2005). North of this basement ridge, a large scale shear zone, the Bole-Nangdoi (BN) shear zone, dissects the West African Craton (WAC), which is thought to represent the eastern continental extension of the St Pauls transform fault (Figure 1)(Jessell et al., 2016). This study focusses on the thermal and exhumation history of the BN shear zone in northern Ghana aiming to characterise the rifting history of the WAC from Gondwana and the associated opening of the Equatorial Atlantic Ocean.

Rifting in the equatorial region of the Atlantic was preceded by extension and initial seafloor spreading in the Central Atlantic since the early Jurassic and in the South Atlantic during the latest Jurassic or earliest Cretaceous (Buiter and Torsvik 2014).

The Benue Trough (Figure 1) was initiated during the early to middle Cretaceous in response to the northward propagating rift axis associated with the South Atlantic.

During the Cretaceous transpressional structures (eg. the Gombe Fault) were inherited by NE-SW trending late Pan-African shear zones and were reactivated forming various isolated basins within the Benue Trough (Benkhelil 1989; Basile et al., 1993; Ngako et al., 2006; Jolly et al., 2015).

Emplacement of voluminous magmatic provinces such as the Central Atlantic Magmatic province (CAMP), the Paraná-Etendeka Large Igneous Province and plume magmatism in the Benue Trough (Coulon et al., 1996) are contemporaneous with the opening of the Central and Southern Atlantic (Peyve 2015b). These magmatic provinces are considered to have been emplaced during periods of extension along Pan African structures (Buiter 2014) and contributed to the thermal weakening of the lithosphere and thus provided a major control on continental break-up (Peyve 2015b; Buiter and Torsvik 2014; Daniels et al., 2014).

Geodynamic and thermochronological studies have been conducted along the off-shore ICG marginal ridge and adjacent Deep Ivorian Basin (DIB) through seismic and Ocean Drilling Program (ODP) drill-hole studies. These studies revealed the main morphological characteristics of the ICG margin and provided constraints on its thermal and mechanical evolution during the break-up of the Gondwana super-continent, and more generally on the resulting ocean-continent transform margin evolution as a whole (Guiraud and Maurin 1992; Basile et al., 1993; Maurin and Guiraud 1993; Bouillin et al., 1997; Benkhelil et al., 1997; Mascle et al., 1998; Antobreh et al., 2009).

The purpose of this study is to constrain the thermal history of northern Ghana, north of the ICG margin using on-shore basement samples across the main structural architecture associated with the BN shear zone (Figure 2). More specifically, the timing of the rifting phase of the continental margin is assessed through the use of Apatite Fission Track (AFT) analysis. The results were obtained using the Adelaide University Autoscan System in combination with LA-ICP-MS equipment and interpreted in combination with previous low-temperature thermochronological data provided by Bigot-Cormier et al., (2005) and Bouillin et al., (1997). Furthermore, the results are

modelled with the software package QTQt (Gallagher 2012) to reveal the thermal history of the study area between 60°C and 120°C and to identify distinct periods of denudation. This in turn will further our understanding of the evolution of transform margins with respect to uplift/subsidence and isostatic/thermal rebound during intra-continental rifting phases, and provide time constraints on Gondwana breakup and the opening of the Equatorial Atlantic Ocean. Additional apatite U-Pb (AU-Pb) data are obtained and primarily used as high temperature constraints for thermal history modelling (Deynoux et al., 2006; Chew and Spikings 2015).

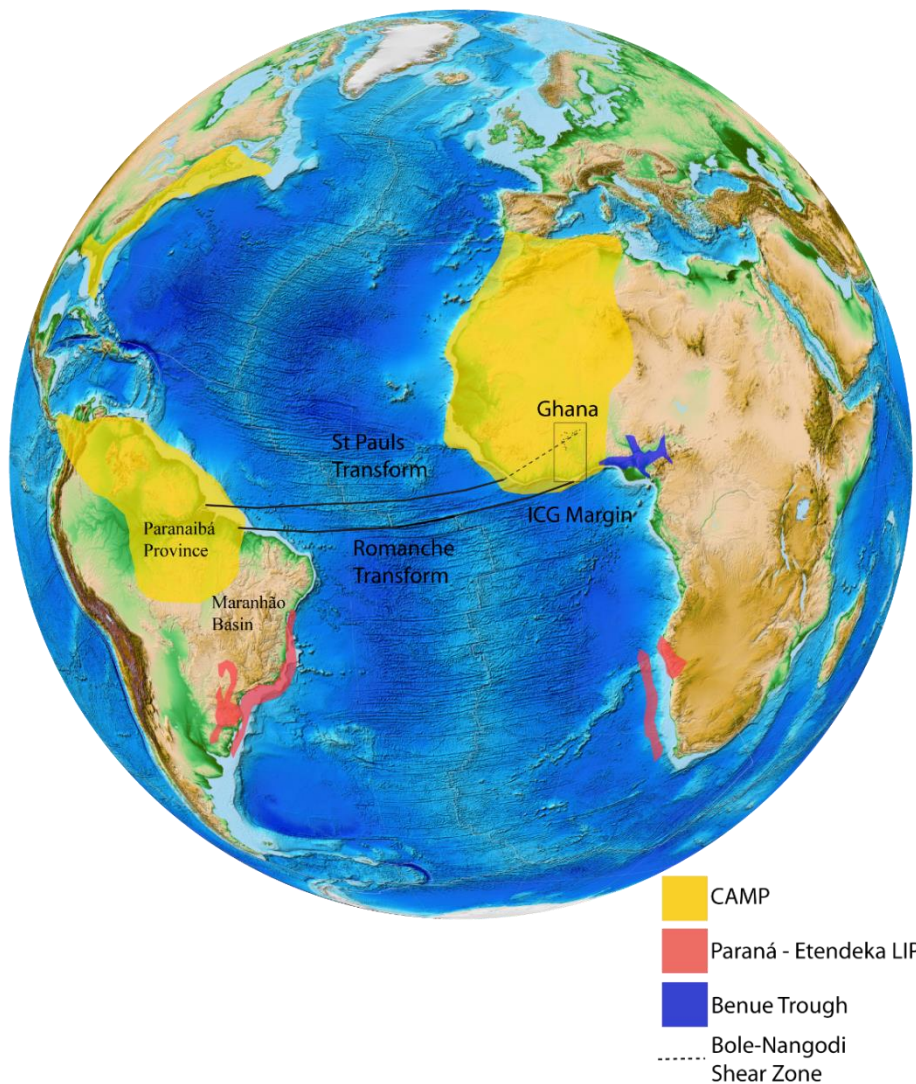


Figure 1 – Globe image with indication of the study area in Ghana (box framed) and showing the approximate locations of CAMP, the Paraná – Etendeka LIP, the Benue Trough (Buiter and Torsvik 2014), Ghana, the Bole-Nangodi shear zones and the Romanche and St Paul’s Transform Zones (Basile et al., 2005; Block et al., 2015). Modified from plate rotation files from Gplates software (Seton et al., 2012)

2. GEOLOGICAL SETTING

The study in northern Ghana forms part of the south-eastern section of the West African Craton (WAC) (Figure 2) (Block et al., 2015) and primarily consists of Paleo-proterozoic basement terranes associated with the Tamnean plutonic suite, Eburnean plutonic suite and the Birimian plutonic supergroup (emplaced between 2250 Ma and 1980 Ma) (Baratoux et al., 2011; Metelka et al., 2011; de Kock et al., 2012; Block et al., 2016). The lithologies within these groups range between granitoids, greenstone volcanics and high/low grade metamorphic units (Block et al., 2015). To the east the study area is bound by the Neo-proterozoic Volta Basin and the Dahomeyide orogen which is thought to have formed during Gondwana assembly in the late Neo-proterozoic and early Cambrian (Figure 2) (Anani 1999; Antobreh et al., 2009; Nude et al., 2009; Carney et al., 2010; Attoh et al., 2013). The different tectono-metamorphic terranes of north-western Ghana are typically bound by high-strain zones and exhibit three deformational phases associated with the Paleo-proterozoic Eburnean orogeny (Tapsoba et al., 2013). The deformational events are thought to have had a strong control on the spatial association of contrasting high and low grade terranes through either nappe style tectonic accretion or diapirism (Block et al., 2016). From those shear zones, the dextral NE-SW striking Bole-Nangodi (BN) shear zone has been interpreted as a major structural control on the orientation of the St Paul's Fracture Zone which trends parallel to the Romanche Fracture Zone and represents the main focus point of this study (Figure 1)(Block et al., 2016; Jessell et al., 2016).

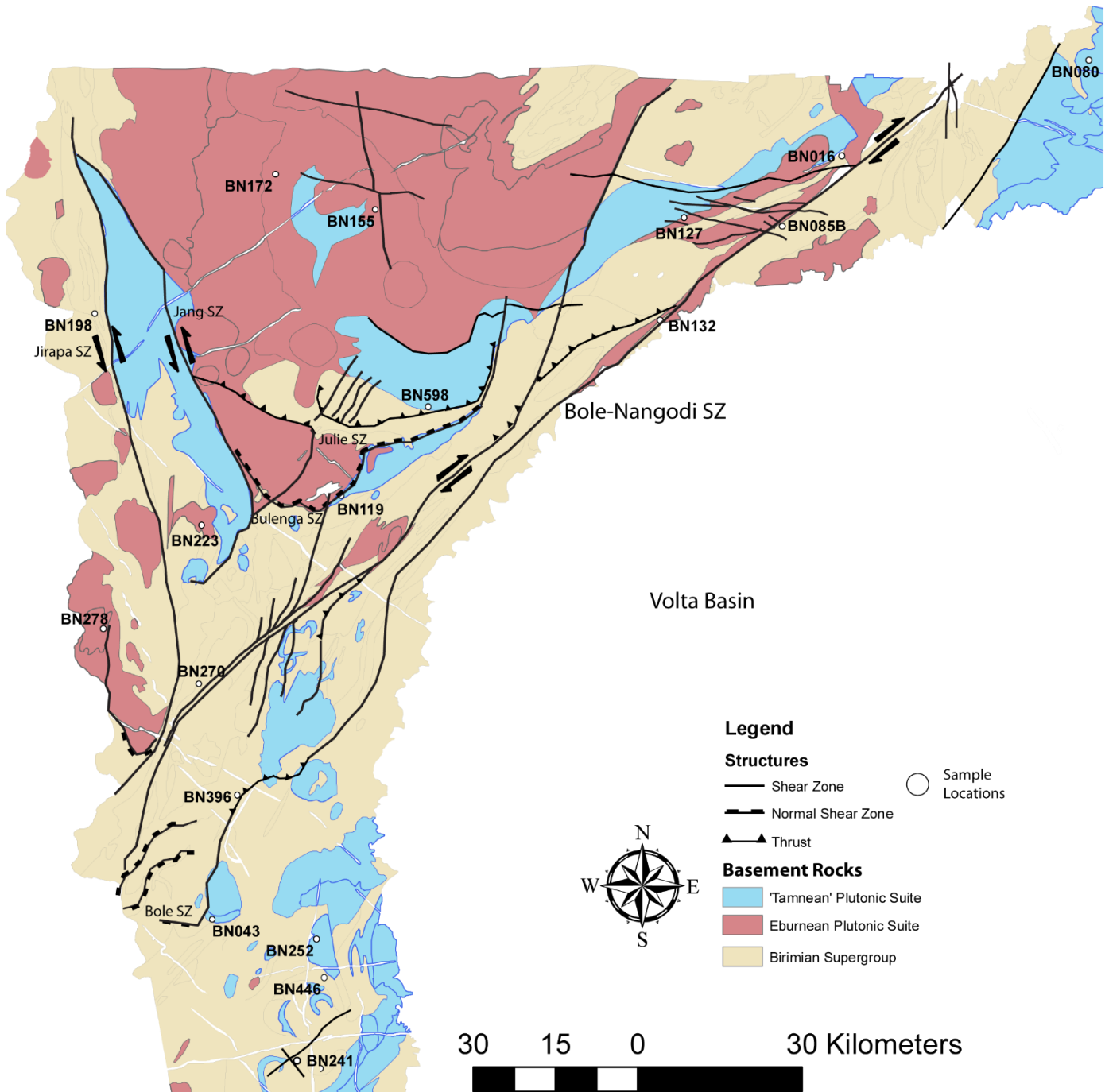


Figure 2 – Schematic geological map of the study area located in northern Ghana. Showing sample locations (Modified after Block *et al.* 2016).

The WAC is considered to have been largely tectonically inactive since the end of the Pan-African orogeny. This period of tectonic quiescence lasted until the Triassic-Jurassic transition at 200Ma (Jessell et al., 2016). The time period between the end of the Triassic and the early Cretaceous is characterised by 2 stages of rifting that precede the opening of the Equatorial Atlantic Rift System (EqRS).

- (1) Break-up within the Central Atlantic transpired at ca. 200Ma, contemporaneous with the emplacement of the Central Atlantic Magmatic Province (CAMP).
- (2) Break-up within the South Atlantic occurred synchronous or marginally preceded the emplacement of the Paraná - Etendeka Large Igneous Province (LIP) at ca. 137Ma as dated by K-Ar methods (Eby and Mariano 1992; Karner and Driscoll 1999; Basile, Mascle, and Guiraud 2005; Buiter and Torsvik 2014; Peyve 2015a).

As a result of rifting in the Central and South Atlantic, the EqRS developed between a southward and northward propagating rift axis (Basile et al., 2005). Rocks related with those igneous events are limited within Ghana and mostly constrained to Guinea, Mali, Morocco, Mauritania and Liberia within the African continent (Deckart et al., 2005; Verati et al., 2005). Crossing the Atlantic from the Ghanese study area, the Maranhão and Paranaíba Basins in north-eastern Brazil (Figure 1) yield abundant volcanoclastic evidence of both distinct periods of magmatism - (with geochemical associations to CAMP and the Paraná - Etendeka LIP) (Basile et al., 2005). Both the African and Brazilian margins thus contain evidence for rifting of the Atlantic Ocean over a 70-80Myr period (Coulon et al., 1996; Baksi and Archibald 1997; Merle et al., 2011; Daniels et al., 2014).

The ICG marginal ridge is the modern expression of the Romanche transform fault associated with rifting and break-up in the Equatorial Atlantic during the early Cretaceous (Masclé et al., 1998). Preliminary on-shore low-temperature AFT studies on the ICG margin have revealed cooling ages that vary between 130Ma and 415Ma. The youngest of those have been interpreted to constrain denudation associated with the initial rifting phase (Lisker et al., 2008). Off-shore low-temperature thermochronology and geophysical studies conducted on the ICG margin reveal its development to have undergone three geodynamic stages since the Aptian (Basile et al., 1993; Bouillin et al., 1997; Clift et al., 1997; Bigot-cormier et al., 2005).

(1) At the start of the Aptian, the first stages of rifting occurred and the Deep Ivorian Basin (DIB) was initiated as a result of E-W to ENE-WSW oblique extension (Clift et al., 1997).

(2) The onset of intra-continental transform faulting between the African & South American plates began in the late Aptian to Cenomanian (Lamarche et al., 1997; Clift et al., 1997; Bouillin et al., 1997).

(3) During the Turonian, transform faulting resulted in newly created oceanic crust to come into contact with the continent and the ICG margin became a passive margin since the Santonian (Clift et al., 1997; Bouillin et al., 1997; Bigot-cormier et al., 2005).

3. METHODS

3.1 Apatite Fission Track thermochronology

Apatite Fission Track thermochronology is based on the spontaneous fission decay of $^{238}\text{Uranium}$. This occurs when the $^{238}\text{Uranium}$ atom splits apart to produce two highly charged daughter isotopes that repulse in opposite directions at high velocities, producing a linear damage track (Chew and Spikings 2015). For samples older than 1Ma, the 1-100 ppm concentration of Uranium in apatite generates a useful quantity of fission tracks for dating purposes. Comparing the fission track density with the Uranium content of the host apatite, a fission track date can be calculated (Chew and Spikings 2015). The fission track density can be acquired through imaging and counting of etched spontaneous fission tracks. The Uranium concentrations are classically acquired indirectly by inducing fission in a nuclear reactor, however, nowadays it can be measured directly in-situ using the LA-ICP-MS method as described by Hasebe et al., (2004). This method was used as it is faster, allows for multi-element analysis and is potentially even more accurate and precise than the classic AFT method (Chew and Spikings 2015).

A fission track date is used to constrain a temperature-time (t-T) cooling path through the apatite fission track partial annealing zone (APAZ). The APAZ represents a temperature zone between 120°C and 60°C where fission tracks get shortened and potentially completely annealed, depending on the rate of heating or cooling (Gleadow et al., 1986). Measurements of fission track lengths (MTL) provide additional information on the rate of cooling or heating through the APAZ with an increased proportion of short fission tracks generally indicating slower cooling or more complex cooling histories (Gleadow et al., 1986).

3.2 Apatite U-Pb Dating

The Apatite Uranium-Lead (AU-Pb) method is based on the diffusion of radiogenic Pb within apatite crystals. Pb can only be retained within the apatite crystal lattice at temperatures below ca.450-550°C. The AU-Pb method thus dates the timing of cooling below this temperature range (a more precise closure temperature estimate is controlled by the cooling rate and grain size geometry) (Chew and Spikings 2015). AU-Pb is conducted synchronously with the AFT method (see below), where the data is collected on the same apatite grain during LA-ICP-MS analysis. Apatite can accommodate a significant amount of initial (common) ^{207}Pb in to the crystal structure which requires a common ^{207}Pb correction, outlined below.

3.3 Laboratory Processing

Samples were processed using standard crushing and sieving procedures and mineral separation was done by conventional magnetic and heavy liquid methods at the University of Toulouse in France. A total of eighteen apatite samples were ‘double dated’ with both the apatite fission track and AU-Pb method.

3.4 Apatite Fission Track and AU-Pb Analysis

Apatite Grains were picked and mounted in epoxy resin and then ground and polished to expose internal sections of the grains. Chemical etching was used to reveal the natural fission tracks within apatite grains and was achieved by submerging the polished mounts into a 5M solution of HNO_3 for 20 seconds followed by cleaning with water to prevent further etching. The fission track density and confined fission track lengths were analysed using an Autoscan System with the FastTracks software package on a Zeiss AXIO Imager M2m utilizing 1000x magnification. The diameter of etch pits

(Dpar) was also measured as this represents a kinetic parameter used in subsequent thermal history modelling (Ketcham et al., 1999). A minimum of 20 grains were analysed per sample to identify and count a minimum of 1000 tracks. The objective was to measure at least 100 confined fission track lengths, where possible. The uranium and lead concentration of each counted grain was measured using spot analyses on a New Wave UP213 laser connected to an Agilent-7500cs ICPMS. Calibrations and data reduction were conducted using Madagascar apatite as the primary standard (U-Pb age of 473.5 ± 0.7 Ma, (Stacey and Kramers 1975)). McClure (U-Pb age of 523.51 ± 1.47 Ma (Schoene and Bowring 2006)) and Durango ($^{40}\text{Ar}/^{39}\text{Ar}$ age of 31.44 ± 0.18 Ma, (McDowell et al., 2005)) apatite were used as secondary standards for accuracy checks. Data reduction was performed using the Iolite software (Paton et al., 2011). Common Pb corrections were undertaken by calculating a best-fit common Pb line through the data in Tera Wasserburg plots. The upper-intercept of this common Pb line with the Concordia estimates the common Pb $^{207}\text{Pb}/^{206}\text{Pb}$ ratio, to which all data are corrected (Chew et al., 2014). This approach assumes that all grains are concordant and requires a large variation of common Pb contributions in individual apatite grains to accurately assess the projected line of best fit through uncorrected data to determine the common Pb ratio (Chew et al., 2014). Outlier analysis of grains that obviously plot away from the common Pb line are assumed to be discordant and/or have analytical problems and are discarded. A weighted mean ^{207}Pb -corrected ^{206}Pb - ^{238}U age was calculated for each sample, which is thought to represent the best estimate of the AU-Pb cooling ages (Chew and Donelick 2012; Chew et al., 2014). More information on the analytical details are listed in Table 1.

Table 1 - Analytical details for the LA-ICP-MS as used for AFT and AUPb double dating

ICPM-MS	
Brand and model	Agilent 7500x
Forward power	1300 W
<i>Gas flows (L/min)</i>	
Cool (Ar)	15.00
Auxiliary (Ar)	0.89
Carrier (He)	0.70
Sample (Ar)	0.93
Laser	
Type of Laser	Nd-YAG
Brand and Model	ESI NWR213
Laser wavelength	213nm
Pulse duration	20 ns
Spot size	32 μm
Repetition rate	10 Hz
Energy attenuation	50%
Laser fluency	$\sim 3\text{-}4 \text{ J/cm}^2$
Laser warm up (background collection)	20 s
Data acquisition parameters	
Data acquisition protocol	Time-resolved analysis
Scanned masses	235, 238, 204, 206, 207, 208, 232, 91, 44, 43, 35
Samples per peak	1
Number of scans per peak	1
Detector mode	Pulse counting
Detector deadtime	35 ns
Background collection	20 s
Ablation for age calculation	30 s
Washout	20 s
<i>Standardisation and data reduction</i>	
Primary standard used	Madagascar Apatite (U-Pb age of $473.5 \pm 0.7 \text{ Ma}$, (Stacey and Kramers 1975)
Secondary standard used	Durango ($^{40}\text{Ar}/^{39}\text{Ar}$ age of $31.44 \pm 0.18 \text{ Ma}$, (McDowell, McIntosh, and Farley 2005) and McClure Mountain apatite (U-Pb age of $523.51 \pm 1.47 \text{ Ma}$ (Schoene and Bowring 2006))
Data reduction software used	Iolite

3.5 Data Presentation and Modelling

AFT central ages were calculated with RadialPlotter which represent the apparent AFT cooling age of analysed samples. This central age is not necessarily a good estimate of a cooling event and therefore subsequent thermal history modelling is needed to derive the tT history preserved in the sample. Furthermore, it is possible to (partially) preserve multiple AFT cooling ages or 'peak ages' in samples which fail Pearsons χ^2 test or where single-grain ages show a dispersion above ~25% which is regarded as a beyond natural spread (Galbraith 2005). In more detail, radial plots often show an open-jaw display of an older event and younger age component that can be related to distinct cooling events (O'Sullivan and Parrish 1995). This is especially the case when two apatite populations have significantly different chemistry. In this regard, Chlorine concentrations are often used as a chemical discriminator (Green et al., 1986). Elevated chlorine concentrations are known to slow fission track annealing but often show only little differences between apatite populations. This study uses Uranium rather than Chlorine concentration as a discriminator, which is thought to have a similar effect on fission track annealing. Hendricks and Redfield (2005) described a model of radiation-enhanced annealing for apatites with elevated Uranium concentrations from old cratonic rocks.

Thermal history (time-temperature) modelling was performed using the software package QTQt which utilizes the Bayesian trans-dimensional Markov Chain Monte Carlo statistical method to derive the most likely thermal history models (Gallagher 2012). The input parameters required in this modelling approach include individual AFT ages, their standard deviations, confined track lengths, sample elevations and a kinetic parameter (Gallagher 2012). Thermal history models are determined from

individual samples or groups of samples in close vicinity of each other and/or position relative to geological structures such as faults and shear zones. The final output of each modelling attempt resolves four different models and generates an average model based on a probability function at each point in the time-temperature space. The probability function is visualised in a colour spectrum ranging from blue (low probability) to red (high probability) where the absolute numerical probability value varies per model.

4. RESULTS

4.1 Sample locations

Table 2 - Sample locations and lithology details. U-Pb formation ages, formation/suite and lithologies are from Block *et al.*, (2015) Block *et al.*, (2016) de Kock *et al.*, (2012) and Baratoux *et al.*, (2011). Migm = migmatite.

<i>Sample ID</i>	<i>Latitude</i>	<i>Longitude</i>	<i>Elevation</i>	<i>Formation/Suite</i>	<i>Lithology</i>	<i>Published U-Pb Formation Age (Ma)</i>
<i>BN-016</i>	10°48'18.00"N	0°53'6.00"W	216 m	Birimian Super Group	Granite	2250 - 1980
<i>BN-043</i>	8°55'44.04"N	2°25'55.20"W	277 m	Tamnean Pluton Suite	Granite	2141.2 ± 6.4
<i>BN-080</i>	11° 2'24.00"N	0°16'40.80"W	219 m	Tamnean Pluton Suite	Granite	2134 - 2118
<i>BN-085B</i>	10°37'55.20"N	1° 1'55.20"W	165 m	Birimian Super Group	Granite	2250 - 1980
<i>BN-119</i>	9°58'9.12"N	2° 6'54.00"W	307 m	Tamnean Plutonic Suite	Granite	2134 - 2118
<i>BN-127</i>	10°39'10.80"N	1°16'19.20"W	181 m	Eburnean Plutonic Suite	Bt-Gneiss	2150 - 2000
<i>BN-132</i>	10°24'3.60"N	1°19'55.20"W	162 m	Eburnean Plutonic Suite	Orthogneiss	2150 - 2000
<i>BN-155</i>	10°40'22.80"N	2° 1'51.60"W	285 m	Eburnean Plutonic Suite	Orthogneiss	2150 - 2000
<i>BN-172</i>	10°45'36.00"N	2°16'37.20"W	306 m	Eburnean Plutonic Suite	Bt-Granite	2150 - 2000
<i>BN-198</i>	10°25'1.20"N	2°43'15.60"W	282 m	Birimian Super Group	Granite	2250 - 1980
<i>BN-223</i>	9°53'53.16"N	2°27'28.80"W	324 m	Eburnean Plutonic Suite	Bt-Msc-Granite	2150 - 2000
<i>BN-241</i>	8°34'54.48"N	2°13'26.40"W	188 m	Birimian Super Group	Bt-Granite	2250 - 1980
<i>BN-252</i>	8°52'50.16"N	2°10'33.60"W	241 m	Tamnean Plutonic Suite	Granite	2134 - 2118
<i>BN-270</i>	9°30'27.00"N	2°27'54.00"W	292 m	Birimian Super Group	Orthogneiss	2250 - 1980
<i>BN-278</i>	9°32'35.88"N	2°42'0.00"W	293 m	Eburnean Plutonic Suite	Bt-Msc-Granite	2150 - 2000
<i>BN-396</i>	9°14'4.56"N	2°22'12.00"W	298 m	Birimian Super Group	Paragneiss	2250 - 1980
<i>BN-446</i>	8°47'10.32"N	2° 9'25.20"W	222 m	Birimian Super Group	Paragneiss	2132 ± 7
<i>BN-598</i>	10°11'20.40"N	1°54'3.60"W	248 m	Tamnean Plutonic Suite	Granodiorite	2134 - 2118

A total of 18 samples were chosen based on their proximity to the main study object, the NE-SW striking Bole-Nangodi shear zone in northern Ghana and based on apatite quality (Figure 2). All samples were sourced from crystalline rock types from three Paleo-proterozoic formations (Figure 2; Table 2). Sample locations and rock descriptions are detailed in Table 2 and locations are shown in Figure 3. AFT and AU-Pb results were obtained from all 18 samples and are grouped according to their location relative to the Bole-Nangodi (BN) shear zone (Figure 3). The four groups yield distinctively different AFT results and are modelled separately for their thermal history, allowing assessment of differential exhumation across the study area with respect to the BN shear zone.

- Group 1 contains three samples BN-080, BN-252 and BN-446, located south of the Bole-Nangodi (BN) shear zone (Figure 3) and represent the area closest to the continental margin.
- Group 2 contains four samples BN-016, BN-085B, BN-119 and BN-270 taken along strike of the BN shear zone.
- Group 3 contains eight samples BN-043, BN-172, BN-198, BN-223, BN-241 BN-278, BN-396 and BN-598 located within the tectonic blocks to the northwest and southwest of the BN shear zone, most distal from the continental margin.
- Group 4 contains three anomalously younger samples (BN-127, BN-132 and BN-155). BN-127 and BN-132 located within the central part of the BN shear zone and BN-155 was taken near an unnamed conjugate fault-set north of the BN shear zone. Their results are discussed following these groupings.

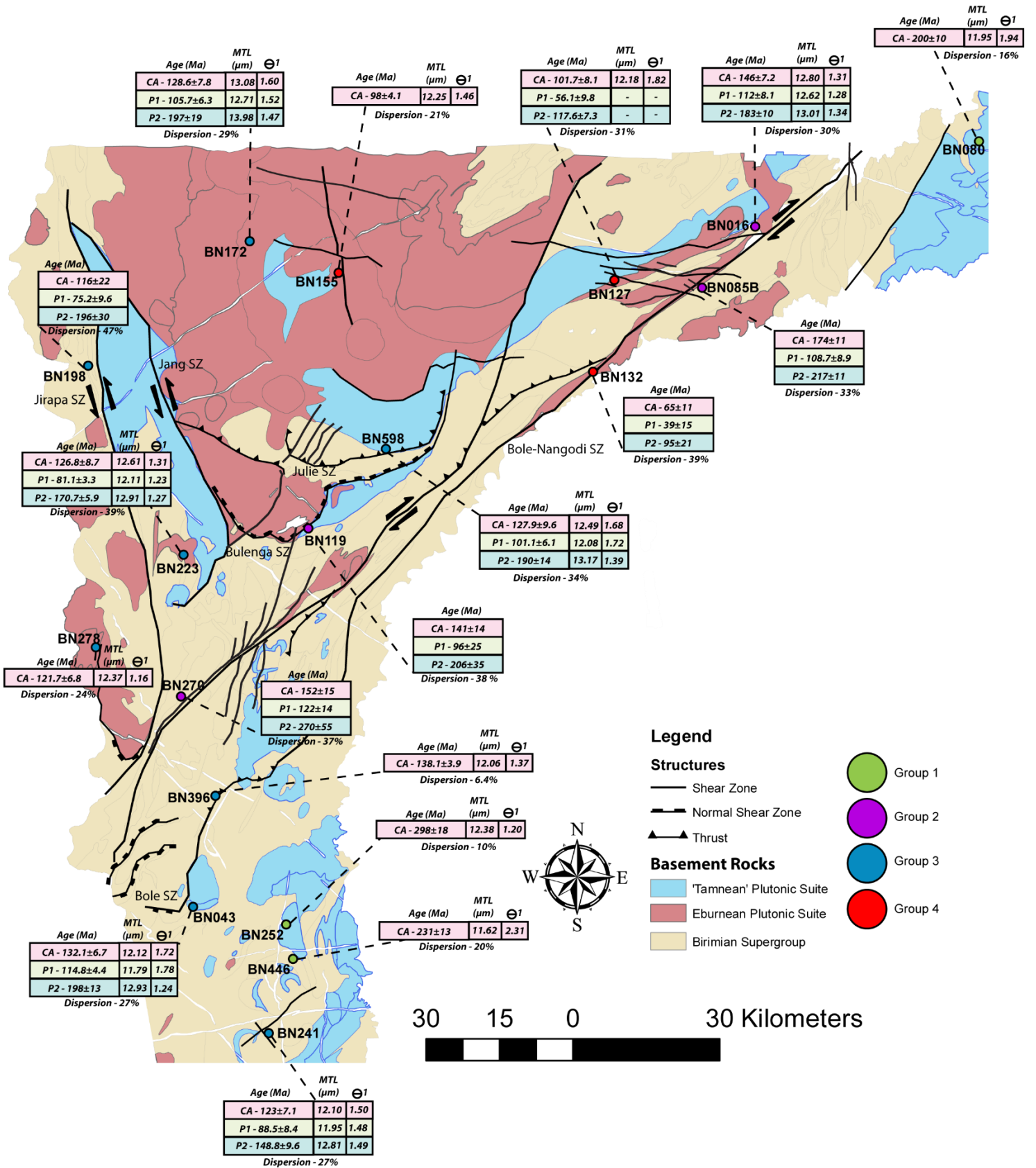


Figure 3 - Map of the study area showing sample locations as coloured circles, lithology's and AFT results. CA – Central Age, P1 – Peak 1 Age, P2 – Peak 2 Age, MTL – Mean Track Length and Θ¹ – MTL Standard Deviation. Modified after Block *et al.* 2016

4.2 Apatite Fission Track Age Results

Table 3 - AFT dating results organised according to groupings. ρ_s = density of spontaneous tracks (10^5 tracks/cm²). N_s = number of counted spontaneous tracks. n = number of counted grains. ^{238}U = mean ^{238}U concentration in ppm. P_1 = Peak one age results (Ma). P_2 = Peak two age results (Ma). nl = Number of measured confined track lengths. MTL = Confined Track Mean Track Lengths in μm . Green rows = Group 1 samples, Purple rows = Group 2 samples, Blue rows = Group 3 samples and Red rows = Group 4 samples.

Sample ID	ρ_s	N_s	n	^{238}U	1σ	Central Age (Ma)	1σ	P_1 (Ma)	1σ	P_2 (Ma)	1σ	Disp (%)	$P(\chi^2)$	nl	MTL (μm)
BN-080	4.3	608	41	4.5	0.34	200	10	-	-	-	-	16	0.07	54	11.95
BN-252	6.69	418	28	4.69	0.476	297	18	-	-	-	-	10	0.25	31	12.38
BN-446	19.24	997	26	14.69	1.21	231	13	-	-	-	-	20	0.00	35	11.62
BN-016	12.53	2952	48	16.94	1.34	146	7.2	112	8.1	183	10	30	0.00	69	12.80
BN-119	3.94	205	34	5.44	0.56	141	14	96	25	206	35	38	0.00	-	-
BN-085B	6.41	890	40	7.63	0.622	174	11	108.7	8.9	217	11	33	0.00	-	-
BN-270	3.01	310	29	3.44	0.32	152	15	122	14	270	55	37	0.00	-	-
BN-043	23.29	1974	41	30.54	2.53	132.1	6.7	114.8	4.4	198	13	27	0.00	60	12.12
BN-172	7.87	814	41	11.39	0.91	128.6	7.8	105.7	6.3	197	19	29	0.00	55	13.08
BN-198	5.31	136	9	9.51	0.82	116	22	75.2	9.7	196	30	56	0.00	-	-
BN-223	20.74	2486	38	38.97	3.49	126.8	8.7	81.1	3.3	170.7	5.9	39	0.00	70	12.61
BN-241	10.58	814	39	19.05	1.56	123	7.1	88.5	8.4	148.8	9.6	27	0.00	45	12.10
BN-278	17.32	1415	30	25.42	2.184	121.7	6.8	-	-	-	-	24	0.00	36	12.37
BN-396	20.34	1916	39	26.13	2.05	138.1	3.9	-	-	-	-	6.4	0.10	87	12.06
BN-598	11.43	1317	36	15.73	1.47	127.9	9.6	101.1	6.1	190	14	34	0.00	64	12.49
BN-127	9.01	468	26	18.26	1.59	101.7	8.1	56.1	9.8	117.6	7.3	31	0.00	33	12.18
BN-132	2.31	72	13	8.72	0.81	65	11	39	15	95	21	39	0.03	-	-
BN-155	15.65	2008	41	32.18	2.22	98	4.1	-	-	-	-	21	0.00	142	12.25

4.2.1 Group 1

Group 1 is defined by samples taken from the south-eastern structural terrane of the study area, at the margin of the Volta basin, and yields the oldest AFT results for this study. The central AFT ages from Group 1 range between $200\pm 10\text{Ma}$ to $297\pm 18\text{Ma}$ (Figure 4). Samples BN-252 and BN-446 were taken in the southwestern corner of the study area and revealed central AFT ages of $298\pm 18\text{Ma}$ and $231\pm 13\text{Ma}$ and MTL of $12.38\mu\text{m}$ and $11.62\mu\text{m}$ respectively (Figure 4; Table 3). Sample BN-080 was taken in the structural terrane within the north-eastern corner of the study area, and has a central AFT age of 200 ± 10 with a MTL of $11.95\mu\text{m}$. A pooled radial plot for Group 1 yields a central AFT age of $230.6\pm 8.6\text{Ma}$ (Figure 4d).

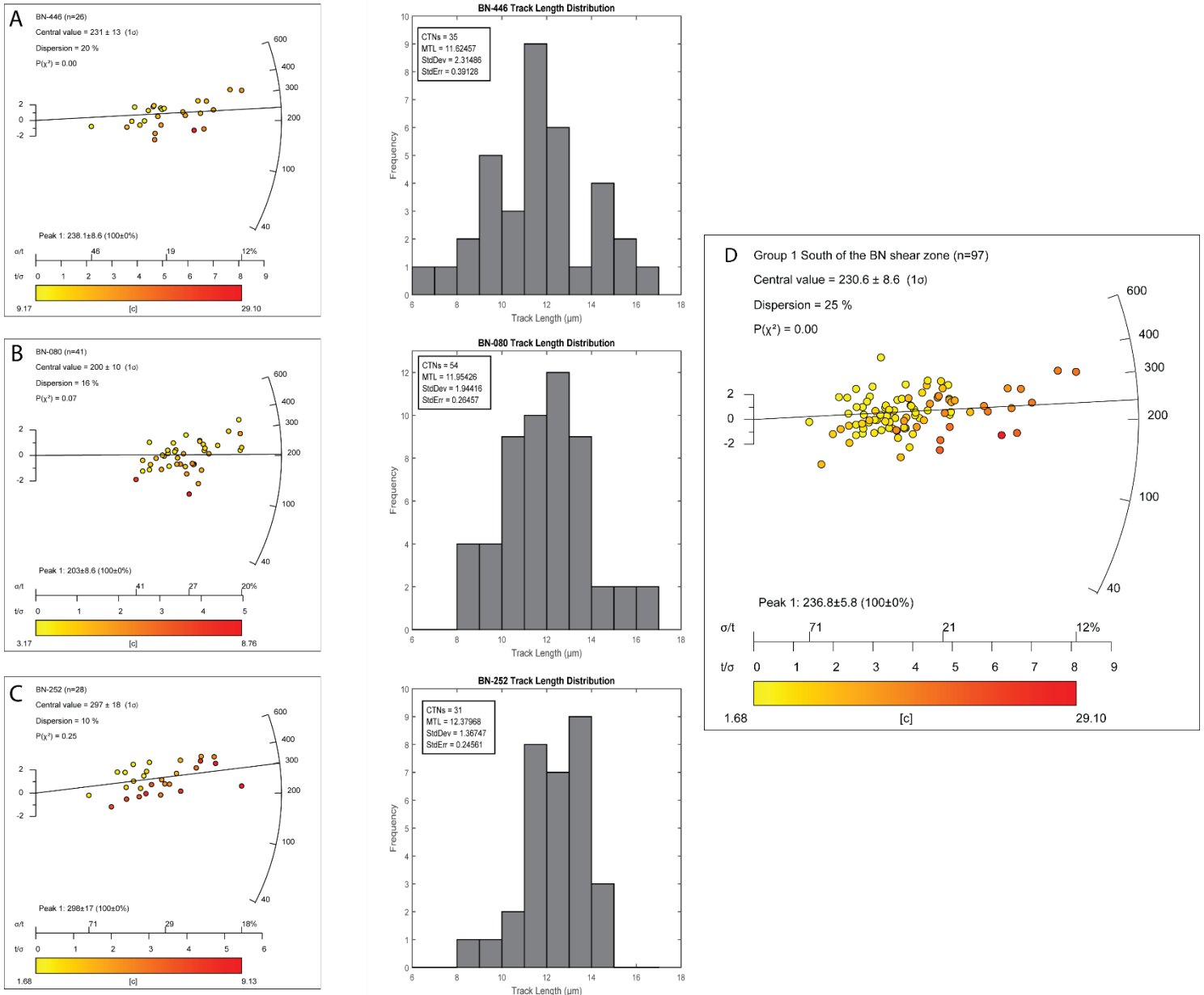


Figure 4 - Radial plots of calculated AFT cooling ages for each sample location associated with sample Group 1 (A-C). D: Represents a pooled radial plot of Group 1 samples. Central age values were calculated using RadialPlotter and for dispersions >25% and $P(\chi^2)$ less than 0.05 age peak discrimination was performed using the RadialPlotter software (Vermeesch 2009). Percentage of data associated with each peak is bracketed adjacent to the age of each peak. [C] on the X- Axis represents the amount of ^{238}U in ppm. The left Y-Axis represents 2 standard deviations from the central age. Right 'curved' Y-Axis shows increasing age in Ma. The values along the X-axis show single-grain age uncertainties. Frequency plots depict track length distributions and are annotated with the number of measured confined track lengths (CTNs), Mean track length (MTL), Standard Deviation (StdDev) and Standard Error (StdErr).

4.2.2 Group 2

Group 2 is defined by samples taken in the NE and SW along strike of the BN shear zone with intermediate central ages and relatively large single-grain age dispersion. The central AFT ages for Group 2 range between 141 ± 14 Ma and 174 ± 11 Ma and are thus somewhat younger than those obtained from Group 1 (Figure 5; Table 3). BN-085B represents the oldest sample in the group has a central AFT age of 174 ± 11 Ma (Figure 5). Samples BN-016, BN-119 and BN-270 have central AFT ages of 146 ± 7.2 Ma, 141 ± 14 Ma and 152 ± 15 Ma respectively. Only for one sample from this group, sufficient confined lengths could be measured for subsequent thermal history modelling. Sample BN-016 has a MTL of $12.80\mu\text{m}$ (Figure 5). All samples fail the χ^2 test and yield single grain dispersion of $>30\%$, suggesting a complex thermal history record. Therefore, two statistical age populations were derived in the data (with peak ages P1 and P2). BN-016 has a P1 of 112 ± 8.1 Ma and a P2 of 183 ± 10 Ma, BN-119 has a P1 of 96 ± 25 Ma and a P2 of 206 ± 35 Ma, BN-270 has a P1 of 122 ± 14 Ma and a P2 of 270 ± 55 Ma and BN-085B has a P1 of 108.7 ± 8.9 Ma and a P2 of 217 ± 11 Ma (Figure 5). The Group 2 pooled radial has a central AFT age of 153.7 ± 5.4 Ma and yields two statistically probable age peaks with a P1 of 117.4 ± 6 Ma and a P2 of 203 ± 11 Ma (Figure 5e).

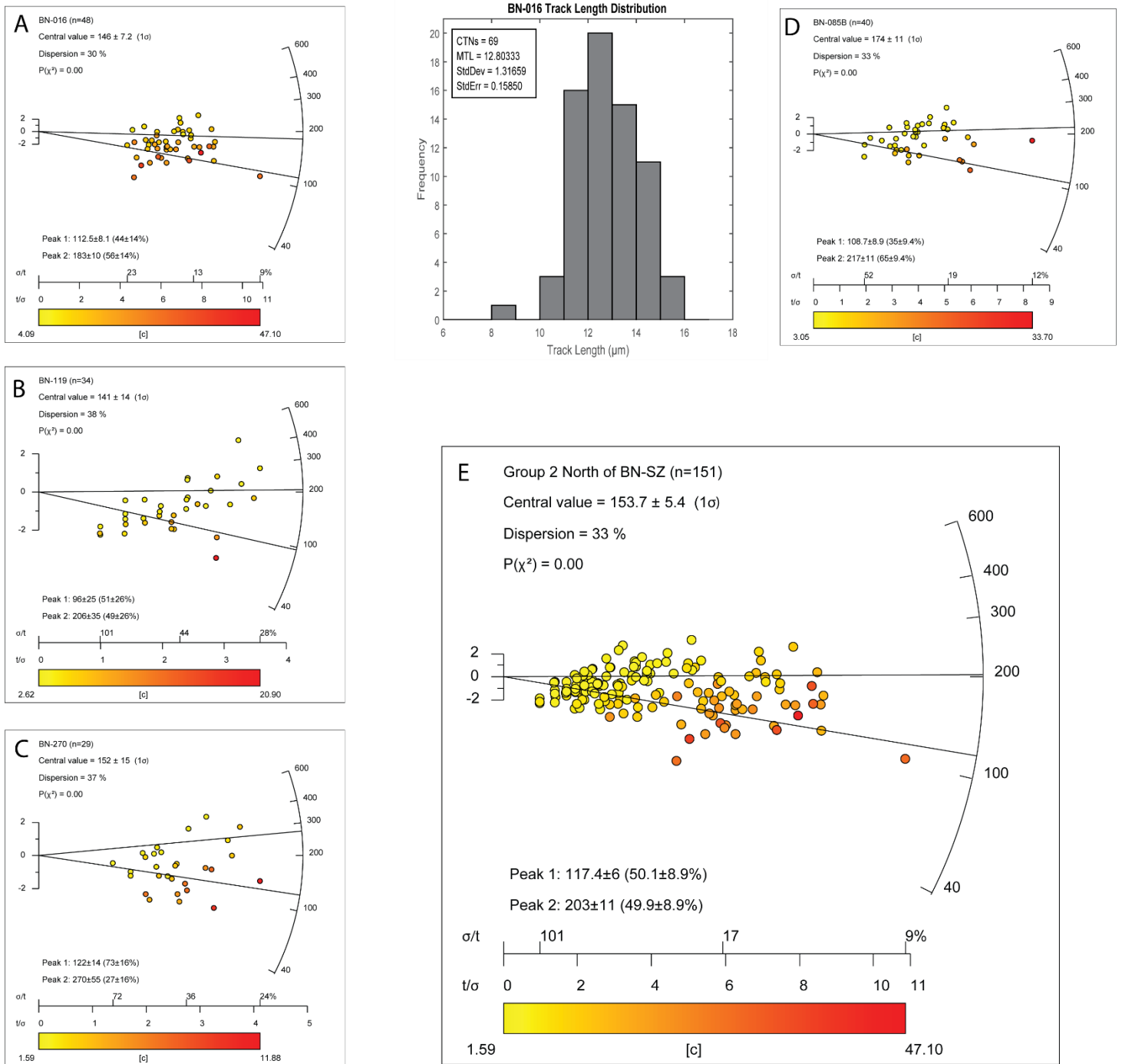


Figure 5 - Radial plots of calculated AFT cooling ages for each sample location associated with sample Group 2 (A-D). E: Represents a pooled radial plot of Group 2 samples. Central age values were calculated using RadialPlotter and for dispersions >25% and $P(\chi^2)$ less than 0.05 age peak discrimination was performed using the RadialPlotter software (Vermeesch 2009). Percentage of data associated with each peak is bracketed adjacent to the age of each peak. [C] on the X-axis represents the amount of ^{238}U in ppm. The left Y-axis represents 2 standard deviations from the central age. Right 'curved' Y-axis shows increasing age in Ma. The values along the X-axis show single-grain age uncertainties. Frequency plots depict track length distributions and are annotated with the number of measured confined track lengths (CTNs), Mean track length (MTL), Standard Deviation (StdDev) and Standard Error (StdErr).

4.2.3 Group 3

Group 3 is defined by most samples for this study, taken to the northwest and southwest of the BN shear zone. The central AFT ages for Group 3 range between 116.7 ± 22 Ma and 132 ± 6.7 Ma (Figure 6). Samples BN-198, BN-278, BN-241, BN-223, BN-598, BN172, BN-043 and BN-396 have central ages of 116 ± 22 Ma, 121.7 ± 6.8 Ma, 123 ± 7.1 Ma, 126.8 ± 8.7 Ma, 127.9 ± 9.6 Ma, 128.6 ± 7.8 Ma, 132.1 ± 6.7 Ma and 138.1 ± 3.9 Ma. Individual AFT age and MTL data can be found in Table 2. RadialPlotter defines two statistically probable peaks for samples BN-043, BN-172, BN-598, BN-241, BN-223 and BN-198 with P1 ages of 114.8 ± 4.4 Ma, 105.7 ± 6.3 Ma, 101.1 ± 6.1 Ma, 88.5 ± 8.4 Ma, 81.1 ± 3.3 Ma and 75.2 ± 9.6 Ma. P2 ages are 198 ± 13 Ma, 197 ± 19 Ma, 190 ± 14 Ma, 148.8 ± 9.6 Ma, 170.7 ± 5.9 Ma, and 196 ± 30 Ma respectively (Figure 6; Table 3). The Group 3 radial plot yields a central AFT age of 129.7 ± 2.7 Ma and two statistically derived age populations, a P1 age of 101.9 ± 3.8 Ma and P2 age of 164.6 ± 5.5 Ma.

Apatite Thermochronology of the Bole-Nangodi Shear Zone

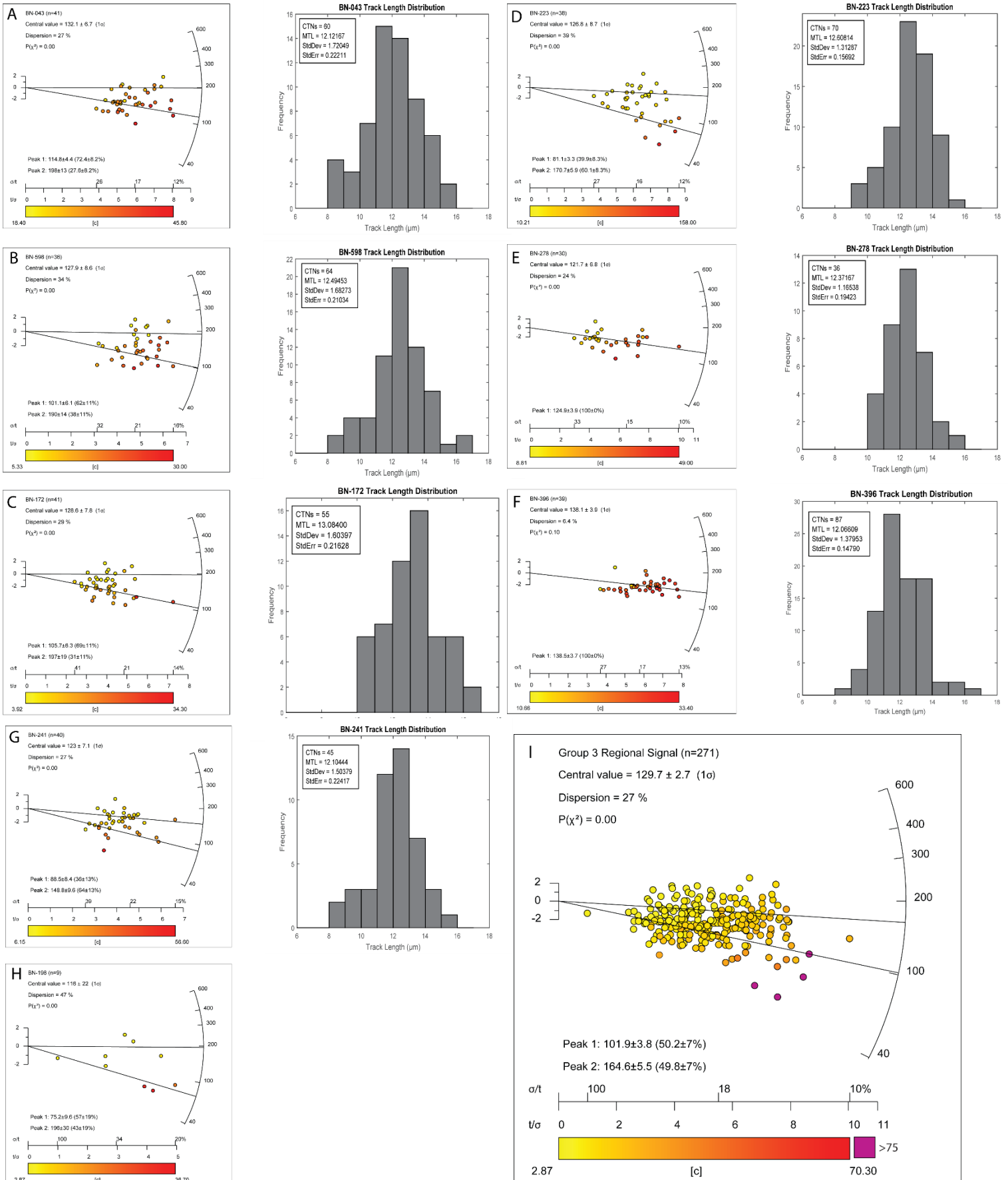


Figure 6 - Radial plots of calculated AFT cooling ages for each sample location associated with sample Group 3 (A-H). I: Represents a pooled radial plot of Group 3 samples. Central age values were calculated using RadialPlotter and for dispersions >25% and $P(\chi^2)$ less than 0.05 age peak discrimination was performed using the RadialPlotter software (Vermeesch 2009). Percentage of data associated with each peak is bracketed adjacent to the age of each peak. [C] on the X- Axis represents the amount of ^{238}U in ppm. The left Y-Axis represents 2 standard deviations from the central age. Right ‘curved’ Y-Axis shows increasing age in Ma. The values along the X-axis show single-grain age uncertainties. Frequency plots depict track length distributions and are annotated with the number of measured confined track lengths (CTNs), Mean track length (MTL), Standard Deviation (StdDev) and Standard Error (StdErr).

4.2.4 Group 4

Group 4 is the youngest group with central AFT ages ranging between 65 ± 11 Ma and $101.7.9\pm 8.1$ Ma (Figure 7). Sample BN-132 represents the youngest sample in the study area and has a central age of 65 ± 11 Ma (Figure 7). Samples BN-127 and BN-155 have central ages of 101.7 ± 8.1 Ma and 96 ± 4.1 Ma and MTL's of and $12.18\mu\text{m}$ and $12.25\mu\text{m}$ respectively (Figure 7; Table 3). RadialPlotter discriminates two statistically probable age peaks for samples BN-132 and BN-127. BN-132 yields a P1 age of 39 ± 15 Ma and a P2 age of 95 ± 21 Ma. BN-127 yields a P1 age of 56.1 ± 9.8 Ma and a P2 age of 117.6 ± 7.3 Ma. The Group 4 pooled radial plot has a central AFT age of 96.6 ± 3.6 Ma and yields two statistically probable age peaks with a P1 age of 67.3 ± 9.1 Ma and a P2 age of 109.9 ± 4.8 Ma.

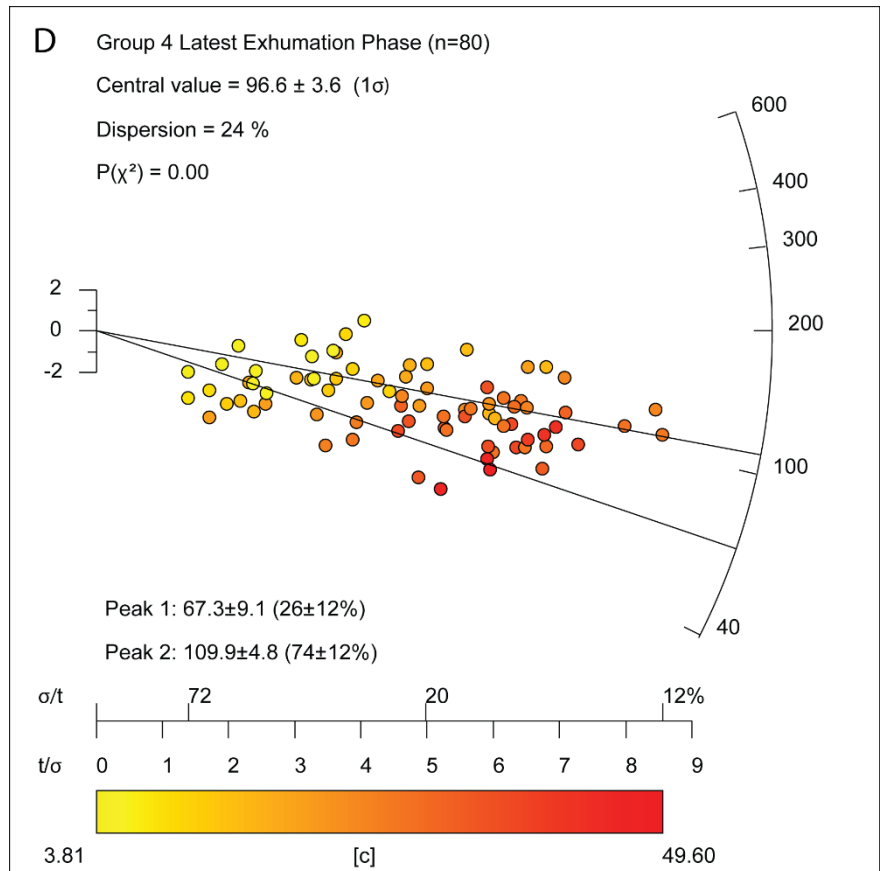
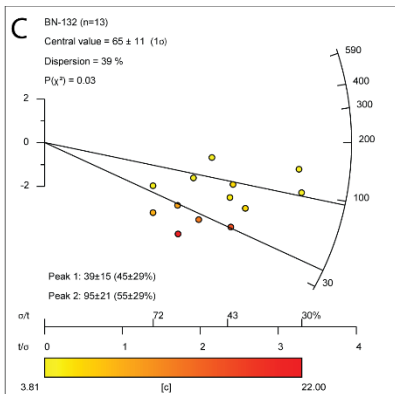
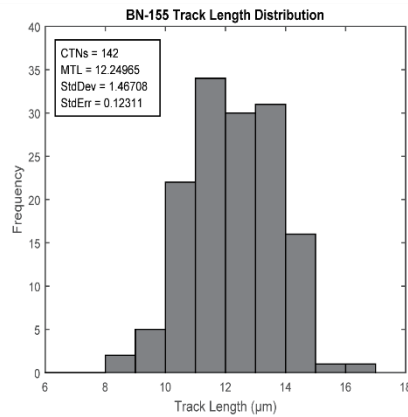
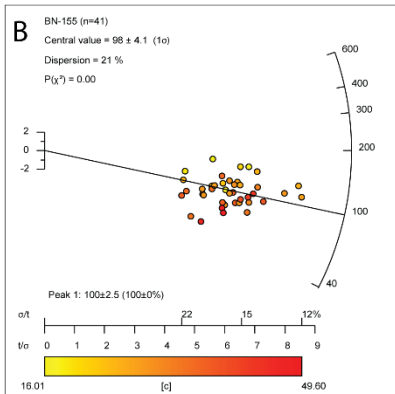
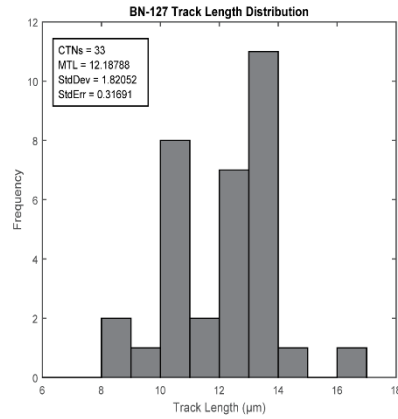
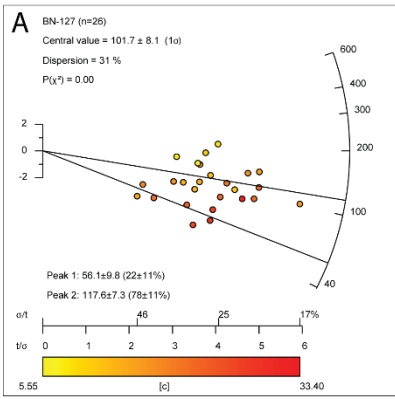


Figure 7 - Radial plots of calculated AFT cooling ages for each sample location associated with sample Group 3 (A-H). I: Represents a pooled radial plot of Group 3 samples. Central age values were calculated using RadialPlotter and for dispersions >25% and $P(\chi^2)$ less than 0.05 age peak discrimination was performed using the RadialPlotter software (Vermeesch 2009). Percentage of data associated with each peak is bracketed adjacent to the age of each peak. [C] on the X- Axis represents the amount of ^{238}U in ppm. The left Y-Axis represents 2 standard deviations from the central age. Right 'curved' Y-Axis shows increasing age in Ma. The values along the X-axis show single-grain age uncertainties. Frequency plots depict track length distributions and are annotated with the number of measured confined track lengths (CTNs), Mean track length (MTL), Standard Deviation (StdDev) and Standard Error (StdErr).

4.2.5 Pooled Study Area

When all data are pooled, the regional thermal history of the entire study area can be derived. The pooled radial plot yields a central AFT age of 139.6 ± 2.6 Ma and high single-grain age dispersion allowing for multiple age peaks. RadialPlotter determines two statistical age peaks with a P1 of 105.4 ± 1.8 Ma and a P2 of 197.8 ± 4 Ma. (Figure 8). Those age peaks are interpreted as two distinct thermal events within the study area during the early Jurassic and late Cretaceous. The pooled radial plots for each defined sample group yield (1) mainly the oldest age-populations; (2) both age populations equally; (3) mainly the younger age-population; and (4) the youngest age population and a significant amount of younger, Cenozoic AFT ages. Each grouping thus preserves different parts of the regional thermal history, discussed below.

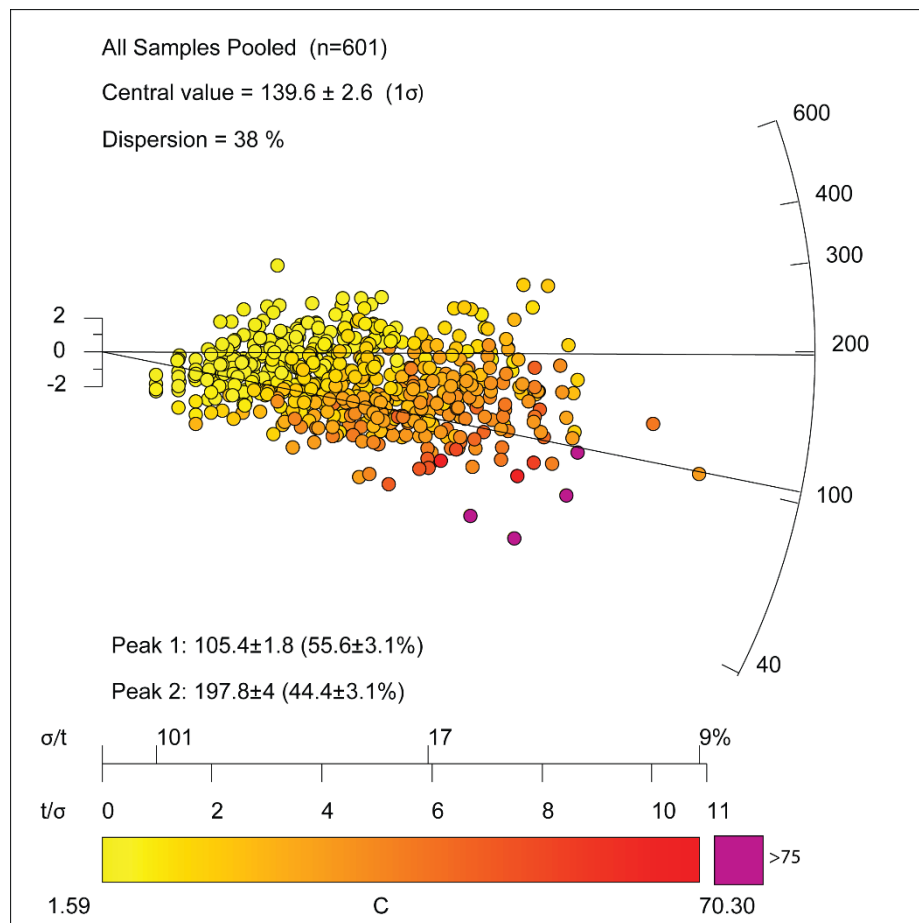


Figure 8 - Radial plots of calculated AFT cooling ages for all samples within the study region. Central age values are by calculated RadialPlotter and for dispersions >25% age peak discrimination was performed using the RadialPlotter software (Vermeesch 2009). Percentage of data associated with each peak is bracketed adjacent to the age of each peak. [C] on the X-Axis represents the amount of ^{238}U in ppm. The left Y-Axis represents 2 standard deviations from central age (Ma). Right 'curved' Y-Axis shows increasing age in Ma. ^{238}U ppm values greater than 75ppm are displayed as purple circles.

4.3 Apatite Fission Track Thermal History Modelling

Thermal history (tT) modelling was conducted on all assigned groups (Figure 9) and on all samples pooled together (Figure 10) to assess the cooling history of the study area.

Given that AFT was the sole low-temperature thermochronometer used in this study and no other published thermochronological data are available for the study area, modelling is limited to a maximum temperature of 120°C without forward modelling constraints.

Interpretations of tT plots are based on the probability output, which acts as a weighted distribution for the most likely or 'expected' tT path with a 90% confidence interval displayed as purple lines.

4.3.1 Group 1 (Oldest AFT ages, southeast of the BN shear zone):

The tT model for the Group 1 samples is well resolved from ~400Ma and exhibits a steady cooling signature through the APAZ and until present day outcrop temperatures (Figure 9a). Given that only old AFT ages were recorded, the model doesn't record <200Ma thermal events that are evident in other parts of the study area.

4.3.2 Group 2 (Two age components, along strike of the BN shear zone):

The Group 2 tT model is poorly resolved prior to the Triassic-Jurassic transition at ca.200Ma. During the period between 200Ma and 160Ma there is a poorly resolved reheating signature evident in both the 'Expected' and the 'Maximum Likelihood' models. Subsequently, the tT model records rapid cooling from ~110°C at the latest Jurassic (ca.160Ma) to above APAZ temperatures of 60°C at 140Ma, where the cooling signature becomes steady until present day outcrop temperatures. Group 2 thus records a poorly resolved thermal event at ~150Ma (Figure 9b).

4.3.3 Group 3 (Young AFT ages, northwest and southwest of the BN shear zone):

The Group 3 thermal history model indicates onset of cooling at ~150Ma, similar to that found for Group 2. The model becomes well resolved between ~130 – 110Ma, indicating cooling from ~90°C until 70°C. Subsequently, cooling stagnates from ~100Ma until ~40Ma, before a well resolved late thermal event cooled the samples to surface temperatures. Group 3 thus records a well-resolved cooling event at ~130-110Ma (Figure 9c).

4.3.4 Group 4 (Youngest AFT ages located in the central BN shear zone):

The tT model for Group 4 is poorly resolved prior to the mid-Cretaceous at ca.120Ma during which a similar fast cooling event was modelled as for Group 3. The model subsequently shows thermal quiescence between ~100Ma and ~30Ma and shows a well-resolved late cooling event from ~30Ma. Group 4 thus records a more recent (Cenozoic) cooling event that is not evident in other parts of the study area (Figure 9d).

Apatite Thermochronology of the Bole-Nangodi Shear Zone
 Group 2 - North of BN-SZ

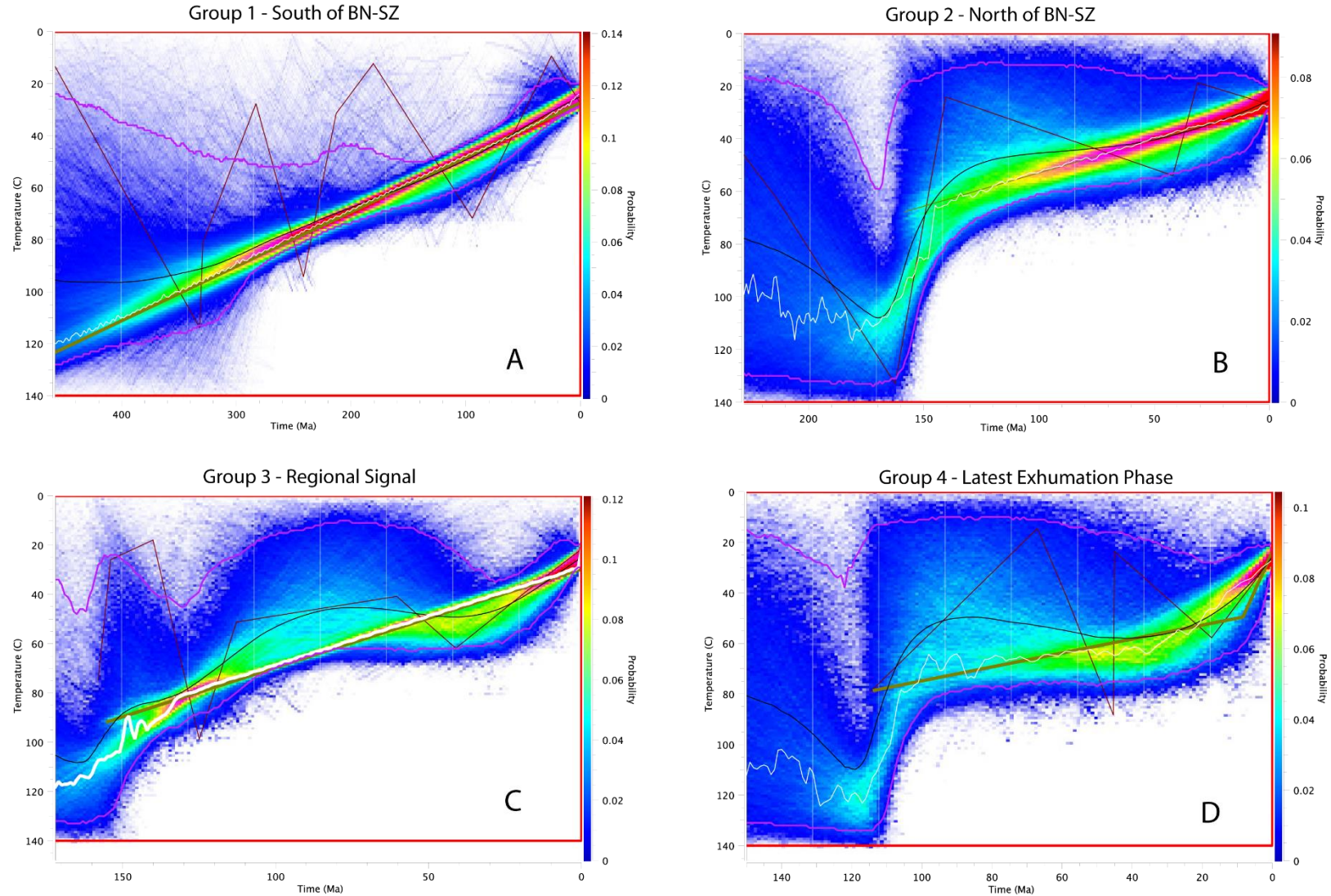


Figure 9 - Thermal History models (tT) for all samples based on AFT and MTL data, developed using QTQt software (Gallagher 2012). Hot to Cold colours represent the probability as displayed on the right Y-Axis. The left Y-Axis represents temperature (°C). The X-Axis represents Time (Ma). Modelling is poorly resolved prior to 200Ma for A, B and C and 140Ma for D as noted by cold colours. A: Model derived from samples, BN-252 and BN-446. B: Model derived from samples BN-016. C: Model derived from samples BN-223, BN-241, BN-043, BN-172, BN-278, BN-396 and BN-598. D: Model derived from samples BN-155, and BN-127. Purple lines represent the 90% confidence interval for the model. The black line represents the average or 'expected' model.

4.3.5 Pooled thermal history model:

Thermal history modelling of pooled sample data from 13 samples was conducted to construct a regional thermal history model for the entire study area (Figure 10). This model was constructed based on 474 single-grain ages and 781 confined fission track lengths. From ~300Ma onwards, the model is poorly constrained and indicates steady cooling and extended residence above the APAZ until an early Jurassic heating event sets in at ca.200Ma. At this point the model becomes better constrained and exhibits maximum heating temperatures of ~110°C at ~140Ma. From the ~130Ma, the model shows fast cooling through the APAZ, reaching temperatures of ~50°C at ~100Ma. From ~100Ma until ~40Ma, the model exhibits thermal quiescence before Cenozoic cooling steadily brings the samples to surface temperatures. The model thus concurs with the pooled radial plot (Figure 8), indicating thermal events at ~200Ma (heating, poorly resolved); at ~130-110Ma (rapid cooling, well resolved); and at ~40Ma (cooling, reasonably well resolved).

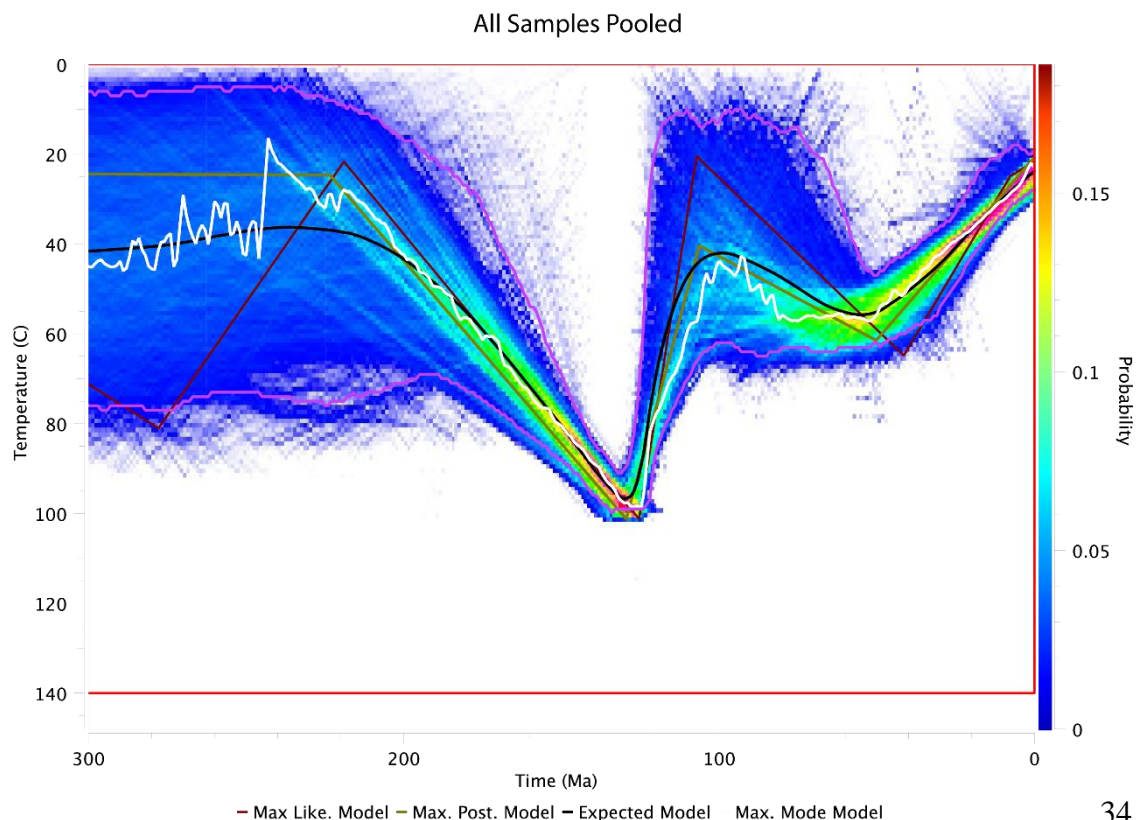


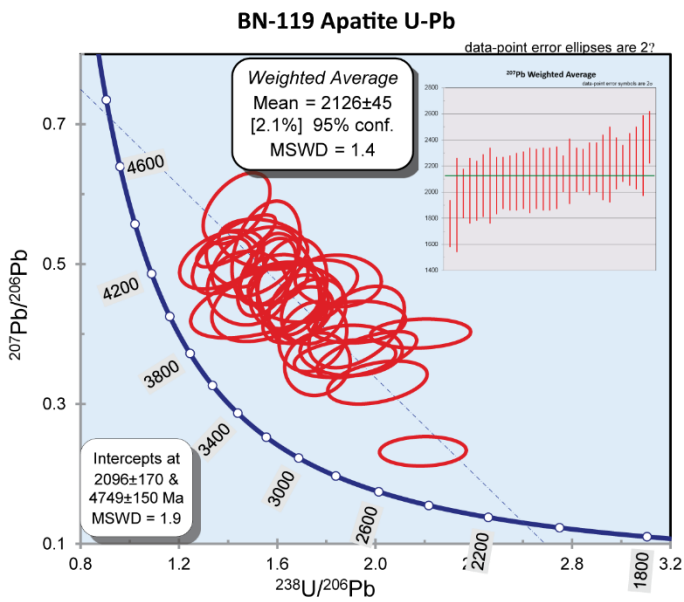
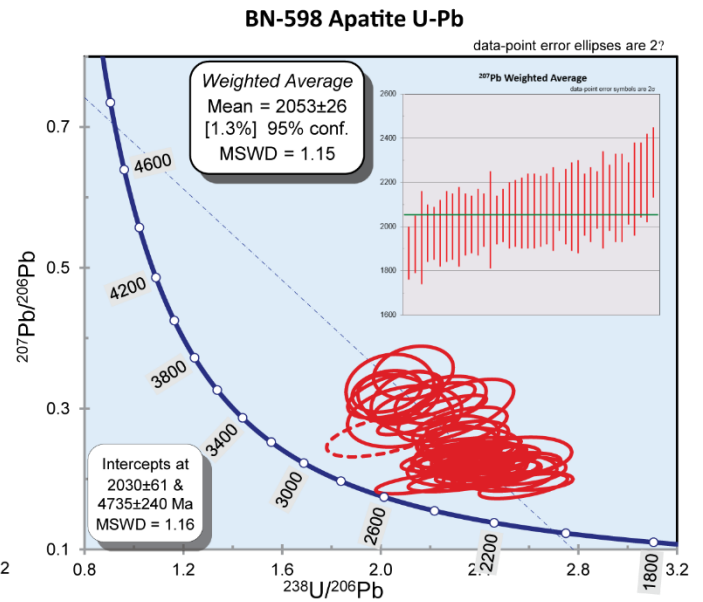
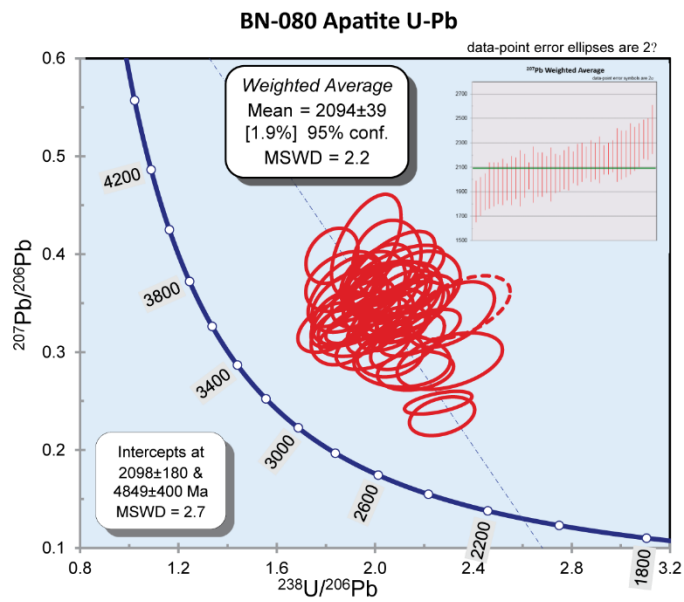
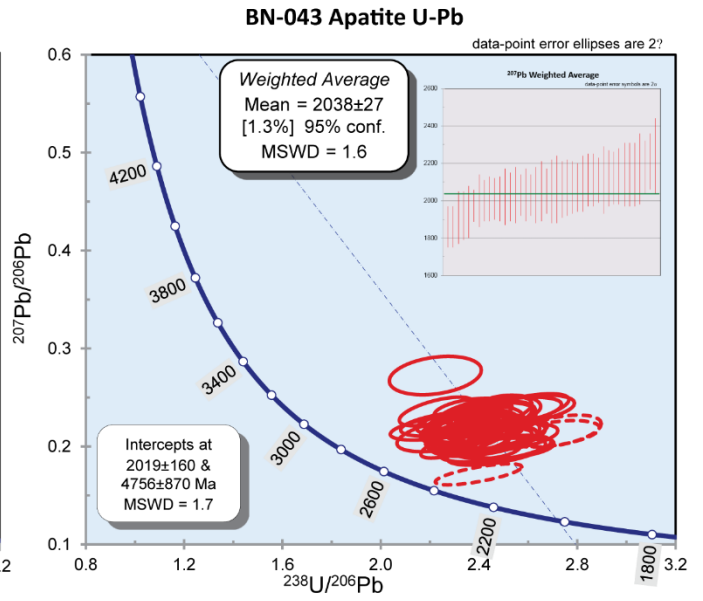
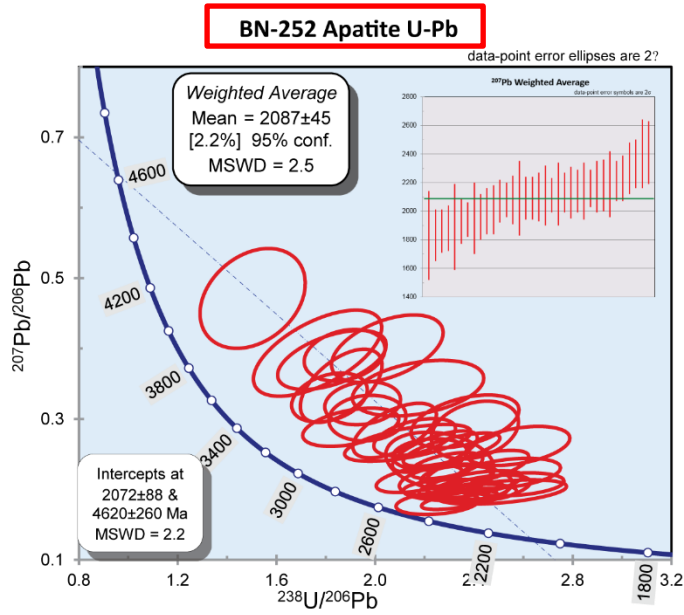
Figure 10 - Thermal History model (tT) of all (13) samples, pooled together. See caption for Figure 9.

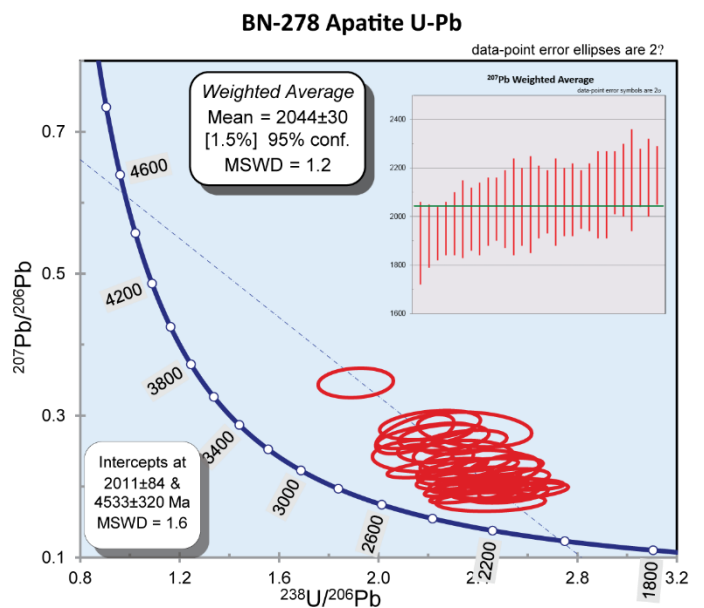
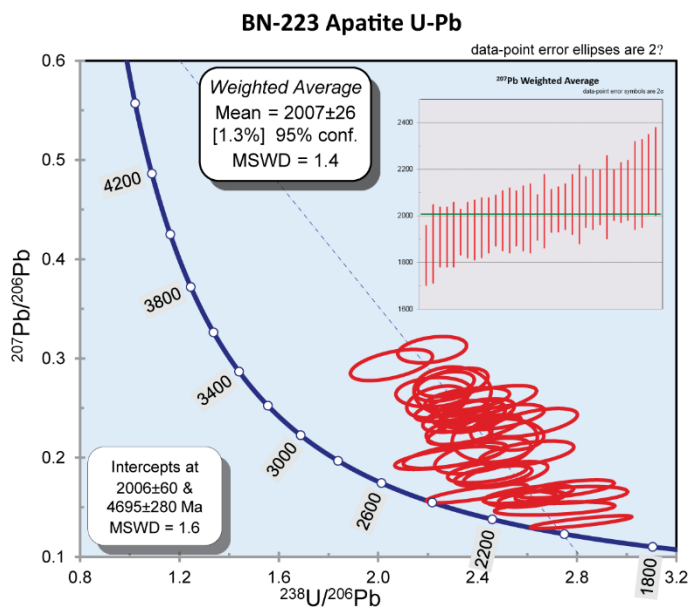
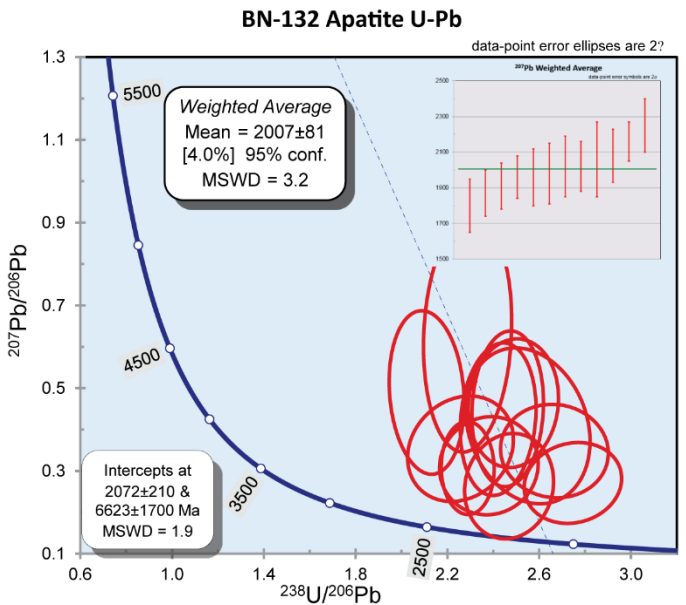
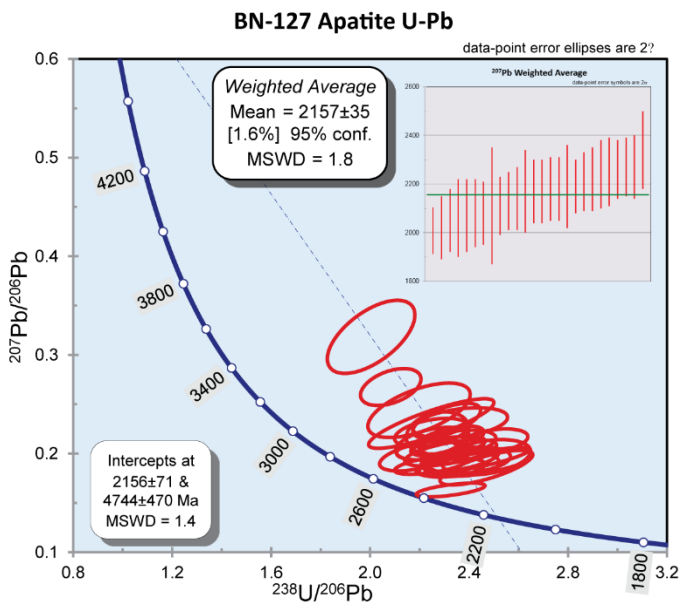
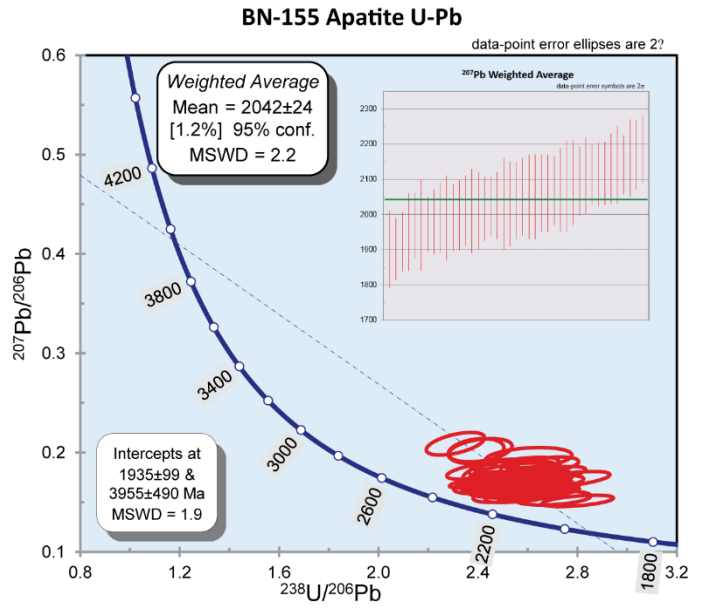
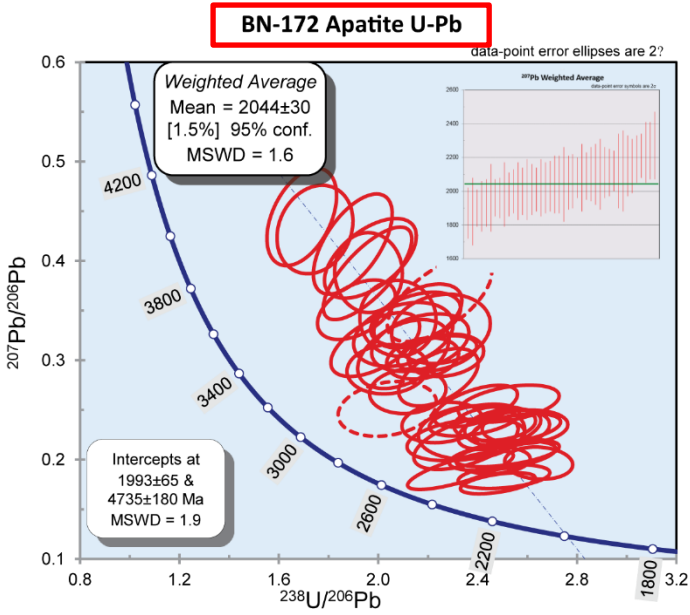
4.4 Apatite U-Pb Results

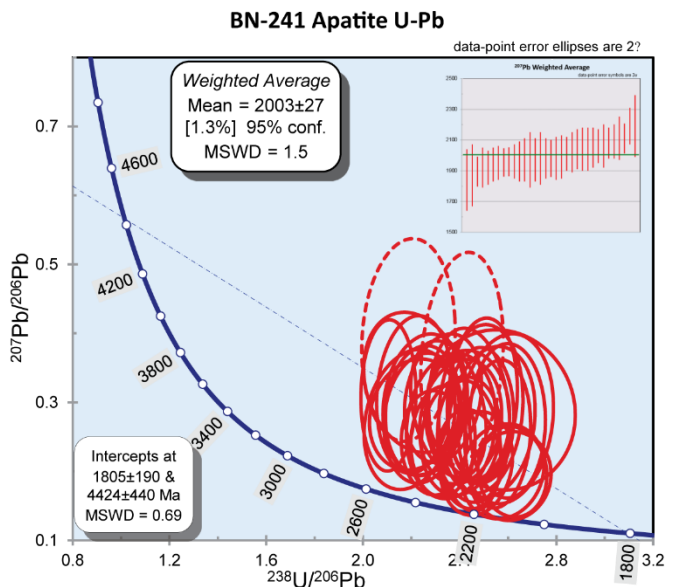
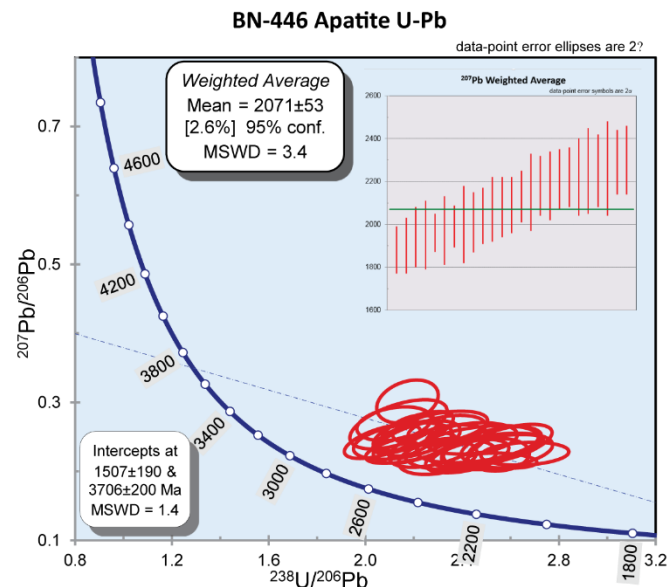
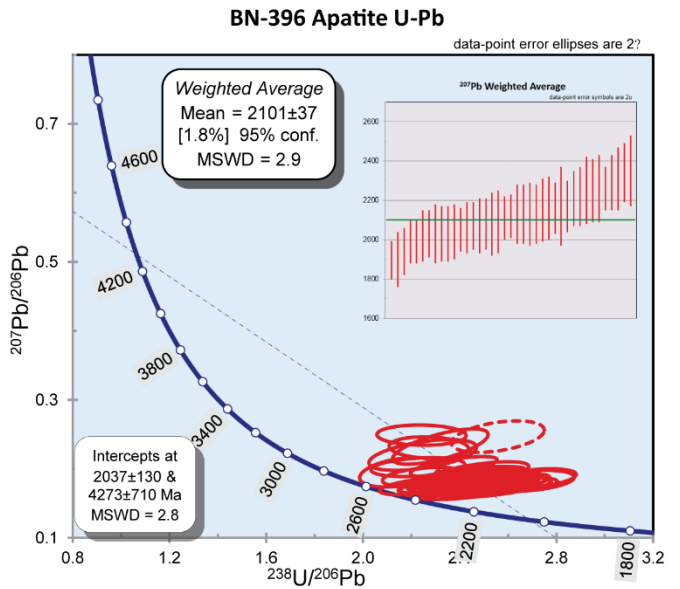
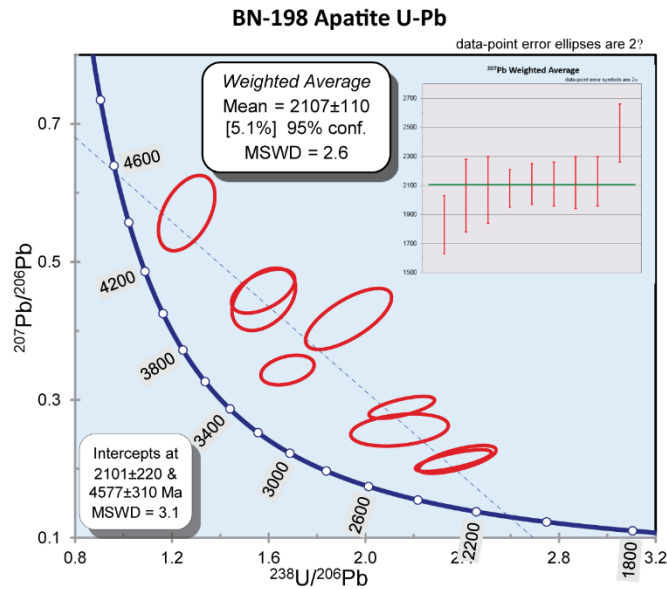
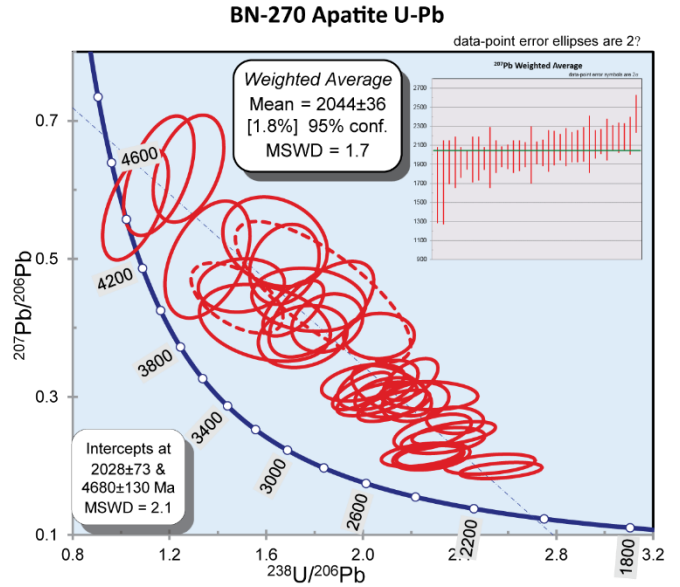
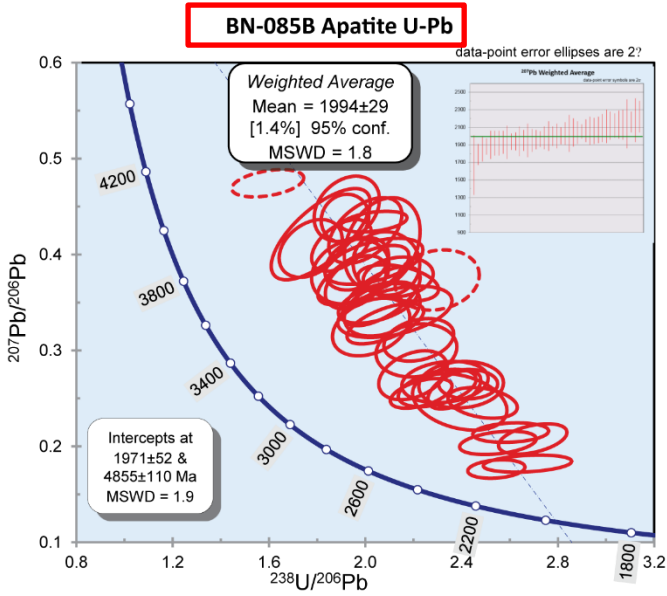
Apatite U-Pb data from 18 samples are presented in Table 4 and exhibit Paleoproterozoic weighted mean ages ranging from 1941±26 Ma to 2157±35 Ma. Samples BN-016, BN-043, BN-080, BN-119, BN-132, BN-155, BN-223, BN-241, BN-278, BN-396, BN-446 and BN-598 display little common Pb variations within individual grains, resulting in poorly constrained intercept ratios with the concordia curve. Therefore, the $^{207}\text{Pb}/^{206}\text{Pb}$ ratio of well constrained samples BN-085B, BN-172 and BN-252 were used to calculate the ^{207}Pb corrections for samples that come from the same rock suite (Figure 11, Table 4). Results are compared to published U-Pb formation and $^{40}\text{Ar}/^{39}\text{Ar}$ ages (Baratoux et al., 2011; Tapsoba et al., 2013; Block et al., 2015; Block et al., 2016).

Table 4 – Apatite U-Pb results for all samples arranged according to Formation/suite. Published U-Pb formation ages, formation/suites and lithologies are from Block *et al.*, (2015) Block *et al.*, (2016) de Kock *et al.*, (2012) & Baratoux *et al.*, (2011). Migm = migmatite. Samples in bold represent the samples which were used to calculate the common Pb contributions for samples from the same rock suite.

Sample ID	Formation/Suite	Lithology	Published U-Pb Formation Age (Ma)	Weighted Mean ^{207}Pb Corrected $^{206}\text{Pb} - ^{238}\text{U}$ age (Ma)	2σ	Apatite Lower Intercept Age (Ma)	2σ
BN-252	Tamnean Plutonic Suite	Granite	2134 - 2118	2087	± 45	2072	± 88
BN-043	Tamnean Plutonic Suite	Granite	2141.2 ± 6.4	2038	± 27	2019	± 160
BN-080	Tamnean Plutonic Suite	Granite	2134 - 2118	2094	± 39	2098	± 180
BN-598	Tamnean Plutonic Suite	Granodiorite	2134 - 2118	2053	± 26	2030	± 61
BN-119	Tamnean Plutonic Suite	Granite	2134 - 2118	2126	± 45	2096	± 170
BN-172	Eburnean Plutonic Suite	Bt-Granite	2150 - 2000	2044	± 30	1993	± 65
BN-155	Eburnean Plutonic Suite	Orthogneiss, Migm	2150 - 2000	2042	± 24	1935	± 99
BN-127	Eburnean Plutonic Suite	Bt-Gneiss, Migm	2150 - 2000	2157	± 35	2157	± 71
BN-132	Eburnean Plutonic Suite	Orthogneiss	2150 - 2000	2007	± 81	2072	± 210
BN-223	Eburnean Plutonic Suite	Bt-Msc-Granite	2150 - 2000	2007	± 26	2006	± 60
BN-278	Eburnean Plutonic Suite	Bt-Msc-Granite	2150 - 2000	2044	± 30	2011	± 84
BN-085B	Birimian Super Group	Granite	2250 - 1980	1994	± 29	1971	± 52
BN-270	Birimian Super Group	Orthogneiss, Migm	2250 - 1980	2044	± 36	2028	± 73
BN-198	Birimian Super Group	Granite	2250 - 1980	2107	± 110	2101	± 220
BN-396	Birimian Super Group	Paragneiss, Migm	2250 - 1980	2101	± 37	2037	± 130
BN-446	Birimian Super Group	Paragneiss	2132 ± 7	2071	± 53	1507	± 190
BN-241	Birimian Super Group	Bt-Granite	2250 - 1980	2003	± 27	1805	± 190
BN-016	Birimian Super Group	Granite	2250 - 1980	1941	± 26	1823	± 71







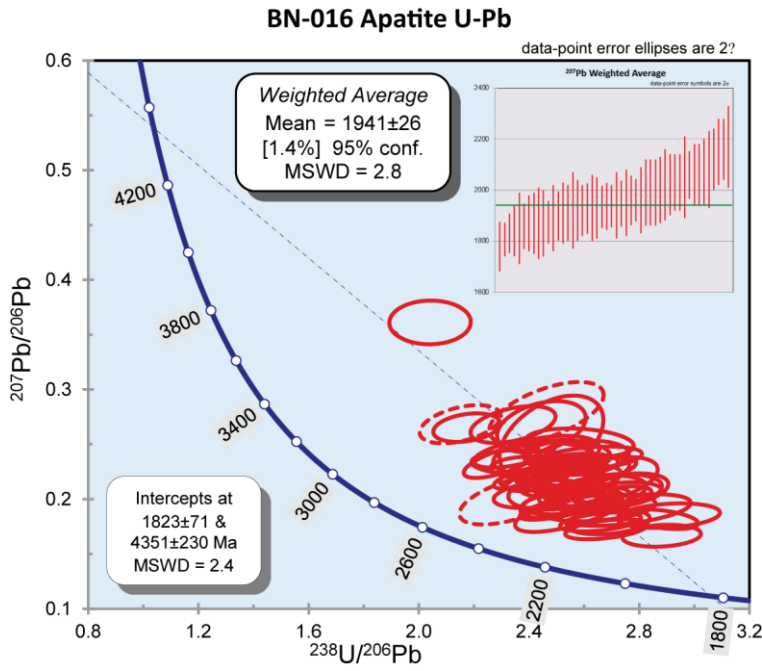


Figure 11 - Results of U-Pb dating of apatite from 18 samples plotted on Tera Wasserburg Concordia diagrams for each sample with ^{207}Pb corrected weighted mean ^{206}Pb - ^{238}U plots as insets. Organised according to Formation/suite as listed in Table 4. Red ellipses represent the uncertainty in isotopic ratios for each single grain spot analysis. Dashed ellipses illustrate apatite grains that had analytical problems and/or obvious discordance and were not utilized in the final calculations. Each plot is annotated with Weighted Average values, Upper and Lower intercept ages and associated MSWDs. Red boxes over sample name represent those samples utilised to calculate the common Pb correction in samples from the same formation/suite.

5. DISCUSSION

5.1 Confined Track Length vs Age comparison

The thermal history models display a rather complex thermal history record (Figure 9, 10) with evidence for multiple thermal events. The identified AFT age-populations (i.e. P1 and P2) preserve different parts of the thermal history record (Figure 5-8), suggesting that apatite grains associated with each population closed at different temperatures (i.e. upper and lower APAZ temperatures). In order to strengthen this observation, fission track length distributions were compared with AFT ages. If the different age-populations indeed preserved different parts of the thermal history, they will likely record different fission track length distributions.

Six samples from Groups 2 and 3 were chosen for this exercise with high single grain dispersions and low $P(\chi^2)$ values that exhibit clear open-jaw signatures in the radial plots (O'Sullivan and Parrish 1995) (samples BN-016, BN-043, BN-172, BN-223, BN-241 and BN-598 (Table 5)). For each of those samples, confined track lengths related to AFT age populations P1 are displayed in blue frequency plots and those related to AFT age populations P2 are displayed in red frequency plots (Figure 12, 13). Figure 12 shows pooled frequency plots. The MTL's for each distribution exhibit a typically lower value for younger P1 lengths ranging between 11.79 μm and 12.62 μm and a higher value for older P2 lengths ranging between 12.81 μm and 13.98 μm (Figure 13; Table 5). The younger P1 age distributions typically exhibit a broad symmetric distribution while the older P2 ages typically exhibit a narrower positively skewed asymmetric distribution.

In addition, the relation between AFT age, confined track length and ^{238}U concentration was evaluated (Figure 12, 13). As shown, there is a positive correlation with older (Peak 2) ages associated with longer confined track lengths (and less dispersion in confined track lengths) and with lower ^{238}U concentrations, while younger (Peak 1) ages correlate with shorter track lengths (and more track length dispersion) and higher ^{238}U concentrations. The fission track length distributions thus support the hypothesis that older (P2) grains preserve a different AFT age record of the thermal history than younger (P1) grains, suggesting different closure temperatures for P1 vs P2 apatites.

Table 5 - Confined track lengths results of six samples and six samples pooled. Central, P1 and P2 ages are given in Ma. Central, P1 and P2 Mean Track Lengths (MTL) are given in μm and 1σ represents one standard deviation from the MTL

<i>Sample ID</i>	<i>Central Age (Ma)</i>	<i>1 σ</i>	<i>Central MTL (μm)</i>	<i>1 σ</i>	<i>P1 Age (Ma)</i>	<i>1 σ</i>	<i>P1 MTL (μm)</i>	<i>1 σ</i>	<i>P2 Age (Ma)</i>	<i>1 σ</i>	<i>P2 MTL (μm)</i>	<i>1 σ</i>
<i>BN-016</i>	146	7.2	12.80	1.31	112	8.1	12.62	1.28	183	10	13.01	1.34
<i>BN-043</i>	132.1	6.7	12.12	1.72	114.8	4.4	11.79	1.78	198	13	12.93	1.24
<i>BN-172</i>	128.6	7.8	13.08	1.60	105.7	6.3	12.71	1.52	197	19	13.98	1.47
<i>BN-223</i>	126.8	8.7	12.61	1.31	81.1	3.3	12.11	1.23	170.7	5.9	12.91	1.27
<i>BN-241</i>	123	7.1	12.1	1.50	88.5	8.4	11.95	1.48	148.8	9.6	12.81	1.49
<i>BN-598</i>	127.9	9.6	12.49	1.68	101.1	6.1	12.08	1.72	190	14	13.17	1.39
<i>Pooled Values</i>	132	3.2	12.55	1.55	98.8	2.8	12.21	1.56	174.4	4.3	13.10	1.36

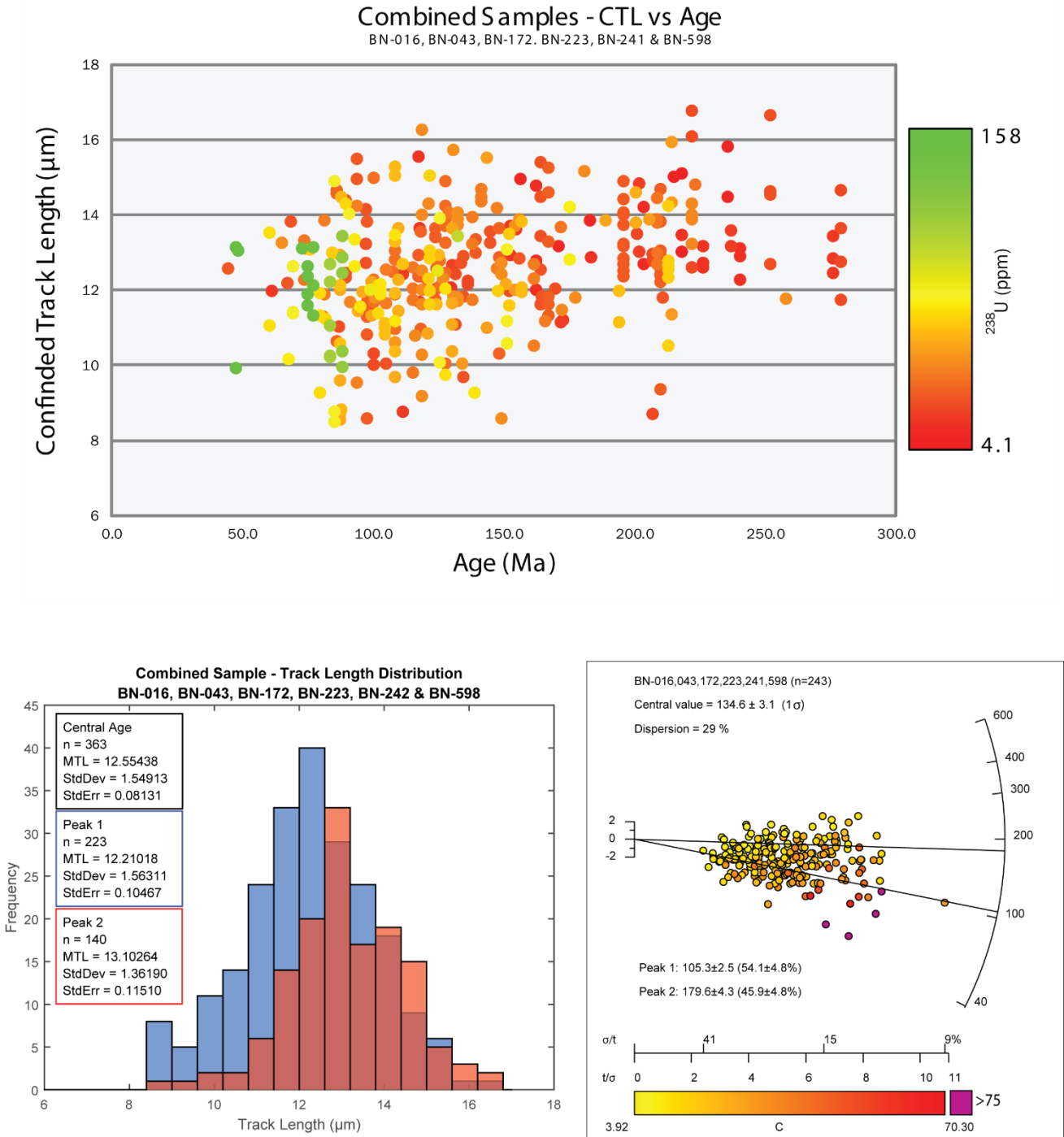


Figure 12 – Above: Pooled Cartesian plot showing the relationship between Age (Ma) on the X-axis, Confined track lengths (μm) on the Y-axis and ^{238}U concentrations displayed as a colour gradient. **Below Left:** Frequency plots showing the Confined track length (μm) relationship between Peak 1 ages and Peak 2 ages (see caption for Figure 11). **Below Right:** - Radial plot of calculated AFT cooling ages for six discriminated samples within the study region. Central age values are by calculated RadialPlotter and for dispersions $>25\%$ age peak discrimination was performed using the RadialPlotter software (Vermeesch 2009). Percentage of data associated with each peak is bracketed adjacent to the age of each peak. [C] on the X- Axis represents the amount of ^{238}U in ppm. The left Y-Axis represents 2 standard deviations from central age (Ma). Right ‘curved’ Y-Axis shows increasing age in Ma. ^{238}U ppm values greater than 75ppm are displayed as purple circles.

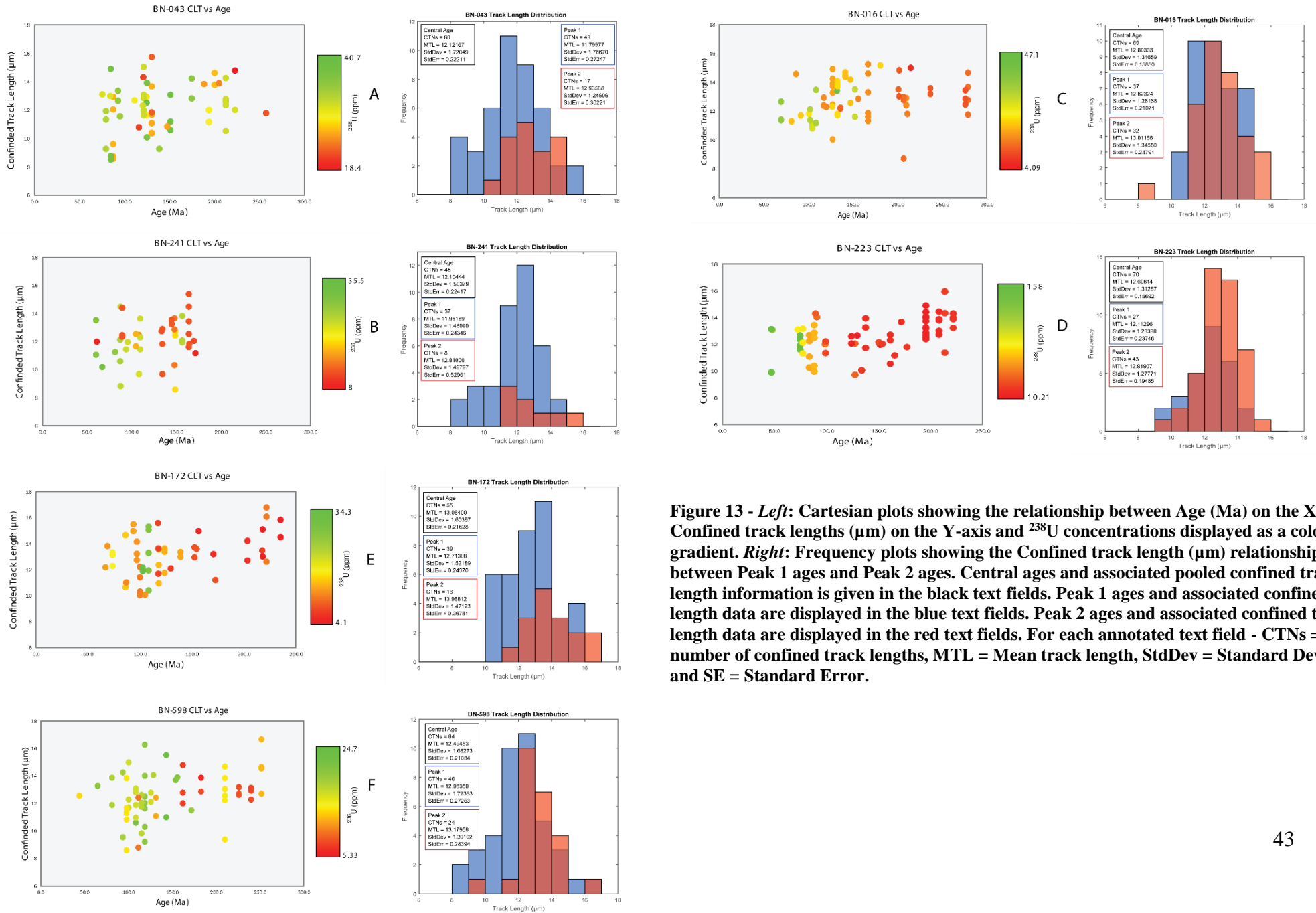


Figure 13 - Left: Cartesian plots showing the relationship between Age (Ma) on the X-axis, Confined track lengths (μm) on the Y-axis and ^{238}U concentrations displayed as a colour gradient. **Right:** Frequency plots showing the Confined track length (μm) relationship between Peak 1 ages and Peak 2 ages. Central ages and associated pooled confined track length information is given in the black text fields. Peak 1 ages and associated confined track length data are displayed in the blue text fields. Peak 2 ages and associated confined track length data are displayed in the red text fields. For each annotated text field - CTNs = number of confined track lengths, MTL = Mean track length, StdDev = Standard Deviation and SE = Standard Error.

5.2 Low-temperature (~120-60°C) thermal events

Thermochronological results for this study reveal two primary age populations (at ~200Ma and 105Ma). Given the significant single-grain age dispersion in most samples, the typical open-jaw displays in radial plots (O'Sullivan and Parrish 1995) (Figure 5-8) and the age-length relationships discussed above (Figure 11, Figure 12) these distinct age-populations are interpreted to preserve a different section of the thermal history record. Subsequent thermal history modelling reveals a two stage thermal history (Figure 9, 10) through APAZ temperatures. A late Triassic-Jurassic heating signal and a mid-Cretaceous cooling signal were modelled, consistent with the two distinct age populations. These thermal events can be interpreted in the context of two major tectono-thermal events that transpired in vicinity of the study area during the Mesozoic that are discussed below.

5.3 Late Triassic to Early Jurassic

Geochronological and $^{40}\text{Ar}/^{39}\text{Ar}$ studies in NE Brazil and the WAC reveal emplacement age of the Central Atlantic Magmatic Province (CAMP) to be consistent with the late Triassic – Jurassic thermal event revealed in this study (Figure 14) (Baksi and Archibald 1997; McHone 2000; Deckart et al., 2005; Verati et al., 2005; Martins et al., 2008; Merle et al., 2011; Buitter and Torsvik 2014; Peyve 2015a). Geochronological and $^{40}\text{Ar}/^{39}\text{Ar}$ studies that measure the emplacement ages for CAMP typically reveal a short duration for the most intense period of magmatism between 202Ma and 189Ma in the central and northern WAC while in western Sierra Leone and towards the east, in Nigeria, manifestations of CAMP related volcanism span between ~234Ma and ~140Ma (Verati et al., 2005; Deckart et al., 2005; Barrie et al., 2010; Merle et al., 2011;

Peyve 2015a). Although outcrop evidence for CAMP related volcanism appears limited within the study area, the massive extent of CAMP emplacement over four continents (Figure 14) including Europe, South America, North America and Africa indicates that CAMP related heatflow likely also affected the study area in Ghana (Baksi and Archibald 1997; Marzoli et al., 1999; Martins et al., 2008; Buitter and Torsvik 2014; Peyve 2015a). This study hence interprets the early Triassic-Jurassic thermal event as being a response to CAMP-related heating of the Ghanese upper crust.

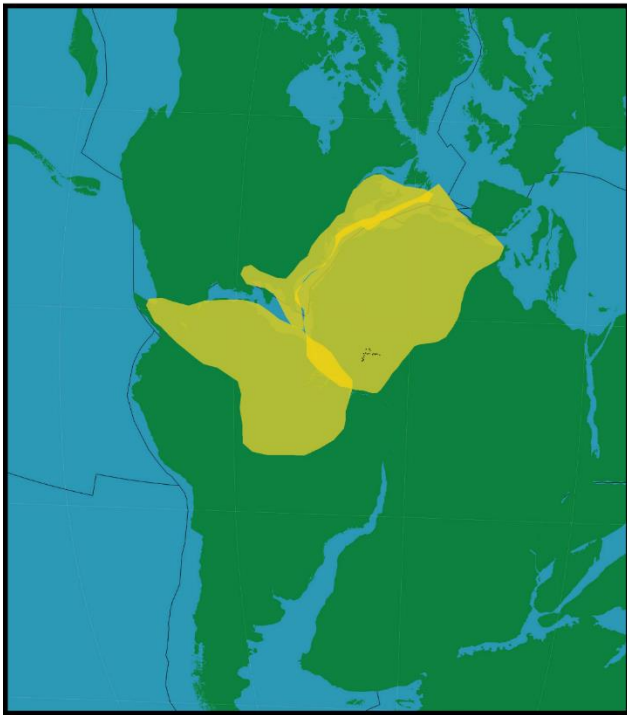
5.4 Early to middle Cretaceous Cooling

Off-shore studies conducted on the exhumed ICG margin indicate the onset of continental rifting and intracontinental deformation between the African and South American continents to be consistent with the younger observed (mid-Cretaceous) thermal event (Guiraud and Maurin 1992; Bouillin et al., 1997; Mascle et al., 1998; Basile et al., 2005; Bigot-cormier et al., 2005; Heine and Brune 2014). Extension in western Africa is generally regarded as occurring since the late Permian and driven by far field tectonics during Pangea break-up with contributions from the emplacement of magmatic provinces through the Jurassic and lower Cretaceous (Figure 14) (Guiraud and Maurin 1992; Martins et al., 2008; Heine and Brune 2014; Buitter and Torsvik 2014; Peyve 2015a). More specifically magmatism in the Benue Trough and break-up in the South Atlantic is considered to be a major pre-cursor which drove the development of the Equatorial transform zone during the latest Jurassic and earliest Cretaceous (Coulon et al., 1996; Peyve 2015a). This event occurred due to a northward propagating rift axis and the emplacement of the St Helena plume head below the Benue Trough creating a triple junction style break-up scenario which induced internal strain on the African plate

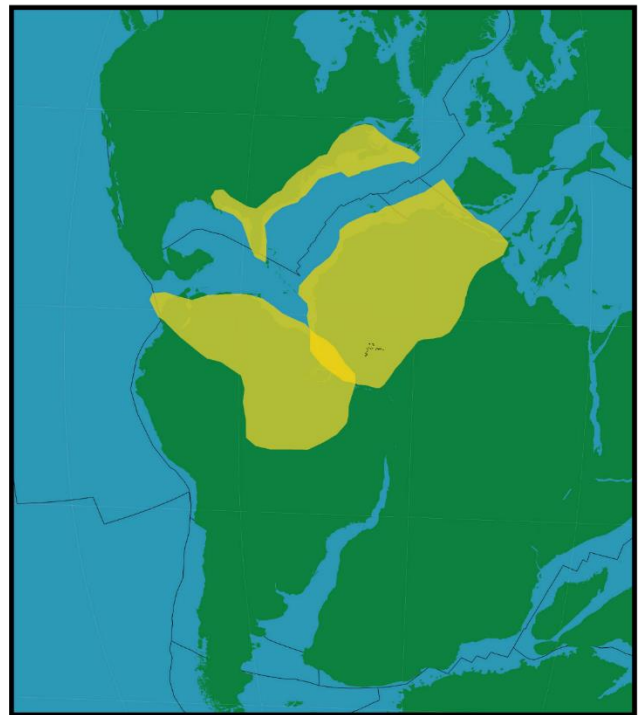
(Figure 14) (Grant 1971; Benkhelil 1989; Guiraud et al., 1992; Coulon et al., 1996; Heine and Brune 2014).

Peak 1 age interpretation on individual samples from sample Groups 2 and 3 reveal ages ranging from 122 ± 14 Ma to 108.7 ± 8.9 Ma (Figure 5) and 75.2 ± 9.6 to 138.5 ± 3.7 (Figure 6) respectively. The associated thermal history models reveal associated fast cooling during the early and middle Cretaceous (Figure 9b,c), coinciding with the earliest stages of Equatorial Atlantic rifting as measured by previous studies (Guiraud et al., 1992; Guiraud and Maurin 1992; Bouillin et al., 1997; Clift et al., 1997; Clift 1999; Bigot-cormier et al., 2005; Heine and Brune 2014; Jessell et al., 2016). The early to middle Cretaceous cooling event is therefore interpreted as a response to the two initial geodynamic stages of break-up. (1) The onset of rifting and the initiation of the DIB during the Aptian and (2) the onset of intracontinental transform faulting between the African and Brazilian margins from the Aptian to the Cenomanian (Figure 14, 15).

200Ma



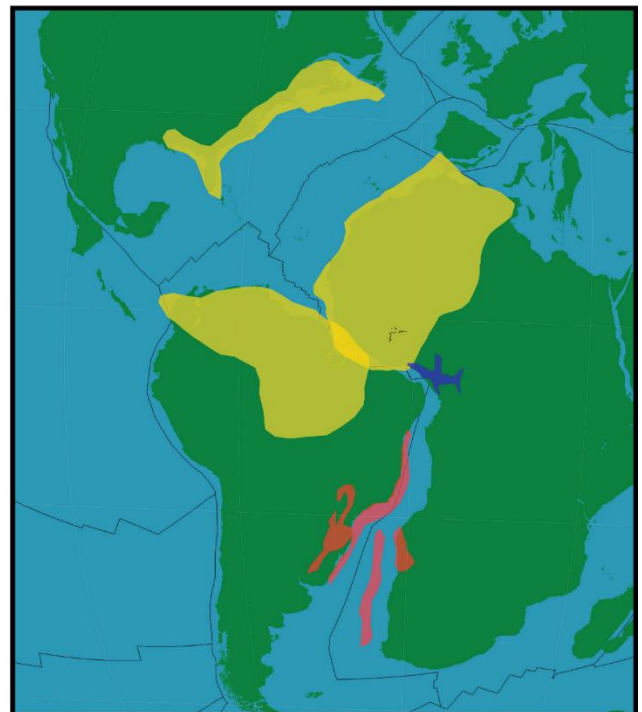
150Ma



130Ma



110Ma






 CAMP  Paran - Etendeka LIP  Benue Trough

Figure 14 – Time sequence showing the evolution of Gondawana break-up between 200Ma and 110Ma in context with late Triassic to mid Cretaceous AFT ages presented in this study. Modified from plate reconstruction models by (Seton et al., 2012).

5.5 Late Cretaceous – Cenozoic Cooling

Peak and central AFT age results for Group 4 are significantly younger (Figure 7).

Central ages for these samples range between 65 ± 11 Ma and 101.7 ± 8.1 Ma. Published off-shore AFT data from Bigot-Cormier et al., (2005) and Bouillin et al., (1997) reveal similar central ages, ranging between 65 Ma and 110 Ma, and are interpreted to constrain the final stages of break-up and uplift of the ICG marginal ridge (Figure 15).

The proximal location of these young ages relative to the BN shear zone which strikes parallel to the NE-SW trending ICG margin supports the interpretation by Jessel et al., (2016) that this structure acted as a major control on the orientation of break-up during the rifting process (Figure 1, 16). The AFT data from this study hence suggests that late Cretaceous reactivation of the BN shear zone induced significant denudation akin to the ICG margin, to (partially) reset the AFT clock. This event is interpreted to be related with the third geodynamic stage of rifting between the Turonian and Santonian which witnessed the introduction of oceanic crust to the continental margin and the transition from an active to a passive margin (Figure 15). Furthermore, the end Cretaceous (~65 Ma) was experiencing NNW-SSE shortening and strike-slip faulting associated with continuing plate movement induced within the African continent. Plate dynamics at this time were recorded in the Benue Trough as an angular unconformity related to strong folding (Benkhelil 1989; Fairhead et al., 2013; Jolly et al., 2015). This could indicate a late Cretaceous – Cenozoic reactivation of the BN shear zone as the compressive stress field was superimposed on western Africa. This interpretation is discussed in more detail below.

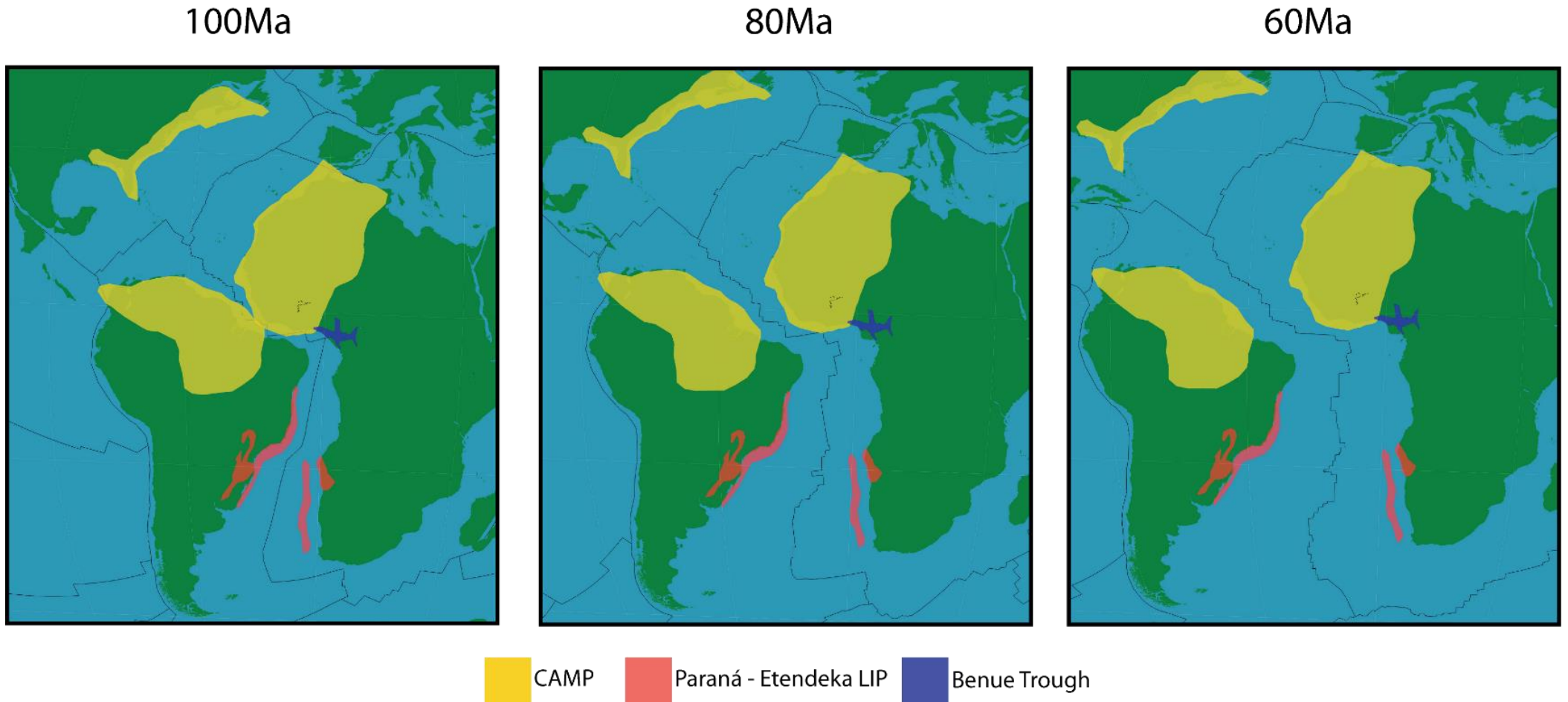


Figure 15 - Time sequence showing the evolution of Gondawana break-up between 100Ma and 60Ma in context with the middle to late Cretaceous AFT ages presented in this study. Modified from plate reconstruction models by (Seton et al., 2012).

5.6 Differential exhumation with respect to the Bole-Nangodi Shear Zone

The BN shear zone acts as the most significant structure within the study area and is oriented parallel to the modern expression of transform zones in the Equatorial Atlantic Ocean (Figure 1). A gridded interpolation map (Figure 16) was constructed to assess the relative differential cooling of samples (according to central AFT age) across the study area. This map reveals a distinct difference between those samples north of the BN shear zone and those samples south of the BN shear zone. This study interprets the clear distinction in cooling ages to display a record of differential exhumation in the north with respect to the south of the BN shear zone. More specifically the BN shear zone is interpreted to be reactivated during the mid-Cretaceous extension which relatively exhumes the northern BN footwall with respect to the subsiding southern hanging wall. In this regard, the north represents an exhumed rift shoulder and exposes a deeper section of the northern Ghanaese thermal history, while the south records the undisturbed pre-rifting section of the thermal history. This study relates exhumation of the Ghanaese continental crust to Cretaceous syn and post rift sediment deposition in coastal basins along the southern Ghanaese margin (Wagner 2002; Yidana et al., 2010; Rüpke et al., 2010; Jianping et al., 2010). This interpretation is supported by a provenance study on Nd isotopes and trace elements of the Sekondian Group which interprets Cretaceous sediments of the Essikado Sandstone to be predominantly sourced from both Birimian and Eburnean plutonic suites. Furthermore, deposition of the Essikado Sandstone is interpreted as occurring as a result of tectonic uplift related to the onset of rifting during the Aptian (Asiedu et al., 2005).

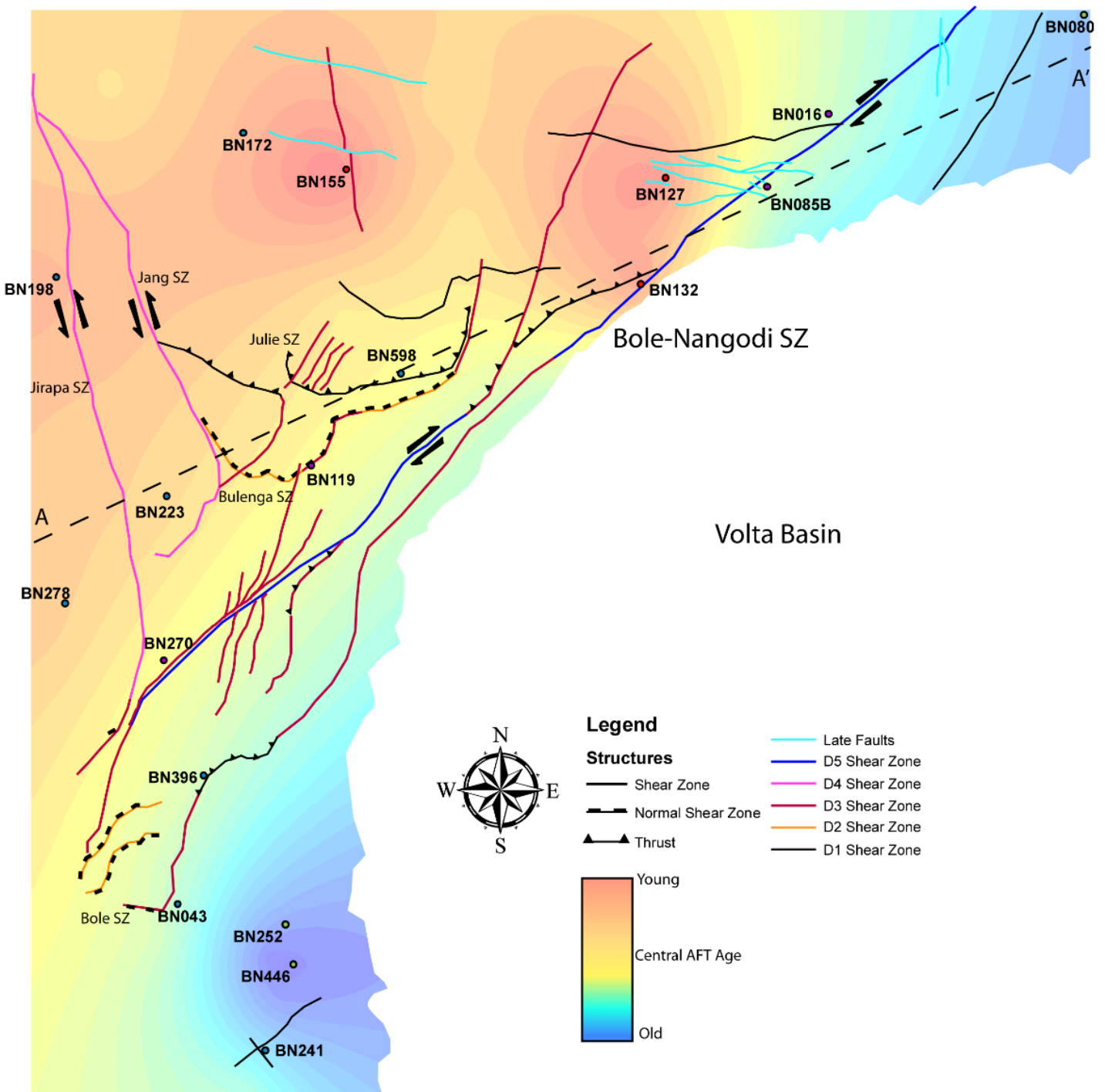


Figure 16 – Gridded ‘heat map’ for the study area defined by AFT central ages. Hot and Cold colours represent young and old AFT ages respectively. Faults are indicated and coloured according to relative deformation events (absolute timings of D4, D5 and ‘Late Fault’ activity are not known). Modified from Block *et al.*, (2016). A to A’ Cross section is visualised in Figure 15.

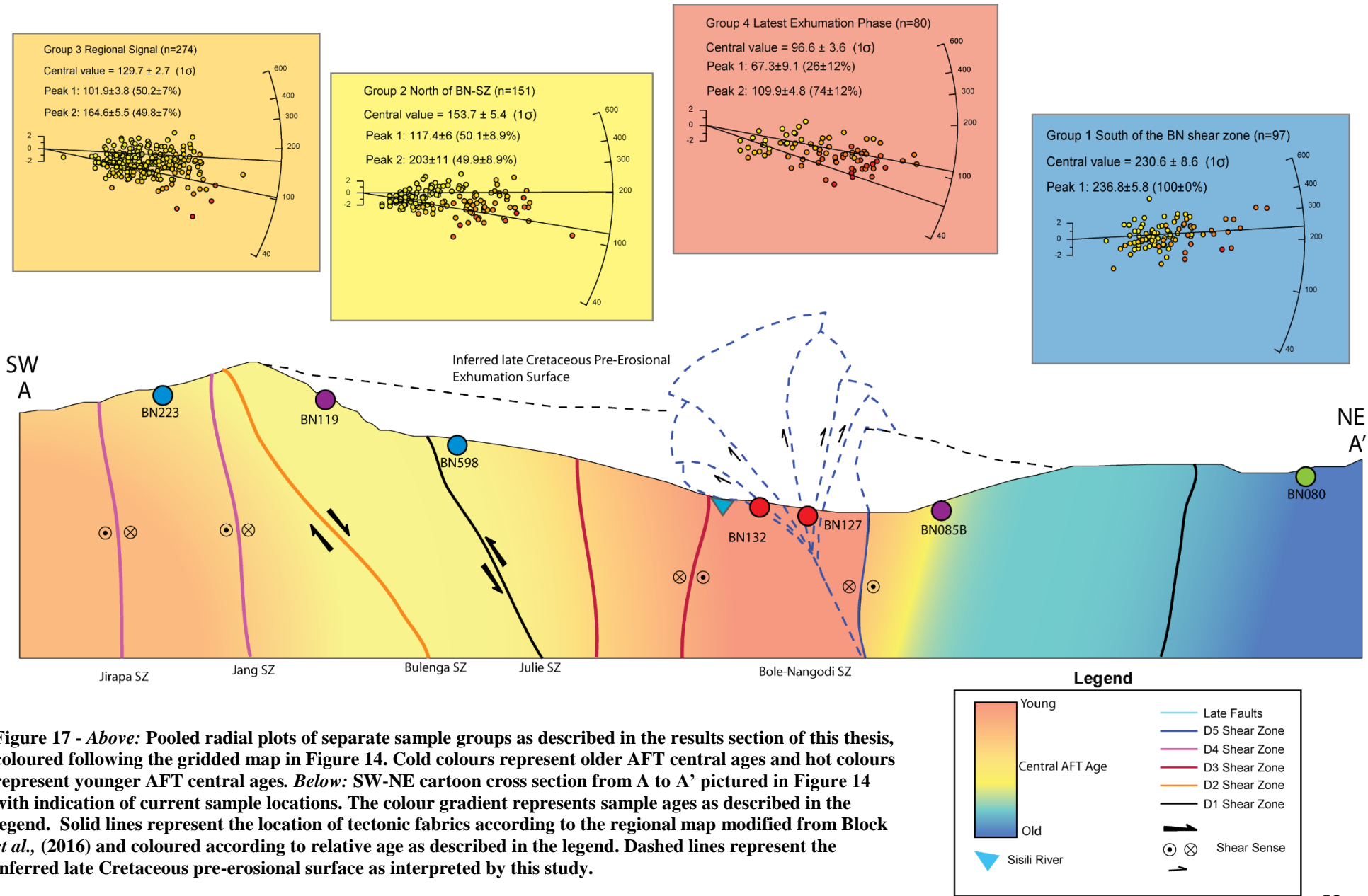


Figure 17 - Above: Pooled radial plots of separate sample groups as described in the results section of this thesis, coloured following the gridded map in Figure 14. Cold colours represent older AFT central ages and hot colours represent younger AFT central ages. **Below:** SW-NE cartoon cross section from A to A' pictured in Figure 14 with indication of current sample locations. The colour gradient represents sample ages as described in the legend. Solid lines represent the location of tectonic fabrics according to the regional map modified from Block *et al.*, (2016) and coloured according to relative age as described in the legend. Dashed lines represent the inferred late Cretaceous pre-erosional surface as interpreted by this study.

Within the study area, seven relative deformation events are described, for which absolute ages are only recorded related with D1 through D3. These early deformation events are interpreted to be associated with the Paleo-proterozoic Eburnean Orogeny (Tapsoba et al., 2013; Block et al., 2015; Block et al., 2016). The latest deformation events in the area, D5 and 'Late Fault' (Figure 16) are described as localised E-W to NE-SW striking brittle deformation associated with shortening and dextral strike-slip shearing under a transcurrent regime (Block et al., 2016). Given the excellent correlation of the D5 fault trend with the significant step in AFT central ages on the gridded AFT heat map (Figure 16), this work interprets the rifting related exhumation event to be related with the D5 deformation and thus constrains brittle stage D5 to the mid-Cretaceous.

The youngest AFT central ages measured in this study are located in the central section of the BN shear zone (Figure 16, 17) where there is a significant wedge shaped geometry. This region is bound by faults of either D5 or 'Late Fault' relative ages. Therefore, in a similar way, the 'Late Faults' are interpreted to be related with the youngest AFT ages for this study (late Cretaceous – Cenozoic). Given the similarities in AFT age data and structural setting, this work further relates the tectonic interpretation for the study area with those obtained for the ICG margin and the Gombe Fault in the Upper Benue Trough (Basile et al., 1993; Clift et al., 1997; Mascle et al., 1998; Jolly et al., 2015).

The Gombe Fault (GF) and the ICG margin are well characterised through field studies as containing positive transpressional flower structures related to strike-slip faults with an element of vertical (either extensional or compressional) deformation (Moody and Hill 1956; Basile et al., 1993; Clift et al., 1997; Mascle et al., 1998; Jolly et al., 2015).

According to field studies, stratigraphic correlations and (for the case of the ICG margin) low temperature thermochronology, both the GF and ICG margin were active and exhumed during the late Cretaceous (towards the end of the Equatorial rifting period) as the Equatorial margin became passive (Bouillin et al., 1997; Bigot-cormier et al., 2005; Fairhead et al., 2013; Jolly et al., 2015).

In light of these relationships, the youngest region of the study area (Figure 16), located in the central BN shear zone, is interpreted as having undergone minor late Cretaceous to early Cenozoic denudation in response to the exhumation of a positive flower structure (Figure 17) which occurred as a result of a continuing compressional stress regime as discussed above (Fairhead et al., 2013). The 'Late Fault' stage brittle faults located at the central BN shear zone between samples BN-127 and BN-016 are interpreted to be stepover faults or restraining bends that developed into contractional duplexes. These structures are typically associated with strike-slip faults of this nature (Woodcock and Fischer 1986). As a result of exhumation in the central BN shear zone, the NE and SE fringes of the fault structure were likely marginally subsided as a flexural response to uplift. In summary, this study interprets the young AFT ages in the central BN shear zone to be related with a restraining bend while the old AFT ages in the SW fringe are interpreted as being associated with a releasing bend (Woodcock and Fischer 1986; Woodcock and Rickards 2003). Further work would be required to confirm this interpretation as structural field observations around brittle deformation zones within the study area are limited.

Current exposure of the interpreted positive flower structure along the centre of the BN shear zone reveals a topographic low relative to other areas in the study area (Figure 17). This study interprets the low topography to be related to an erosional surface and

migration path of the Sisili River. Rivers are known to follow paths of low resistance such as fault zones and therefore it's likely that the river further aided in revealing deeper crustal exposure and associated younger AFT ages at the centre of the BN shear zone (Holbrook and Schumm 1999; Tooth et al., 2002). Although the river erosion could have played a role in the differential cooling pattern observed for the study area, structurally induced exhumation and denudation are interpreted as more major controls on the observed trends in the data.

5.7 U-Pb Data

Apatite U-Pb results from in this study are closely related to published zircon U-Pb ages (Baratoux et al., 2011; de Kock et al., 2012; Block et al., 2015; Block et al., 2016), indicating that the samples have not been at temperatures >450 °C since the Paleoproterozoic. The obtained results (Figure 11) are only used as high-temperature constraints in the thermal history models and, since they don't relate to the Mesozoic tectono-thermal evolution of the study area, a more in-depth interpretation of the U-Pb ages in terms of the Precambrian tectonic history is beyond the scope of this thesis.

6. Conclusions

Low temperature thermochronological results from northern Ghana characterise the thermal and deformation history of the NE-SW striking Bole-Nangodi shear zone and the surrounding area in context with continental rifting between West Africa and Brazil.

- During the late Triassic and early Jurassic heating of the upper crust is preserved in AFT age data and thus provides a spatial constraint on the southern extent of CAMP related heat flow.

- Early to middle Cretaceous exhumation is marked by differential AFT age preservation in the north with respect to the south of the BN shear zone and is contemporaneous with the initiation of rifting in the Equatorial Atlantic.
- A late Cretaceous to Cenozoic thermal event in the central BN shear zone is evident and is likely a product of a compressional stress regime transposed by plate motions within the African continent.
- Structurally, the central BN shear zone has been exhumed as a positive flower structure along a reactivated strike-slip fault and is marked by restraining bends that developed into contractional duplexes.

7. ACKNOWLEDGMENTS

Thanks to my supervisor Stijn Glorie and co-supervisor Alan Collins and their PhD team Jack Gillespie, Gilby Jepson and James Hall for their tireless assistance. Katie Howard and Juraj Farkas for their support to myself and the entire honours cohort, providing information and advice throughout the year. Thanks to Aoife McFadden, Benjamin Wade and Tony Hall for laboratory training. Finally thank you to Mark Jessel and Sylvian Block for gathering and providing the sample materials utilized in this study.

8. REFERENCES

- Anani, Chris. 1999. 'Sandstone petrology and provenance of the Neoproterozoic Voltaian Group in the southeastern Voltaian Basin, Ghana', *Sedimentary Geology*, 128: 83-98.
- Antobreh, A. A., J. I. Faleide, F. Tsikalas, and S. Planke. 2009. 'Rift–shear architecture and tectonic development of the Ghana margin deduced from multichannel seismic reflection and potential field data', *Marine and Petroleum Geology*, 26: 345-68.
- Asiedu, D. K., E. Hegner, A. Rocholl, and D. Atta-Peters. 2005. 'Provenance of late Ordovician to early Cretaceous sedimentary rocks from southern Ghana, as inferred from Nd isotopes and trace elements', *Journal of African Earth Sciences*, 41: 316-28.
- Attoh, Kodjopa, Scott Samson, Yao Agbossoumondé, Prosper M. Nudé, and Jennifer Morgan. 2013. 'Geochemical characteristics and U–Pb zircon LA-ICPMS ages

- of granitoids from the Pan-African Dahomeyide orogen, West Africa', *Journal of African Earth Sciences*, 79: 1-9.
- Baksi, Ajoy K., and D. A. Archibald. 1997. 'Mesozoic igneous activity in the Maranhão province, northern Brazil: $^{40}\text{Ar}/^{39}\text{Ar}$ evidence for separate episodes of basaltic magmatism', *Earth and Planetary Science Letters*, 151: 139-53.
- Baratoux, Lenka, Václav Metelka, Séta Naba, Mark W. Jessell, Michel Grégoire, and Jérôme Ganne. 2011. 'Juvenile Paleoproterozoic crust evolution during the Eburnean orogeny (~2.2–2.0 Ga), western Burkina Faso', *Precambrian Research*, 191: 18-45.
- Barrie, Ibrahim, Jan Wijbrans, Paul Andriessen, Frank Beunk, Victor Strasser-King, and Daniel Fode. 2010. "Combined (super 40) Ar/ (super 39) Ar and fission-track study of the Freetown layered igneous complex, Freetown, Sierra Leone, West Africa implications for the initial break-up of Pangea to form the central Atlantic Ocean and insight into the post-rift evolution of the Sierra Leone passive margin." In. Katlenburg-Lindau: Katlenburg-Lindau, Germany: Copernicus GmbH on behalf of the European Geosciences Union (EGU).
- Basile, C., J. Mascle, M. Popoff, J. P. Bouillin, and G. Mascle. 1993. 'The Ivory Coast-Ghana transform margin: A marginal ridge structure deduced from seismic data', *Tectonophysics*, 222: 1-19.
- Basile, Christophe, Jean Mascle, and René Guiraud. 2005. 'Phanerozoic geological evolution of the Equatorial Atlantic domain', *Journal of African Earth Sciences*, 43: 275-82.
- Benkhelil, J. 1989. 'The origin and evolution of the Cretaceous Benue Trough (Nigeria)', *Journal of African Earth Sciences*, 8: 251-82.
- Benkhelil, J., J. Mascle, M. Guiraud, and C. Basile. 1997. 'Submersible observations of Cretaceous deformations along the Côte d'Ivoire–Ghana transform margin', *An International Journal of Marine Geology*, 17: 49-54.
- Bigot-cormier, Florence, Christophe Basile, Gérard Poupeau, Jean-pierre Bouillin, and Erika Labrin. 2005. 'Denudation of the Côte d'Ivoire-Ghana transform continental margin from apatite fission tracks', *Terra Nova*, 17: 189-95.
- Block, S., J. Ganne, L. Baratoux, A. Zeh, L. A. Parra-Avila, M. Jessell, L. Aillères, and L. Siebenaller. 2015. 'Petrological and geochronological constraints on lower crust exhumation during Paleoproterozoic (Eburnean) orogeny, NW Ghana, West African Craton', *Journal of Metamorphic Geology*, 33: 463-94.
- Block, S., M. Jessell, L. Aillères, L. Baratoux, O. Bruguier, A. Zeh, D. Bosch, R. Caby, and E. Mensah. 2016. 'Lower crust exhumation during Paleoproterozoic (Eburnean) orogeny, NW Ghana, West African Craton: Interplay of coeval contractional deformation and extensional gravitational collapse', *Precambrian Research*, 274: 82-109.
- Bouillin, J. P., G. Poupeau, E. Labrin, C. Basile, N. Sabil, J. Mascle, G. Mascle, F. Gillot, and L. Riou. 1997. 'Fission track study: heating and denudation of marginal ridge of the Ivory Coast–Ghana transform margin', *An International Journal of Marine Geology*, 17: 55-61.
- Buiter, Susanne. 2014. 'How plumes help to break plates.(GEODYNAMICS)', *Nature*, 513: 36.

- Buiter, Susanne J. H., and Trond H. Torsvik. 2014. 'A review of Wilson Cycle plate margins: A role for mantle plumes in continental break-up along sutures?', *Gondwana Research*, 26: 627-53.
- Carney, John N., Colm J. Jordan, Christopher W. Thomas, Daniel J. Condon, Simon J. Kemp, and John A. Duodo. 2010. 'Lithostratigraphy, sedimentation and evolution of the Volta Basin in Ghana', *Precambrian Research*, 183: 701-24.
- Chew, D. M., and R. A. Donelick. 2012. "Combined apatite fission track and U-Pb dating by LA-ICPMS." In. Katlenburg-Lindau: Katlenburg-Lindau, Germany: Copernicus GmbH on behalf of the European Geosciences Union (EGU).
- Chew, D. M., J. A. Petrus, and B. S. Kamber. 2014. 'U-Pb LA-ICPMS dating using accessory mineral standards with variable common Pb', *Chemical Geology*, 363: 185-99.
- Chew, D. M., and Ra Spikings. 2015. 'Geochronology and Thermochronology Using Apatite: Time and Temperature, Lower Crust to Surface', *Elements*, 11: 189-94.
- Clift, P. D. 1999. 'Flexural unloading and uplift along the Côte d'Ivoire-Ghana Transform Margin, equatorial Atlantic', *Journal of Geophysical Research: Solid Earth*, 104: 25257-74.
- Clift, P. D., J. Lorenzo, A. Carter, and Aj Hurford. 1997. 'Transform tectonics and thermal rejuvenation on the Cote d'Ivoire Ghana margin, West Africa', *J. Geol. Soc.*, 154: 483-89.
- Coulon, C., P. Vidal, C. Dupuy, P. Baudin, M. Popoff, H. Maluski, and D. Hermitte. 1996. 'The Mesozoic to Early Cenozoic Magmatism of the Benue Trough (Nigeria); Geochemical Evidence for the Involvement of the St Helena Plume', *Journal of Petrology*, 37: 1341-58.
- Daniels, K. A., I. D. Bastow, D. Keir, R. S. J. Sparks, and T. Menand. 2014. 'Thermal models of dyke intrusion during development of continent-ocean transition', *Earth and Planetary Science Letters*, 385: 145-53.
- de Kock, G. S., H. Théveniaut, P. M. W. Botha, and W. Gyapong. 2012. 'Timing the structural events in the Palaeoproterozoic Bolé-Nangodi belt terrane and adjacent Maluwe basin, West African craton, in central-west Ghana', *Journal of African Earth Sciences*, 65: 1-24.
- Deckart, Katja, Hervé Bertrand, and Jean-Paul Liégeois. 2005. 'Geochemistry and Sr, Nd, Pb isotopic composition of the Central Atlantic Magmatic Province (CAMP) in Guyana and Guinea', *Lithos*, 82: 289-314.
- Deynoux, Max, Pascal Affaton, Roland Trompette, and Michel Villeneuve. 2006. 'Pan-African tectonic evolution and glacial events registered in Neoproterozoic to Cambrian cratonic and foreland basins of West Africa', *Journal of African Earth Sciences*, 46: 397-426.
- Eby, G. N., and A. N. Mariano. 1992. 'Geology and geochronology of carbonatites and associated alkaline rocks peripheral to the Paraná Basin, Brazil-Paraguay', *Journal of South American Earth Sciences*, 6: 207-16.
- Fairhead, J. D., C. M. Green, S. M. Masterton, and R. Guiraud. 2013. 'The role that plate tectonics, inferred stress changes and stratigraphic unconformities have on the evolution of the West and Central African Rift System and the Atlantic continental margins', *Tectonophysics*, 594: 118-27.

- Galbraith, Rex. 2005. *Statistics for fission track analysis* (Chapman & Hall/CRC: Boca Raton).
- Gallagher, Kerry. 2012. 'Transdimensional inverse thermal history modeling for quantitative thermochronology', *Journal of Geophysical Research: Solid Earth*, 117: n/a-n/a.
- Gleadow, A., I. Duddy, P. Green, and J. Lovering. 1986. 'Confined fission track lengths in apatite: a diagnostic tool for thermal history analysis', *Contributions to Mineralogy and Petrology*, 94: 405-15.
- Gleadow, Andrew J. W., Ian R. Duddy, Paul F. Green, and Kerry A. Hegarty. 1986. 'Fission track lengths in the apatite annealing zone and the interpretation of mixed ages', *Earth and Planetary Science Letters*, 78: 245-54.
- Grant, Norman Kennedy. 1971. 'South Atlantic, Benue Trough, and Gulf of Guinea Cretaceous triple junction', *Geological Society of America Bulletin*, 82: 2295-98.
- Green, P. F., I. R. Duddy, A. J. W. Gleadow, P. R. Tingate, and G. M. Laslett. 1986. 'Thermal annealing of fission tracks in apatite. 1. A qualitative description', *Chemical Geology*, 59: 237-53.
- Guiraud, R., R. M. Binks, J. D. Fairhead, and M. Wilson. 1992. 'Chronology and geodynamic setting of Cretaceous–Cenozoic rifting in West and Central Africa A2 - Ziegler, P.A.' in *Geodynamics of Rifting* (Elsevier: Amsterdam).
- Guiraud, René, and Jean-Christophe Maurin. 1992. 'Early Cretaceous rifts of Western and Central Africa: an overview', *Tectonophysics*, 213: 153-68.
- Heine, Christian, and Sascha Brune. 2014. 'Oblique rifting of the Equatorial Atlantic why there is no Saharan Atlantic Ocean', *Geology (Boulder)*, 42: 211-14.
- Holbrook, John, and S. A. Schumm. 1999. 'Geomorphic and sedimentary response of rivers to tectonic deformation: a brief review and critique of a tool for recognizing subtle epeirogenic deformation in modern and ancient settings', *Tectonophysics*, 305: 287-306.
- Jessell, Mark W., Graham C. Begg, and Meghan S. Miller. 2016. 'The geophysical signatures of the West African Craton', *Precambrian Research*, 274: 3-24.
- Jianping, Liu, Pan Xiaohua, Ma Jun, Tian Zuoji, and Wan Lunkun. 2010. 'Exploration targets in the Côte d'Ivoire-Ghana transform margin in Equatorial West Africa', *Petroleum Exploration and Development*, 37: 43-50.
- Jolly, Byami A., Peter M. Zaborski, Okwudiri A. Anyiam, and Ebere I. Nzekwe. 2015. 'Field study of the positive flower structures of the Gombe inlier, upper Benue trough, northeastern Nigeria system', *Journal of the Geological Society of India*, 85: 183-96.
- Karner, Garry D., and Neal W. Driscoll. 1999. 'Tectonic and stratigraphic development of the West African and eastern Brazilian margins insights from quantitative basin modelling', *Geological Society Special Publications*, 153: 11-40.
- Ketcham, Richard A., Raymond A. Donelick, and William D. Carlson. 1999. 'Variability of apatite fission-track annealing kinetics III, Extrapolation to geological time scales', *American Mineralogist*, 84: 1235-55.

- Lamarche, G., C. Basile, J. Mascle, and F. Sage. 1997. 'The Cote d'Ivoire Ghana transform margin: Sedimentary and tectonic structure from multichannel seismic data', *Geo-Mar. Lett.*, 17: 62-69.
- Lisker, F., T. John, and B. Ventura. 2008. "Denudation and uplift across the Ghana transform margin as indicated by new apatite fission track data." In. Katlenburg-Lindau: Katlenburg-Lindau, Germany: Copernicus GmbH on behalf of the European Geosciences Union (EGU).
- Martins, L. T., J. Madeira, N. Youbi, J. Munhá, J. Mata, and R. Kerrich. 2008. 'Rift-related magmatism of the Central Atlantic magmatic province in Algarve, Southern Portugal', *Lithos*, 101: 102-24.
- Marzoli, Andrea, Paul R. Renne, Enzo M. Piccirillo, Marcia Ernesto, Giuliano Bellieni, and Angelo De Min. 1999. 'Extensive 200-million-year-old continental flood basalts of the Central Atlantic Magmatic Province', *Science*, 284: 616-18.
- Mascle, Jean, Michel Guiraud, Jean Benkhelil, Christophe Basile, Jean-Pierre Bouillin, Georges Mascle, Michel Cousin, Marc Durand, Jean Dejax, and Michel Moullade. 1998. 'A geological field trip to the Côte d'Ivoire-Ghana transform margin', *Oceanologica Acta*, 21: 1-20.
- Maurin, Jean-Christophe, and René Guiraud. 1993. 'Basement control in the development of the early cretaceous West and Central African rift system', *Tectonophysics*, 228: 81-95.
- McDowell, Fw, Wc McIntosh, and Ka Farley. 2005. 'A precise Ar-40-Ar-39 reference age for the Durango apatite (U-Th)/He and fission-track dating standard', *Chem. Geol.*, 214: 249-63.
- McHone, J. G. 2000. 'Non-plume magmatism and rifting during the opening of the central Atlantic Ocean', *Tectonophysics*, 316: 287-96.
- Merle, Renaud, Andrea Marzoli, Hervé Bertrand, Laurie Reisberg, Chrystèle Verati, Catherine Zimmermann, Massimo Chiaradia, Giuliano Bellieni, and Marcia Ernesto. 2011. '⁴⁰Ar/³⁹Ar ages and Sr-Nd-Pb-Os geochemistry of CAMP tholeiites from Western Maranhão basin (NE Brazil)', *Lithos*, 122: 137-51.
- Metelka, Václav, Lenka Baratoux, Séta Naba, and Mark W. Jessell. 2011. 'A geophysically constrained litho-structural analysis of the Eburnean greenstone belts and associated granitoid domains, Burkina Faso, West Africa', *Precambrian Research*, 190: 48-69.
- Moody, J. D., and M. J. Hill. 1956. 'Wrench-fault tectonics', *Bulletin of the Geological Society of America*, 67: 1207-46.
- Ngako, Vincent, Emmanuel Njonfang, Festus Tongwa Aka, Pascal Affaton, and Joseph Metuk Nnange. 2006. 'The North-South Paleozoic to Quaternary trend of alkaline magmatism from Niger-Nigeria to Cameroon: Complex interaction between hotspots and Precambrian faults', *Journal of African Earth Sciences*, 45: 241-56.
- Nude, Prosper M., John W. Shervais, Kodjopa Attoh, Scott K. Vetter, and Corey Barton. 2009. 'Petrology and geochemistry of nepheline syenite and related carbonate-rich rocks in the Pan-African Dahomeyide orogen, southeastern Ghana, West Africa', *Journal of African Earth Sciences*, 55: 147-57.
- O'Sullivan, Paul B., and Randall R. Parrish. 1995. 'The importance of apatite composition and single-grain ages when interpreting fission track data from

- plutonic rocks: a case study from the Coast Ranges, British Columbia', *Earth and Planetary Science Letters*, 132: 213-24.
- Paton, Chad, John Hellstrom, Bence Paul, Jon Woodhead, and Janet Hergt. 2011. 'Iolite: Freeware for the visualisation and processing of mass spectrometric data', *Journal of Analytical Atomic Spectrometry*, 26: 2508-18.
- Peyve, A. 2015a. 'The role of mantle plumes in the evolution of the African segment of Pangea and the formation of the Atlantic Ocean', *Geotectonics*, 49: 379-94.
- Peyve, A. A. 2015b. 'The role of mantle plumes in the evolution of the African segment of Pangea and the formation of the Atlantic Ocean', *Geotectonics*, 49: 379-94.
- Rüpke, Lars H., Daniel W. Schmid, Ebbe H. Hartz, and Bjørn Martinsen. 2010. 'Basin modelling of a transform margin setting: structural, thermal and hydrocarbon evolution of the Tano Basin, Ghana', *Petroleum Geoscience*, 16: 283-98.
- Schoene, Blair, and Samuel Bowring. 2006. 'U-Pb systematics of the McClure Mountain syenite: thermochronological constraints on the age of the 40 Ar/39 Ar standard MMhb', *Contributions to Mineralogy and Petrology*, 151: 615-30.
- Seton, M., R. D. Müller, S. Zahirovic, C. Gaina, T. Torsvik, G. Shephard, A. Talsma, M. Gurnis, M. Turner, S. Maus, and M. Chandler. 2012. 'Global continental and ocean basin reconstructions since 200 Ma', *Earth-Science Reviews*, 113: 212-70.
- Stacey, J. S., and J. D. Kramers. 1975. 'Approximation of terrestrial lead isotope evolution by a two-stage model', *Earth and Planetary Science Letters*, 26: 207-21.
- Tapsoba, Boukare, Ching-Hua Lo, Urbain Wenmenga, Bor-Ming Jahn, and Sun-Lin Chung. 2013. '(super 40) Ar/ (super 39) Ar thermochronology of Paleoproterozoic granitoids of northeast Burkina Faso, West African Craton implications for regional tectonics', *Precambrian Research*, 235: 208-29.
- Tooth, S., T. S. McCarthy, D. Brandt, P. J. Hancox, and R. Morris. 2002. 'Geological controls on the formation of alluvial meanders and floodplain wetlands: the example of the Klip River, eastern Free State, South Africa', *Earth Surface Processes and Landforms*, 27: 797-815.
- Verati, Chrystèle, Hervé Bertrand, and Gilbert Féraud. 2005. 'The farthest record of the Central Atlantic Magmatic Province into West Africa craton: Precise 40Ar/39Ar dating and geochemistry of Taoudenni basin intrusives (northern Mali)', *Earth and Planetary Science Letters*, 235: 391-407.
- Vermeesch, Pieter. 2009. 'RadialPlotter: A Java application for fission track, luminescence and other radial plots', *Radiation Measurements*, 44: 409-10.
- Wagner, Thomas. 2002. 'Late Cretaceous to early Quaternary organic sedimentation in the eastern Equatorial Atlantic', *Palaeogeography, Palaeoclimatology, Palaeoecology*, 179: 113-47.
- Woodcock, Nigel H., and Mike Fischer. 1986. 'Strike-slip duplexes', *Journal of Structural Geology*, 8: 725-35.
- Woodcock, Nigel H., and Barrie Rickards. 2003. 'Transpressive duplex and flower structure: Dent Fault System, NW England', *Journal of Structural Geology*, 25: 1981-92.

Yidana, Sandow Mark, Bruce Banoeng-Yakubo, and Thomas M. Akabzaa. 2010.
'Analysis of groundwater quality using multivariate and spatial analyses in
the Keta basin, Ghana', *Journal of African Earth Sciences*, 58: 220-34.

9. APPENDIX A: DATA TABLE

Age calculation spreadsheet containing LA-ICP-MS data and AFT counting data to produce ages that are used in the RadialPlotter software.

Name	238U Dur	SD	RF	Ns	A (unadjusted)	A	rho s	t (Ma)	SD t
016_1.D	14.3	0.68	4.75524476	86	5.63E-05	5627	1528345.477	209.7763371	24.72
016_2.D	9.49	0.6	6.32244468	30	2.62E-05	2615	1147227.533	236.7770365	45.75
016_3.D	11.06	0.65	5.87703436	69	7.08E-05	7079	974713.9426	173.4690971	23.24
016_4.D	29	1.1	3.79310345	142	9.28E-05	9277	1530667.242	104.45183	9.62
016_5.D	9.81	0.49	4.99490316	65	7.00E-05	6998	928836.8105	186.1830825	24.90
016_6.D	14.53	0.85	5.84996559	99	1.15E-04	11480	862369.338	117.3345086	13.64
016_7.D	14.8	1.2	8.10810811	148	1.18E-04	11790	1255301.103	167.0336584	19.29
016_8.D	18.9	1.2	6.34920635	58	3.83E-05	3832	1513569.937	157.8229125	23.02
016_9.D	22.8	2	8.77192982	50	4.31E-05	4305	1161440.186	100.8364095	16.78
016_10.D	11.35	0.89	7.84140969	69	4.81E-05	4814	1433319.485	247.1450653	35.51
016_11.D	13.08	0.78	5.96330275	56	3.99E-05	3985	1405269.762	210.8562039	30.86
016_12.D	16.79	0.94	5.59857058	45	4.15E-05	4154	1083293.211	127.4534097	20.30
016_13.D	14.25	0.89	6.24561404	35	3.07E-05	3072	1139322.917	157.5686927	28.39
016_14.D	14.8	1.4	9.45945946	61	5.96E-05	5962	1023146.595	136.4669932	21.72
016_15.D	11.32	0.85	7.50883392	79	6.63E-05	6628	1191913.096	206.7153975	27.96
016_16.D	11.41	0.67	5.87204207	78	4.78E-05	4782	1631116.688	279.0752378	35.60
016_17.D	19.7	1.1	5.58375635	33	4.10E-05	4098	805270.8638	81.04002007	14.82
016_18.D	20	1.3	6.5	107	6.96E-05	6955	1538461.538	151.6680725	17.67
016_19.D	47.1	3.8	8.06794055	108	3.43E-05	3426	3152364.273	132.163771	16.60
016_20.D	11.3	1.1	9.73451327	23	3.27E-05	3270	703363.9144	123.0008865	28.30
016_21.D	12.44	0.77	6.18971061	62	4.89E-05	4894	1266857.376	200.0360104	28.26
016_22.D	37.6	3.9	10.3723404	35	2.66E-05	2657	1317275.122	69.51864168	13.79
016_23.D	12.36	0.78	6.31067961	46	4.67E-05	4667	985643.8826	157.164049	25.21
016_24.D	16.57	0.88	5.31080266	63	6.67E-05	6669	944669.3657	112.7483858	15.42
016_25.D	17.7	1.1	6.21468927	75	5.69E-05	5693	1317407.342	146.8076504	19.25

016_26.D	22.1	2.4	10.8597285	98	6.61E-05	6607	1483275.314	132.5299549	19.66
016_28.D	9.47	0.79	8.34213305	64	6.57E-05	6572	973828.3628	201.9612691	30.35
016_29.D	30.8	2.1	6.81818182	104	4.37E-05	4373	2378230.048	152.2374187	18.18
016_30.D	19.7	1.4	7.10659898	91	6.19E-05	6185	1471301.536	147.3060166	18.66
016_31.D	32.8	2.5	7.62195122	43	2.55E-05	2546	1688923.802	101.9189692	17.38
016_32.D	13.7	1.2	8.75912409	35	3.23E-05	3226	1084934.904	156.0885826	29.72
016_33.D	10.74	0.72	6.70391061	40	3.64E-05	3637	1099807.534	201.1297051	34.54
016_34.D	21.3	2.6	12.2065728	67	3.43E-05	3426	1955633.392	180.6200364	31.19
016_35.D	24.4	1.8	7.37704918	25	1.44E-05	1442	1733703.19	140.2198601	29.89
016_36.D	13.9	1.3	9.35251799	50	4.69E-05	4694	1065189.604	151.1015078	25.62
016_37.D	20.4	1.6	7.84313725	52	5.53E-05	5529	940495.5688	91.32781145	14.55
016_38.D	27.8	3.7	13.3093525	36	6.03E-05	6026	597411.2181	42.73117692	9.11
016_39.D	4.09	0.3	7.33496333	24	5.36E-05	5358	447928.3315	214.8738531	46.61
016_40.D	15.49	0.91	5.87475791	49	4.81E-05	4812	1018287.614	129.8358594	20.06
016_41.D	19.6	1.5	7.65306122	52	3.77E-05	3772	1378579.003	138.8185707	21.99
016_42.D	21.6	1.9	8.7962963	46	3.32E-05	3316	1387213.51	126.8718712	21.78
016_43.D	10.62	0.66	6.21468927	33	4.50E-05	4503	732844.7702	136.221994	25.18
016_44.D	7.37	0.48	6.51289009	64	9.00E-05	8995	711506.3924	189.7838456	26.75
016_45.D	19.4	1.4	7.21649485	39	2.81E-05	2806	1389878.831	141.3711838	24.83
016_46.D	15.9	1.1	6.91823899	26	3.77E-05	3767	690204.4067	86.02724725	17.89
016_47.D	34.2	2.4	7.01754386	75	4.00E-05	4000	1875000	108.4608525	14.66
016_48.D	14	0.85	6.07142857	32	3.76E-05	3755	852197.0706	120.3121418	22.49
016_49.D	8.7	0.75	8.62068966	74	6.02E-05	6019	1229440.106	275.9410878	39.94
	238U				A				
Name	Dur	SD	RF	Ns	(unadjusted)	A	rho s	t (Ma)	SD t
043_1.D	26.1	2.2	8.42911877	53	2.73E-05	2730	1941391.941	130.2976436	21.00
043_2.D	26.4	2.2	8.33333333	31	2.36E-05	2357	1315231.226	87.55998968	17.34
043_3.D	25.5	1.9	7.45098039	47	2.60E-05	2599	1808387.841	124.2849235	20.36
043_4.D	28.3	2.3	8.12720848	33	1.64E-05	1636	2017114.914	124.9079846	24.00
043_5.D	33.2	3.2	9.63855422	25	1.66E-05	1661	1505117.399	79.72678321	17.70
043_6.D	37.8	2.7	7.14285714	29	1.58E-05	1581	1834282.1	85.30177792	16.97
043_7.D	22.4	1.4	6.25	33	1.98E-05	1975	1670886.076	130.6623133	24.17
043_8.D	25.5	1.7	6.66666667	16	1.43E-05	1432	1117318.436	77.07230201	19.94

043_9.D	30.9	2.4	7.76699029	20	1.50E-05	1504	1329787.234	75.70618037	17.92
043_10.D	34.2	3.2	9.35672515	34	1.83E-05	1833	1854882.706	95.26594394	18.61
043_11.D	30.7	2.8	9.12052117	41	2.78E-05	2778	1475881.929	84.51302026	15.28
043_12.D	45.8	3.7	8.07860262	47	2.60E-05	2599	1808387.841	69.49337858	11.59
043_13.D	29.7	2.8	9.42760943	32	1.70E-05	1700	1882352.941	111.1870489	22.28
043_14.D	34.8	3.4	9.77011494	38	2.06E-05	2061	1843765.163	93.07811219	17.63
043_15.D	38	2.8	7.36842105	96	2.92E-05	2920	3287671.233	151.3067711	19.05
043_16.D	37.1	2.8	7.54716981	53	2.00E-05	1998	2652652.653	125.2966151	19.64
043_17.D	36.1	3.2	8.86426593	43	1.41E-05	1405	3060498.221	148.2996733	26.16
043_18.D	25.3	3.2	12.6482213	34	1.24E-05	1240	2741935.484	188.9799318	40.27
043_19.D	31.7	3.2	10.0946372	57	2.59E-05	2593	2198225.993	121.5548752	20.24
043_20.D	26.7	2.8	10.4868914	50	1.63E-05	1629	3069367.71	200.2784087	35.26
043_21.D	21	1.3	6.19047619	30	2.16E-05	2156	1391465.677	116.1966361	22.40
043_22.D	29.2	3.1	10.6164384	111	3.41E-05	3412	3253223.916	194.1930173	27.65
043_23.D	43.6	2.5	5.73394495	82	3.03E-05	3034	2702702.703	108.768486	13.53
043_24.D	31.4	2.5	7.96178344	72	1.87E-05	1874	3842049.093	212.9610786	30.29
043_25.D	25.5	2.4	9.41176471	68	2.47E-05	2468	2755267.423	188.4176518	28.92
043_26.D	34.4	2	5.81395349	60	2.20E-05	2200	2727272.727	138.7864394	19.65
043_27.D	21.9	1.9	8.67579909	98	3.01E-05	3009	3256895.979	257.9305203	34.35
043_28.D	35.6	3.5	9.83146067	78	2.18E-05	2184	3571428.571	175.1216979	26.26
043_29.D	40.7	2.6	6.38820639	83	2.87E-05	2869	2892994.075	124.5691728	15.82
043_30.D	24.3	2	8.23045267	87	3.03E-05	3034	2867501.648	205.5024394	27.78
043_31.D	18.4	1.1	5.97826087	31	1.31E-05	1313	2361005.331	223.1520611	42.24
043_32.D	29.5	2.7	9.15254237	40	1.45E-05	1451	2756719.504	163.2748739	29.83
043_33.D	31.1	1.9	6.10932476	41	1.56E-05	1560	2628205.128	147.8325033	24.79
043_34.D	25.6	1.7	6.640625	26	1.48E-05	1476	1761517.615	120.6251169	24.98
043_35.D	26.6	2.2	8.27067669	27	1.52E-05	1517	1779828.609	117.3271985	24.58
043_36.D	31.4	2.1	6.68789809	30	1.38E-05	1382	2170767.004	121.1867968	23.56
043_37.D	21.1	1.8	8.53080569	22	1.51E-05	1508	1458885.942	121.2020903	27.83
043_38.D	29	2.2	7.5862069	26	1.35E-05	1354	1920236.337	116.1180391	24.42
043_39.D	44.2	3.9	8.82352941	73	2.32E-05	2317	3150625.809	124.9166304	18.31
043_40.D	29.9	3.4	11.3712375	42	1.16E-05	1158	3626943.005	211.1532398	40.47
043_41.D	31.6	3.3	10.443038	35	1.58E-05	1576	2220812.183	123.1768924	24.47

Name	²³⁸ U Dur	SD	RF	Ns	A (unadjusted)	A	rho s	t (Ma)	SD t
80_1.D	4.2	0.31	7.38095238	18	3.49E-05	3490	515759.3123	248.4030282	61.35
80_2.D	4.62	0.35	7.57575758	16	4.20E-05	4202	380771.0614	167.7690412	43.83
80_3.D	5.01	0.42	8.38323353	14	2.71E-05	2714	515843.773	208.9187666	58.52
80_4.D	3.69	0.23	6.23306233	27	6.84E-05	6838	394852.296	216.986164	43.89
80_5.D	4.4	0.34	7.72727273	29	5.87E-05	5868	494205.8623	227.5727712	45.77
80_6.D	4.28	0.36	8.41121495	7	1.92E-05	1916	365344.4676	173.6795384	67.25
80_7.D	5.52	0.28	5.07246377	26	3.36E-05	3361	773579.2919	282.7228159	57.27
80_8.D	3.77	0.31	8.22281167	11	2.81E-05	2814	390902.6297	210.3658405	65.74
80_9.D	4.58	0.28	6.11353712	10	2.25E-05	2245	445434.2984	197.5155527	63.62
80_10.D	3.2	0.71	22.1875	12	2.58E-05	2579	465296.6266	293.1046516	106.72
80_11.D	5.65	0.39	6.90265487	13	2.85E-05	2849	456300.4563	164.4390545	47.00
80_12.D	3.61	0.31	8.58725762	8	3.37E-05	3372	237247.9241	134.1289945	48.80
80_13.D	4.39	0.21	4.78359909	15	4.17E-05	4167	359971.2023	166.925103	43.83
80_14.D	4.18	0.38	9.09090909	23	4.66E-05	4656	493986.2543	239.2262046	54.42
80_15.D	5.53	0.34	6.1482821	14	3.84E-05	3835	365058.6701	134.7239707	36.95
80_18.D	8.76	0.69	7.87671233	15	3.96E-05	3959	378883.5565	88.5865145	23.91
80_19.D	3.17	0.26	8.20189274	7	3.61E-05	3609	193959.5456	124.9651922	48.33
80_20.D	4	0.33	8.25	10	2.51E-05	2513	397930.76	201.9667739	66.01
80_21.D	5.88	0.5	8.50340136	16	3.26E-05	3263	490346.3071	169.7263327	44.82
80_22.D	4.78	0.32	6.69456067	19	3.89E-05	3893	488055.4842	207.2031666	49.52
80_23.D	3.77	0.26	6.89655172	17	3.39E-05	3390	501474.9263	268.6460916	67.74
80_24.D	4.93	0.25	5.07099391	12	3.01E-05	3005	399334.4426	164.9210387	48.34
80_25.D	4.22	0.28	6.63507109	24	3.80E-05	3798	631911.5324	301.6454013	64.74
80_26.D	4.07	0.28	6.87960688	18	4.07E-05	4073	441934.6919	220.1308444	54.05
80_27.D	3.44	0.19	5.52325581	26	4.27E-05	4274	608329.4338	354.75545	72.28
80_28.D	4.8	0.28	5.83333333	17	4.80E-05	4800	354166.6667	150.3986157	37.52
80_29.D	3.58	0.26	7.26256983	11	4.07E-05	4072	270137.5246	153.7677802	47.69
80_30.D	4.21	0.27	6.41330166	12	2.53E-05	2533	473746.5456	227.9895392	67.42
80_31.D	4.34	0.31	7.14285714	14	4.18E-05	4175	335329.3413	157.4063413	43.55
80_32.D	4.78	0.41	8.57740586	9	2.06E-05	2061	436681.2227	185.7032949	63.92
80_34.D	4.82	0.44	9.12863071	10	3.01E-05	3007	332557.3661	140.7419085	46.32

80_35.D	3.57	0.24	6.72268908	14	2.53E-05	2528	553797.4684	312.2311427	86.05
80_37.D	5.07	0.25	4.93096647	16	5.65E-05	5652	283085.6334	114.1334722	29.08
80_39.D	4.03	0.34	8.43672457	19	4.13E-05	4133	459714.4931	231.0627692	56.48
80_40.D	4.64	0.42	9.05172414	13	3.00E-05	3003	432900.4329	189.5925995	55.31
80_41.D	7.81	0.46	5.88988476	6	1.70E-05	1699	353148.9111	92.58440009	38.19
80_42.D	4.5	0.31	6.88888889	17	2.88E-05	2877	590893.2916	265.2673493	66.88
80_43.D	3.65	0.31	8.49315068	12	2.46E-05	2460	487804.878	269.8881389	81.21
80_45.D	3.84	0.28	7.29166667	12	2.88E-05	2882	416377.5156	219.8282535	65.45
80_46.D	4.38	0.32	7.30593607	8	2.39E-05	2393	334308.3995	155.5168605	56.15
80_47.D	4.02	0.34	8.45771144	11	2.43E-05	2430	452674.8971	228.1424689	71.44
	238U				A				
Name	Dur	SD	RF	Ns	(unadjusted)	A	rho s	t (Ma)	SD t
85_1.D	3.91	0.41	10.4859335	14	3.35E-05	3346	418410.0418	207.0657564	59.45
85_2.D	4.57	0.23	5.03282276	28	5.25E-05	5248	533536.5854	225.5816408	44.12
85_3.D	22.5	1.1	4.88888889	39	3.51E-05	3509	1111427.757	96.41036082	16.14
85_5.D	3.14	0.35	11.1464968	5	1.88E-05	1875	266666.6667	164.8732176	75.99
85_6.D	5.45	0.43	7.88990826	20	4.91E-05	4905	407747.1967	145.4661219	34.49
85_7.D	33.7	2	5.9347181	92	2.90E-05	2901	3171320.234	182.4428042	21.89
85_8.D	12.7	1.1	8.66141732	31	2.62E-05	2624	1181402.439	180.3767693	35.97
85_9.D	3.55	0.32	9.01408451	23	4.61E-05	4609	499023.6494	270.6577053	61.48
85_10.D	0.848	0.063	7.42924528	4	3.07E-05	3068	130378.0965	295.4574283	149.35
85_11.D	5.55	0.34	6.12612613	32	4.25E-05	4254	752233.1923	261.161532	48.86
85_12.D	10.05	0.69	6.86567164	14	3.50E-05	3502	399771.5591	77.7500731	21.45
85_13.D	6.84	0.6	8.77192982	31	3.45E-05	3448	899071.9258	253.4255242	50.66
85_14.D	7.8	1	12.8205128	12	2.73E-05	2727	440044.0044	109.9936765	34.74
85_15.D	17.3	1.2	6.93641618	38	3.85E-05	3845	988296.4889	111.3681311	19.65
85_16.D	5.82	0.64	10.9965636	11	2.85E-05	2848	386235.9551	129.1954202	41.46
85_17.D	3.46	0.23	6.64739884	17	4.41E-05	4409	385574.9603	215.4915732	54.19
85_18.D	3.69	0.36	9.75609756	11	3.44E-05	3438	319953.4613	168.2890727	53.33
85_19.D	5.26	0.38	7.2243346	22	2.49E-05	2487	884599.9196	322.4995345	72.60
85_20.D	5.03	0.44	8.74751491	18	2.64E-05	2639	682076.5441	261.2827374	65.69
85_21.D	4.09	0.3	7.33496333	30	3.69E-05	3692	812567.714	379.2920895	74.63
85_22.D	8.85	0.5	5.64971751	39	4.52E-05	4524	862068.9655	188.7563579	32.05

85_23.D	5.9	0.73	12.3728814	4	2.69E-05	2689	148754.1837	49.38886749	25.44
85_24.D	8.25	0.78	9.45454545	15	3.62E-05	3624	413907.2848	97.90919818	26.92
85_25.D	14.1	1.5	10.6382979	65	5.45E-05	5453	1192004.401	164.1325926	26.82
85_26.D	4.65	0.35	7.52688172	12	4.46E-05	4461	268997.9825	112.7635427	33.64
85_27.D	3.97	0.4	10.0755668	18	4.76E-05	4762	377992.4402	184.5599627	47.31
85_28.D	3.73	0.3	8.04289544	14	2.82E-05	2821	496277.9156	256.4632469	71.58
85_29.D	19.43	0.86	4.42614514	33	2.91E-05	2909	1134410.45	113.7981253	20.44
85_30.D	3.47	0.21	6.0518732	16	4.08E-05	4082	391964.7232	218.3821613	56.17
85_31.D	3.83	0.25	6.52741514	7	2.37E-05	2368	295608.1081	150.0137868	57.54
85_32.D	5.08	0.32	6.2992126	16	2.63E-05	2629	608596.4245	231.3795513	59.65
85_33.D	5.13	0.25	4.87329435	18	2.51E-05	2514	715990.4535	268.7704404	64.69
85_34.D	3.7	0.27	7.2972973	9	3.89E-05	3888	231481.4815	121.8651851	41.58
85_35.D	10.05	0.94	9.35323383	19	3.51E-05	3507	541773.5957	105.1433533	26.05
85_36.D	10.27	0.6	5.84225901	10	2.00E-05	1996	501002.004	95.22131161	30.62
85_38.D	3.55	0.4	11.2676056	15	2.76E-05	2759	543675.2447	294.3307099	82.92
85_39.D	7.67	0.87	11.3428944	36	3.88E-05	3881	927595.9804	233.5338192	47.08
85_40.D	14.9	2.8	18.7919463	23	2.50E-05	2495	921843.6874	120.5261785	33.83
85_41.D	3.05	0.27	8.85245902	9	2.14E-05	2138	420954.1628	265.8434009	91.69
85_42.D	3.61	0.37	10.2493075	4	2.08E-05	2076	192678.2274	104.1095118	53.14
85_44.D	4.31	0.35	8.12064965	16	3.87E-05	3872	413223.1405	185.827232	48.85
	238U				A				
Name	Dur	SD	RF	Ns	(unadjusted)	A	rho s	t (Ma)	SD t
119_1.D	4.37	0.29	6.63615561	10	2.46E-05	2459	406669.3778	162.6041098	52.54
119_2.D	7.4	1.2	16.2162162	8	1.20E-05	1204	664451.8272	156.96185	61.05
119_3.D	3.6	0.27	7.5	6	1.06E-05	1059	566572.238	272.6444816	113.17
119_4.D	3.64	0.39	10.7142857	8	2.50E-05	2497	320384.4614	153.8990623	56.86
119_5.D	9.2	2.5	27.173913	7	1.38E-05	1379	507614.2132	96.90317092	45.11
119_6.D	5.63	0.42	7.46003552	2	1.04E-05	1035	193236.715	60.45102651	42.98
119_7.D	3.25	0.21	6.46153846	8	2.08E-05	2075	385542.1687	206.5722011	74.24
119_8.D	2.62	0.26	9.92366412	2	1.51E-05	1511	132362.6737	88.78313206	63.39
119_9.D	4.39	0.47	10.7061503	15	2.08E-05	2075	722891.5663	284.9926208	79.66
119_10.D	6.57	0.46	7.00152207	3	1.02E-05	1020	294117.6471	78.73379405	45.79
119_11.D	6.55	0.69	10.5343511	14	2.03E-05	2034	688298.9184	183.3185384	52.66

119_12.D	4.09	0.3	7.33496333	6	1.44E-05	1436	417827.2981	178.2848555	73.95
119_13.D	4.1	0.37	9.02439024	1	1.31E-05	1309	76394.19404	32.88732335	33.02
119_14.D	3.64	0.27	7.41758242	4	1.38E-05	1383	289226.3196	139.0922703	70.31
119_15.D	3.43	0.27	7.87172012	6	1.16E-05	1158	518134.715	261.9126606	108.89
119_16.D	3.56	0.35	9.83146067	12	2.57E-05	2567	467471.7569	228.2725277	69.61
119_17.D	3.86	0.36	9.32642487	1	2.13E-05	2129	46970.40864	21.4967609	21.59
119_18.D	6.61	0.62	9.37972769	5	1.61E-05	1609	310752.0199	82.65811571	37.77
119_19.D	4.49	0.41	9.13140312	6	1.37E-05	1372	437317.7843	170.0862331	71.15
119_20.D	4.16	0.48	11.5384615	3	1.41E-05	1411	212615.1665	89.81159483	52.88
119_21.D	4.75	0.62	13.0526316	2	1.76E-05	1755	113960.114	42.31490988	30.43
119_22.D	5.85	0.64	10.9401709	4	1.13E-05	1125	355555.5556	106.663055	54.59
119_24.D	10.4	1	9.61538462	9	1.72E-05	1722	522648.0836	88.31976182	30.64
119_25.D	20.9	2.1	10.0478469	9	1.25E-05	1253	718276.1373	60.52920137	21.07
119_26.D	6.77	0.73	10.7828656	1	1.12E-05	1120	89285.71429	23.29532004	23.43
119_27.D	3.43	0.28	8.16326531	2	1.38E-05	1384	144508.6705	74.12433807	52.76
119_28.D	7.19	0.69	9.59666203	5	1.06E-05	1062	470809.7928	114.8425161	52.53
119_29.D	5.43	0.51	9.39226519	9	1.08E-05	1078	834879.4063	266.487405	92.29
119_31.D	6.92	0.9	13.0057803	5	1.55E-05	1551	322372.6628	81.91251886	38.15
119_32.D	4.13	0.35	8.47457627	3	7.93E-06	792.5	378548.8959	160.1862379	93.47
119_33.D	3.04	0.25	8.22368421	2	7.80E-06	779.7	256508.9137	147.6072053	105.08
119_34.D	4.17	0.43	10.3117506	4	1.41E-05	1414	282885.4314	118.9384407	60.72
119_36.D	3.66	0.41	11.2021858	12	1.20E-05	1200	1000000	466.2086865	144.36
119_37.D	3.17	0.3	9.4637224	6	2.39E-05	2389	251151.1093	138.6934303	58.12
	238U				A				
Name	Dur	SD	RF	Ns	(unadjusted)	A	rho s	t (Ma)	SD t
127_1.D	8.67	0.56	6.45905421	9	1.28E-05	1277	704776.8207	157.8990255	53.61
127_2.D	21	1.5	7.14285714	18	1.62E-05	1624	1108374.384	102.9605753	25.36
127_4.D	33.4	2.8	8.38323353	25	1.58E-05	1584	1578282.828	92.25790083	20.01
127_5.D	17.9	1.7	9.4972067	15	1.08E-05	1076	1394052.045	151.3541167	41.64
127_6.D	7.63	0.69	9.04325033	19	2.12E-05	2117	897496.4573	227.2518159	56.04
127_7.D	12.15	0.88	7.24279835	25	3.39E-05	3392	737028.3019	118.1944388	25.14
127_9.D	22.6	2.2	9.73451327	19	2.00E-05	1999	950475.2376	82.1746742	20.48
127_10.D	12.5	1.6	12.8	21	2.49E-05	2492	842696.6292	131.2230466	33.20

127_11.D	16.1	1.5	9.31677019	34	2.64E-05	2636	1289833.08	155.6434529	30.38
127_12.D	17.3	1	5.78034682	39	4.38E-05	4384	889598.5401	100.3322385	17.08
127_13.D	18.1	1.2	6.62983425	23	1.90E-05	1898	1211801.897	130.3263502	28.52
127_14.D	15.6	1.5	9.61538462	5	1.46E-05	1456	343406.5934	43.14262612	19.73
127_15.D	22.2	1.9	8.55855856	32	2.65E-05	2648	1208459.215	106.1633517	20.85
127_16.D	21.6	2	9.25925926	7	1.24E-05	1235	566801.6194	51.39508093	20.00
127_19.D	11.3	1	8.84955752	16	1.42E-05	1420	1126760.563	193.1555211	51.22
127_20.D	22.8	2	8.77192982	29	2.28E-05	2284	1269702.277	108.5877308	22.30
127_21.D	5.55	0.44	7.92792793	15	3.15E-05	3150	476190.4762	166.5490119	44.98
127_22.D	29.4	3.1	10.5442177	18	2.30E-05	2298	783289.8172	52.17866255	13.47
127_23.D	15	1	6.66666667	14	1.71E-05	1714	816802.8005	106.198982	29.25
127_24.D	14.6	0.85	5.82191781	11	1.50E-05	1502	732356.8575	97.89147395	30.06
127_25.D	27.7	2.1	7.58122744	19	1.82E-05	1820	1043956.044	73.68761993	17.80
127_26.D	17.9	1.7	9.4972067	10	1.15E-05	1147	871839.5815	95.07223964	31.39
127_27.D	27.3	2.1	7.69230769	13	2.28E-05	2280	570175.4386	40.93951534	11.78
127_28.D	23.7	2.7	11.3924051	13	1.78E-05	1783	729108.2445	60.21302216	18.05
127_29.D	13.92	0.85	6.10632184	13	2.05E-05	2050	634146.3415	88.96651732	25.27
127_30.D	18.9	2.6	13.7566138	6	9.05E-06	904.9	663056.6913	68.62019587	29.56
238U A									
Name	Dur	SD	RF	Ns	(unadjusted)	A	rho s	t (Ma)	SD t
132_1.D	6.64	0.4	6.02409639	6	1.93E-05	1927	311364.8158	91.55674305	37.78
132_2.D	5.57	0.56	10.05386	6	3.02E-05	3019	198741.3051	69.78414467	29.34
132_3.D	4.43	0.68	15.3498871	4	2.03E-05	2031	196947.3166	86.83496631	45.42
132_5.D	4.43	0.41	9.25507901	12	5.28E-05	5277	227401.9329	100.1587345	30.36
132_6.D	10.51	0.96	9.13415794	3	1.48E-05	1483	202292.65	37.73828582	22.06
132_8.D	6.69	0.59	8.81913303	7	3.27E-05	3274	213805.7422	62.54051936	24.27
132_9.D	16.9	1.5	8.87573964	6	1.74E-05	1742	344431.6877	39.95273441	16.69
132_10.D	4.34	0.56	12.9032258	5	1.53E-05	1534	325945.2412	146.017082	67.96
132_11.D	13.54	0.91	6.72082718	4	1.70E-05	1704	234741.784	34.00184606	17.15
132_12.D	4.83	0.49	10.1449275	12	3.49E-05	3487	344135.3599	138.6058258	42.41
132_13.D	9.7	1.2	12.371134	2	2.01E-05	2005	99750.62344	20.19018118	14.49
132_14.D	22	1.9	8.63636364	3	1.52E-05	1519	197498.3542	17.62882851	10.29
132_15.D	3.81	0.43	11.2860892	2	2.10E-05	2097	95374.3443	49.03772604	35.11

Name	²³⁸ U Dur	SD	RF	Ns	A (unadjusted)	A	rho s	t (Ma)	SD t
155_01.D	32.2	1.8	5.59006211	54	3.77E-05	3774	1430842.607	102.2769885	15.05
155_02.D	24	1.7	7.08333333	43	3.18E-05	3180	1352201.258	129.4063078	21.76
155_03.D	17.51	0.76	4.34037693	39	4.41E-05	4407	884955.7522	116.2002389	19.28
155_04.D	32.9	2	6.07902736	62	3.23E-05	3231	1918910.554	133.9157837	18.86
155_05.D	29.9	2	6.68896321	43	3.76E-05	3758	1144225.652	88.17765314	14.68
155_06.D	26.7	1.4	5.24344569	89	5.14E-05	5136	1732866.044	148.8408278	17.60
155_07.D	37.8	2.4	6.34920635	41	2.75E-05	2752	1489825.581	90.79736031	15.31
155_08.D	47.6	4.6	9.66386555	52	3.07E-05	3065	1696574.225	82.16501482	13.89
155_09.D	29	2.2	7.5862069	54	3.10E-05	3095	1744749.596	138.0914817	21.51
155_10.D	38.9	2.7	6.94087404	50	3.07E-05	3069	1629195.178	96.44118496	15.19
155_11.D	22	1.7	7.72727273	57	3.33E-05	3326	1713770.295	178.2394356	27.33
155_13.D	29.4	1.6	5.44217687	48	3.83E-05	3829	1253591.016	98.17233113	15.14
155_14.D	27	1.7	6.2962963	51	3.30E-05	3299	1545923.007	131.4858934	20.19
155_15.D	30.1	2	6.64451827	89	5.19E-05	5192	1714175.655	130.7878754	16.36
155_16.D	25	1.8	7.2	37	2.90E-05	2897	1277183.293	117.4472088	21.08
155_17.D	28.8	1.3	4.51388889	86	5.30E-05	5298	1623254.058	129.4546716	15.13
155_18.D	26.3	1.9	7.2243346	68	3.49E-05	3490	1948424.069	169.6262438	23.94
155_19.D	38.1	2.3	6.03674541	46	2.43E-05	2432	1891447.368	114.1589229	18.19
155_20.D	35.2	3.1	8.80681818	29	3.49E-05	3494	829994.2759	54.47382659	11.20
155_21.D	47.2	3.8	8.05084746	33	3.00E-05	2995	1101836.394	53.93228639	10.34
155_22.D	34.3	2.5	7.28862974	60	4.64E-05	4639	1293382.194	86.89486457	12.88
155_23.D	29.8	1.9	6.37583893	45	2.52E-05	2518	1787132.645	137.6534537	22.32
155_24.D	16.86	0.88	5.21945433	53	3.98E-05	3979	1331992.963	180.7315167	26.56
155_27.D	26.5	2.2	8.30188679	25	1.84E-05	1838	1360174.102	117.9939216	25.55
155_28.D	16.01	0.79	4.93441599	34	2.44E-05	2437	1395157.981	199.067747	35.52
155_30.D	44.3	3.3	7.44920993	66	2.86E-05	2860	2307692.308	119.7364305	17.23
155_31.D	29.7	1.5	5.05050505	42	2.95E-05	2950	1423728.814	110.266326	17.90
155_32.D	36.8	2.7	7.33695652	43	1.82E-05	1821	2361339.923	147.1754426	24.91
155_33.D	36.3	2.5	6.88705234	25	1.70E-05	1702	1468860.165	93.20136052	19.71
155_36.D	35.6	2.9	8.14606742	34	2.30E-05	2303	1476335.215	95.50052719	18.13
155_37.D	19.5	1.8	9.23076923	27	2.18E-05	2183	1236830.05	145.4979243	31.06

155_38.D	30.1	2	6.64451827	32	2.59E-05	2591	1235044.384	94.49758823	17.85
155_39.D	39.1	1.7	4.34782609	59	3.17E-05	3169	1861786.052	109.5342214	15.03
155_40.D	30	2.3	7.66666667	33	2.38E-05	2378	1387720.774	106.4344821	20.25
155_41.D	38.1	3.7	9.71128609	26	1.94E-05	1941	1339515.714	81.05528235	17.74
155_42.D	40.9	2.1	5.13447433	48	2.59E-05	2591	1852566.577	104.2380364	15.97
155_45.D	43.7	2.5	5.7208238	54	2.57E-05	2565	2105263.158	110.8099271	16.36
155_46.D	36.2	2.6	7.18232044	37	2.11E-05	2106	1756885.09	111.6248716	20.03
155_47.D	49.6	3.3	6.65322581	42	2.59E-05	2588	1622874.807	75.46585358	12.68
155_48.D	31.3	2.6	8.30670927	55	3.09E-05	3086	1782242.385	130.7680829	20.71
155_50.D	29.2	2.4	8.21917808	41	2.69E-05	2693	1522465.652	119.8431394	21.15
	238U				A				
Name	Dur	SD	RF	Ns	(unadjusted)	A	rho s	t (Ma)	SD t
172_1.D	28.5	1.7	5.96491228	65	3.69E-05	3692	1760563.38	108.3953632	14.92
172_2.D	7.35	0.52	7.07482993	8	1.93E-05	1927	415153.0877	99.18271543	35.76
172_3.D	11.5	1.2	10.4347826	32	2.18E-05	2181	1467216.873	221.9016806	45.55
172_4.D	13.1	1	7.63358779	21	4.11E-05	4111	510824.6169	68.63518492	15.87
172_5.D	15.2	1	6.57894737	27	2.64E-05	2636	1024279.211	118.154151	24.03
172_6.D	14.1	1.7	12.0567376	27	2.41E-05	2410	1120331.95	139.0894762	31.59
172_7.D	6.36	0.55	8.64779874	23	3.09E-05	3093	743614.6136	203.6447814	45.97
172_8.D	5.5	0.54	9.81818182	16	3.25E-05	3250	492307.6923	156.4777645	42.03
172_9.D	13.7	0.87	6.35036496	12	2.30E-05	2300	521739.1304	67.03983892	19.82
172_10.D	5.6	0.42	7.5	13	2.37E-05	2373	547829.7514	170.8248166	49.08
172_11.D	3.92	0.31	7.90816327	17	2.43E-05	2425	701030.9278	308.9324199	78.81
172_12.D	5.56	0.51	9.17266187	19	3.59E-05	3590	529247.9109	166.2767797	41.08
172_13.D	11.58	0.8	6.90846287	21	3.18E-05	3178	660792.9515	100.1930924	22.93
172_14.D	15.9	1.3	8.17610063	22	2.82E-05	2823	779312.7878	86.15286038	19.67
172_15.D	18.4	1.2	6.52173913	27	3.50E-05	3502	770988.0069	73.72323417	14.98
172_16.D	7.79	0.78	10.012837	38	3.35E-05	3348	1135005.974	252.8003102	48.19
172_18.D	8.69	0.71	8.1703107	36	4.19E-05	4189	859393.65	172.6646726	32.05
172_19.D	12.97	0.71	5.47417116	31	4.32E-05	4317	718091.2671	97.23453044	18.26
172_20.D	7.89	0.89	11.2801014	24	3.30E-05	3304	726392.2518	160.8880291	37.52
172_21.D	7.7	0.84	10.9090909	21	4.06E-05	4063	516859.4635	117.6986149	28.71
172_22.D	7.25	0.54	7.44827586	21	3.91E-05	3907	537496.8006	129.872172	29.95

172_23.D	7.46	0.6	8.04289544	18	1.93E-05	1926	934579.4393	217.9591339	54.28
172_24.D	4.1	0.31	7.56097561	10	1.95E-05	1945	514138.8175	218.166069	70.93
172_25.D	7.81	0.55	7.04225352	13	2.49E-05	2487	522718.1343	117.3593247	33.58
172_26.D	19.4	1.8	9.27835052	12	1.96E-05	1961	611932.6874	55.57619456	16.85
172_28.D	34.3	2.4	6.99708455	35	1.75E-05	1746	2004581.901	102.5957752	18.77
172_29.D	8.55	0.58	6.78362573	17	2.28E-05	2278	746268.6567	152.62931	38.44
172_30.D	13.76	0.94	6.83139535	18	2.45E-05	2449	734993.8751	93.83415828	23.03
172_31.D	14.4	1.4	9.72222222	14	1.61E-05	1608	870646.7662	106.1110374	30.18
172_32.D	8.92	0.51	5.71748879	6	9.67E-06	967.1	620411.5397	121.9163921	50.26
172_34.D	7.59	0.68	8.95915679	14	2.07E-05	2065	677966.1017	156.1549738	44.02
172_35.D	11.8	1.1	9.3220339	10	1.44E-05	1436	696378.8301	103.5928235	34.15
172_36.D	12.1	1.4	11.5702479	10	1.67E-05	1672	598086.1244	86.87781796	29.25
172_38.D	4.73	0.31	6.55391121	18	2.81E-05	2806	641482.5374	235.6257701	57.64
172_39.D	11.9	1.1	9.24369748	20	2.81E-05	2809	711997.152	105.01453	25.41
172_40.D	19.3	1.5	7.77202073	15	1.34E-05	1344	1116071.429	101.5244526	27.38
172_41.D	9.26	0.7	7.55939525	12	1.72E-05	1720	697674.4186	131.9621552	39.38
172_42.D	8.96	0.83	9.26339286	11	1.39E-05	1387	793078.5869	154.7551727	48.81
172_43.D	6.34	0.55	8.67507886	8	1.92E-05	1919	416883.7936	115.3176553	41.98
172_44.D	13.1	1.1	8.39694656	13	1.66E-05	1661	782661.0476	104.8638052	30.39
172_45.D	14.6	1.1	7.53424658	19	1.84E-05	1841	1032047.8	123.8874856	29.92
Name	238U Dur	SD	RF	Ns	A (unadjusted)	A	rho s	t (Ma)	SD t
198_1.D	5.03	0.33	6.56063618	7	2.15E-05	2151	325430.0325	132.0647361	50.66
198_2.D	4.99	0.45	9.01803607	14	2.43E-05	2427	576843.8401	234.100106	66.03
198_3.D	33.4	2.7	8.08383234	17	1.61E-05	1611	1055245.189	64.82980397	16.57
198_4.D	6.85	0.46	6.71532847	22	4.13E-05	4130	532687.6513	158.4121314	35.41
198_5.D	0.687	0.072	10.4803493	3	2.98E-05	2981	100637.37	295.2384411	173.24
198_6.D	0.415	0.055	13.253012	6	3.74E-05	3736	160599.5717	752.4161285	322.95
198_7.D	1.38	0.16	11.5942029	5	1.91E-05	1909	261917.2342	379.9928993	175.56
198_8.D	0.595	0.058	9.74789916	6	3.58E-05	3583	167457.4379	555.7579892	233.27
198_9.D	36.7	2.3	6.26702997	19	1.68E-05	1683	1128936.423	63.12895536	15.01
198_11.D	20.8	1.3	6.25	27	3.14E-05	3140	859872.6115	84.69700548	17.14
198_14.D	1.33	0.34	25.5639098	5	1.81E-05	1805	277008.3102	415.8265144	214.20

198_15.D	3.43	0.36	10.4956268	12	2.39E-05	2389	502302.2185	295.1510313	90.66
198_16.D	2.87	0.24	8.36236934	1	1.29E-05	1291	77459.33385	55.4213463	55.61
198_17.D	0.601	0.061	10.1497504	3	2.09E-05	2094	143266.4756	473.7692647	277.73
198_18.D	0.56	0.06	10.7142857	3	3.10E-05	3098	96836.66882	347.1047482	203.82
198_19.D	5.83	0.36	6.17495712	7	2.82E-05	2817	248491.3028	87.30754601	33.44
198_21.D	0.476	0.045	9.45378151	5	3.52E-05	3523	141924.4962	587.3135153	268.46
198_22.D	0.601	0.056	9.31780366	5	4.09E-05	4085	122399.0208	406.8915464	185.88
198_23.D	0.554	0.073	13.1768953	1	1.82E-05	1818	55005.50055	201.5774502	203.32
198_25.D	0.628	0.048	7.6433121	5	3.79E-05	3788	131995.7761	419.5134373	190.33
198_26.D	0.606	0.051	8.41584158	8	2.80E-05	2804	285306.7047	904.4221872	328.70
198_27.D	0.641	0.059	9.20436817	2	2.34E-05	2335	85653.10493	269.8466388	192.42
198_28.D	0.558	0.048	8.60215054	5	2.53E-05	2526	197941.4093	692.954393	315.58
198_29.D	0.54	0.049	9.07407407	10	4.03E-05	4025	248447.205	885.1871982	291.22
198_30.D	0.587	0.05	8.51788756	2	2.14E-05	2140	93457.94393	320.2572859	228.09
198_31.D	0.502	0.05	9.96015936	4	2.45E-05	2446	163532.2976	639.0698972	325.81
198_32.D	0.561	0.062	11.0516934	2	2.77E-05	2768	72254.33526	260.2897756	186.29
198_33.D	0.546	0.052	9.52380952	3	2.56E-05	2555	117416.8297	428.9071598	250.98
198_34.D	0.59	0.058	9.83050847	7	1.96E-05	1959	357325.1659	1141.669718	445.87
198_35.D	0.552	0.064	11.5942029	3	2.53E-05	2528	118670.8861	428.780484	252.50
198_36.D	0.585	0.079	13.5042735	2	2.08E-05	2075	96385.54217	331.1367381	238.38
	238U				A				
Name	Dur	SD	RF	Ns	(unadjusted)	A	rho s	t (Ma)	SD t
223_1.D	70.3	8.9	12.6600284	98	3.94E-05	3935	2490470.14	72.64905159	11.77
223_2.D	23.9	1.8	7.53138075	44	1.74E-05	1744	2522935.78	214.1063668	36.08
223_3.D	39.7	7.9	19.8992443	61	3.18E-05	3183	1916431.04	98.79251269	23.38
223_4.D	19.9	1.2	6.03015075	58	3.76E-05	3755	1544607.19	158.1179969	22.85
223_5.D	18.2	1.4	7.69230769	45	2.93E-05	2926	1537935.748	171.9550922	28.85
223_6.D	19.5	1.2	6.15384615	58	3.66E-05	3655	1586867.305	165.6786634	24.03
223_7.D	18.1	1.1	6.07734807	49	2.63E-05	2634	1860288.535	208.5504801	32.38
223_8.D	25	2.2	8.8	41	3.40E-05	3404	1204465.335	98.6011772	17.68
223_9.D	131	12	9.16030534	178	3.73E-05	3728	4774678.112	74.73197181	8.85
223_10.D	13.5	1.1	8.14814815	41	2.79E-05	2789	1470060.954	220.748551	38.89
223_11.D	37.2	2.8	7.52688172	108	6.54E-05	6535	1652639.633	90.9746838	11.11

223_12.D	45.8	4.3	9.38864629	136	3.37E-05	3366	4040404.04	179.4135245	22.81
223_13.D	16.7	2	11.9760479	34	2.37E-05	2369	1435204.728	174.842864	36.57
223_14.D	33.8	2.7	7.98816568	82	3.88E-05	3879	2113946.894	127.7090894	17.41
223_15.D	21	1.6	7.61904762	79	3.43E-05	3433	2301194.291	222.1180666	30.18
223_16.D	19.6	1.2	6.12244898	54	3.48E-05	3478	1552616.446	161.3302429	24.07
223_17.D	19.2	1.4	7.29166667	37	2.86E-05	2855	1295971.979	137.7210763	24.77
223_18.D	21.8	1.5	6.88073394	65	3.42E-05	3418	1901696.899	177.4383556	25.17
223_19.D	25.6	2.4	9.375	45	3.62E-05	3619	1243437.414	99.39963823	17.50
223_20.D	52.9	5.1	9.64083176	68	3.15E-05	3147	2160788.052	83.69271863	12.97
223_21.D	34.7	3.3	9.51008646	69	4.33E-05	4332	1592797.784	93.97561385	14.42
223_22.D	11.16	0.9	8.06451613	23	2.77E-05	2766	831525.6688	151.8586326	33.95
223_23.D	14.5	0.74	5.10344828	43	4.88E-05	4877	881689.5633	124.1969201	19.97
223_24.D	26.4	1.5	5.68181818	79	4.05E-05	4049	1951099.037	150.6414777	18.99
223_25.D	68.9	5.4	7.83744557	88	3.39E-05	3390	2595870.206	77.23478069	10.22
223_26.D	13.9	1.3	9.35251799	63	4.70E-05	4699	1340710.79	195.910524	30.74
223_27.D	32.6	3.5	10.7361963	27	1.90E-05	1895	1424802.111	89.51003617	19.73
223_28.D	16.9	1.4	8.28402367	62	2.48E-05	2483	2496979.46	297.7242775	45.14
223_29.D	56.2	3.8	6.76156584	86	3.55E-05	3546	2425267.908	88.38855847	11.25
223_30.D	99	10	10.1010101	83	3.56E-05	3558	2332771.22	48.41261819	7.22
223_31.D	158	13	8.2278481	91	2.50E-05	2496	3645833.333	47.41274098	6.32
223_32.D	23.5	1.4	5.95744681	35	2.27E-05	2270	1541850.22	133.9088303	24.00
223_34.D	33.6	3.1	9.22619048	44	1.88E-05	1884	2335456.476	141.7755877	25.06
223_35.D	45.5	4.7	10.3296703	42	1.89E-05	1892	2219873.15	99.83957934	18.54
223_38.D	103.3	8.3	8.03484995	145	2.80E-05	2802	5174875.089	102.4934006	11.84
223_40.D	10.21	0.78	7.63956905	15	2.31E-05	2307	650195.0585	130.0123222	35.01
223_41.D	23.4	1.8	7.69230769	57	3.22E-05	3221	1769636.759	154.1062605	23.60
223_42.D	36.4	4.1	11.2637363	53	1.76E-05	1756	3018223.235	168.7741132	29.98
	238U				A				
Name	Dur	SD	RF	Ns	(unadjusted)	A	rho s	t (Ma)	SD t
241_1.D	6.15	0.47	7.64227642	17	1.94E-05	1944	874485.5967	286.7710306	72.92
241_2.D	28.6	1.5	5.24475524	50	2.27E-05	2273	2199736.032	156.6999382	23.64
241_3.D	17	1	5.88235294	13	1.45E-05	1452	895316.8044	107.7080185	30.54
241_4.D	26.9	2.5	9.2936803	23	1.60E-05	1595	1442006.27	109.6151714	25.02

241_5.D	13.3	1.1	8.27067669	34	3.87E-05	3874	877645.8441	134.6718296	25.64
241_6.D	21.8	1.7	7.79816514	26	1.63E-05	1631	1594114.04	149.0682905	31.46
241_7.D	14.4	1	6.94444444	16	1.84E-05	1842	868621.0641	123.2151668	31.97
241_8.D	26.5	2.1	7.9245283	24	1.71E-05	1712	1401869.159	108.1846709	23.69
241_9.D	12.9	1.1	8.52713178	15	1.77E-05	1773	846023.6887	133.8534522	36.40
241_10.D	20	1.4	7	21	1.44E-05	1444	1454293.629	148.2423909	33.97
241_11.D	11.37	0.87	7.65171504	14	1.57E-05	1568	892857.1429	159.9469559	44.47
241_12.D	9.54	0.7	7.33752621	16	1.99E-05	1986	805639.4763	171.8478994	44.77
241_13.D	11.02	0.69	6.26134301	18	2.64E-05	2639	682076.5441	126.3980182	30.83
241_14.D	12.98	0.94	7.24191063	26	2.48E-05	2483	1047120.419	164.2595109	34.34
241_15.D	29.6	2.1	7.09459459	42	3.33E-05	3325	1263157.895	87.41209783	14.85
241_16.D	11	1.1	10	23	2.47E-05	2472	930420.712	172.1192197	39.80
241_17.D	8	0.6	7.5	7	2.93E-05	2934	238582.1404	61.21217288	23.59
241_18.D	14.4	1.1	7.63888889	8	1.25E-05	1253	638467.6776	90.79622253	32.84
241_19.D	25.1	1.6	6.37450199	27	2.24E-05	2237	1206973.625	98.41429216	19.95
241_20.D	11.05	0.92	8.32579186	13	1.33E-05	1329	978179.082	180.0243621	52.13
241_21.D	27.1	1.7	6.27306273	28	2.25E-05	2249	1244997.777	94.05472477	18.73
241_22.D	26.7	1.4	5.24344569	37	2.96E-05	2959	1250422.44	95.86623226	16.54
241_23.D	19.4	2.3	11.8556701	13	1.31E-05	1306	995405.8193	104.9570434	31.66
241_24.D	16.8	1.5	8.92857143	15	1.20E-05	1200	1250000	151.6477193	41.43
241_25.D	28.1	2.3	8.18505338	11	9.14E-06	914	1203501.094	87.72737587	27.41
241_26.D	33.5	2.3	6.86567164	14	1.42E-05	1417	988002.8229	60.53770964	16.70
241_27.D	14.7	1	6.80272109	23	2.01E-05	2005	1147132.17	158.9585969	34.86
241_28.D	13.29	0.65	4.89089541	15	2.02E-05	2018	743310.2081	114.3251553	30.04
241_29.D	6.36	0.64	10.0628931	11	1.74E-05	1738	632911.3924	202.030092	64.22
241_30.D	16.5	1.4	8.48484848	15	2.04E-05	2041	734933.856	91.20984156	24.79
241_31.D	20	1	5	19	1.52E-05	1523	1247537.754	127.3736152	29.91
241_32.D	13.1	1.3	9.92366412	10	1.75E-05	1745	573065.9026	89.59119219	29.69
241_33.D	35.5	7.2	20.2816901	25	2.14E-05	2142	1167133.52	67.44839589	19.21
241_34.D	15.36	0.91	5.92447917	23	2.06E-05	2059	1117047.11	148.2620207	32.14
241_35.D	13.27	0.7	5.27505652	26	2.42E-05	2424	1072607.261	164.5764453	33.42
241_36.D	16.8	1.8	10.7142857	24	1.42E-05	1420	1690140.845	204.2067873	47.08
241_37.D	32.4	2.7	8.33333333	11	8.50E-06	850.3	1293661.061	81.82194994	25.60

241_38.D	56.6	6.6	11.6607774	14	1.54E-05	1538	910273.0819	33.08215828	9.65
241_39.D	13.15	0.96	7.30038023	20	2.14E-05	2140	934579.4393	144.9281794	34.09
241_40.D	12.03	0.71	5.90191189	27	2.69E-05	2691	1003344.482	169.7490356	34.17
	238U				A				
Name	Dur	SD	RF	Ns	(unadjusted)	A	rho s	t (Ma)	SD t
252_1.D	8.09	0.68	8.40543881	22	1.37E-05	1374	1601164.483	377.8961266	86.60
252_2.D	8.81	0.51	5.78887628	33	3.23E-05	3229	1021988.232	224.1680056	41.12
252_3.D	0.74	0.1	13.5135135	6	1.74E-05	1738	345224.3959	857.6982951	368.84
252_4.D	1.73	0.14	8.09248555	7	1.46E-05	1460	479452.0548	523.159264	202.22
252_5.D	2.54	0.26	10.2362205	10	1.53E-05	1531	653167.8641	486.8173945	161.81
252_6.D	5.45	0.48	8.80733945	27	2.43E-05	2431	1110654.052	388.7740452	82.28
252_8.D	1.28	0.17	13.28125	4	9.38E-06	938.2	426348.3266	623.805099	322.72
252_9.D	1.43	0.11	7.69230769	8	2.53E-05	2529	316330.5654	420.9447235	152.31
252_10.D	9.13	0.76	8.32420591	27	1.65E-05	1652	1634382.567	342.738793	71.87
252_11.D	5.14	0.27	5.25291829	13	1.96E-05	1957	664282.0644	249.2544055	70.36
252_12.D	7.95	0.57	7.16981132	16	1.85E-05	1849	865332.6122	210.5622293	54.76
252_13.D	5.68	0.5	8.8028169	12	2.13E-05	2131	563115.908	192.0615485	57.96
252_14.D	3.12	0.22	7.05128205	9	1.45E-05	1451	620261.8884	379.533251	129.31
252_15.D	1.68	0.18	10.7142857	6	1.59E-05	1591	377121.3074	426.9597183	180.21
252_16.D	7.37	0.57	7.73405699	6	9.69E-06	969.4	618939.5502	163.0621042	67.75
252_17.D	2.6	0.21	8.07692308	11	7.99E-06	798.5	1377582.968	965.789247	301.46
252_18.D	3.63	0.35	9.64187328	17	2.12E-05	2115	803782.5059	421.3453754	109.97
252_19.D	4.89	0.66	13.4969325	14	1.94E-05	1943	720535.2548	283.4267207	84.86
252_20.D	1.94	0.2	10.3092784	9	2.64E-05	2642	340651.022	336.3605263	117.36
252_21.D	1.27	0.13	10.2362205	9	1.48E-05	1481	607697.5017	878.2926244	306.26
252_22.D	1.54	0.11	7.14285714	4	1.19E-05	1185	337552.7426	417.222398	210.73
252_24.D	6.77	0.84	12.4076809	11	1.23E-05	1230	894308.9431	254.6647907	83.03
252_25.D	7.1	2.5	35.2112676	8	1.96E-05	1957	408788.9627	112.2357684	56.00
252_26.D	2.92	0.26	8.90410959	6	1.61E-05	1607	373366.5215	246.657316	103.06
252_27.D	6.82	0.61	8.94428152	8	1.27E-05	1265	632411.0672	179.8128125	65.58
252_28.D	6.03	0.78	12.9353234	26	2.47E-05	2470	1052631.579	334.4423855	78.57
252_29.D	8.3	1.1	13.253012	10	1.17E-05	1173	852514.919	198.8768027	68.19
252_30.D	4.96	0.23	4.63709677	12	1.84E-05	1843	651112.3169	253.1029402	74.00

252_31.D	4.54	0.42	9.25110132	23	2.34E-05	2344	981228.6689	411.5789973	93.89
252_32.D	19.3	1.9	9.84455959	3	1.25E-05	1248	240384.6154	24.4456879	14.32
252_33.D	4.03	0.29	7.19602978	15	2.25E-05	2251	666370.502	317.2181535	85.03
252_34.D	1.44	0.16	11.11111111	4	1.69E-05	1690	236686.3905	315.3703512	161.53
252_35.D	3.37	0.23	6.82492582	8	1.97E-05	1970	406091.3706	232.7063262	83.79
252_36.D	2.48	0.16	6.4516129	2	8.82E-06	881.7	226834.5242	177.3963966	125.96
252_38.D	2.84	0.22	7.74647887	7	1.58E-05	1578	443599.493	300.0562835	115.77
252_39.D	2.27	0.27	11.8942731	5	9.00E-06	899.5	555864.3691	464.3898657	214.90
Name	238U Dur	SD	RF	Ns	A (unadjusted)	A	rho s	t (Ma)	SD t
270_1.D	3.53	0.32	9.06515581	7	2.44E-05	2442	286650.2867	165.3293932	64.26
270_2.D	7.81	0.58	7.42637644	11	1.86E-05	1858	592034.4456	154.4670135	47.97
270_3.D	2.04	0.26	12.745098	4	1.82E-05	1818	220022.0022	218.6766544	112.83
270_4.D	3.95	0.72	18.2278481	6	2.68E-05	2678	224047.7969	115.9274101	51.83
270_5.D	1.68	0.27	16.0714286	6	3.30E-05	3295	182094.0819	219.7439217	96.41
270_6.D	2.01	0.26	12.9353234	5	2.40E-05	2398	208507.0892	210.4599957	97.98
270_7.D	4.88	0.25	5.12295082	7	4.22E-05	4220	165876.7773	69.7217836	26.59
270_8.D	1.87	0.15	8.02139037	3	2.89E-05	2886	103950.104	113.632719	66.24
270_9.D	1.318	0.091	6.90440061	15	3.71E-05	3713	403985.9952	603.0220644	161.17
270_10.D	0.326	0.044	13.4969325	7	1.84E-05	1844	379609.5445	2041.267861	819.24
270_11.D	0.604	0.052	8.60927152	15	3.86E-05	3856	389004.1494	1207.688277	328.70
270_12.D	7.58	0.61	8.0474934	8	2.30E-05	2300	347826.087	93.94592589	34.06
270_13.D	4.08	0.45	11.0294118	7	2.21E-05	2212	316455.6962	158.0057454	62.21
270_14.D	4.69	0.88	18.7633262	5	3.97E-05	3966	126071.6087	55.19975336	26.77
270_15.D	1.76	0.19	10.7954545	11	2.93E-05	2932	375170.5321	425.270723	136.20
270_16.D	1.595	0.094	5.89341693	8	2.81E-05	2806	285103.35	358.4790145	128.49
270_17.D	10.5	1.1	10.4761905	12	3.08E-05	3075	390243.9024	76.19580467	23.40
270_18.D	2.6	0.24	9.23076923	5	2.67E-05	2670	187265.9176	146.8529522	67.06
270_19.D	1.4	0.12	8.57142857	7	3.45E-05	3446	203134.0685	292.4948429	113.36
270_20.D	11.88	0.7	5.89225589	18	2.23E-05	2234	805729.6329	138.3747418	33.62
270_21.D	1.07	0.17	15.8878505	7	4.60E-05	4601	152140.8389	286.76101	117.57
270_22.D	3.96	0.41	10.3535354	15	3.83E-05	3830	391644.9086	200.8025067	55.86
270_23.D	2.12	0.32	15.0943396	2	1.33E-05	1332	150150.1502	144.433851	104.43

270_24.D	2.72	0.23	8.45588235	3	2.28E-05	2282	131463.6284	98.91313772	57.72
270_25.D	2.11	0.18	8.53080569	6	4.86E-05	4863	123380.6292	119.477773	49.83
270_26.D	0.728	0.068	9.34065934	4	2.45E-05	2452	163132.137	446.3142406	227.02
270_27.D	3.36	0.19	5.6547619	4	1.26E-05	1256	318471.3376	192.5669406	96.90
270_28.D	2.51	0.2	7.96812749	5	1.60E-05	1601	312304.8095	251.6255839	114.30
270_29.D	0.552	0.054	9.7826087	5	1.60E-05	1601	312304.8095	1072.426793	490.94
270_30.D	0.101	0.012	11.8811881	10	3.54E-05	3543	282246.6836	4117.302866	1390.87
270_31.D	5.96	0.5	8.38926174	7	2.94E-05	2935	238500.8518	82.00340367	31.75
270_32.D	6.19	0.39	6.30048465	10	2.09E-05	2090	478468.8995	157.4712473	50.78
270_33.D	3	0.18	6	13	3.37E-05	3369	385871.1784	259.9493239	73.76
270_34.D	0.64	0.079	12.34375	11	3.54E-05	3536	311085.9729	931.73108	303.56
270_35.D	7.32	0.4	5.46448087	4	1.79E-05	1790	223463.6872	62.65231791	31.51
270_36.D	4.19	0.59	14.0811456	7	3.00E-05	3004	233022.6365	113.6848011	45.85
270_37.D	7.31	0.72	9.8495212	8	2.08E-05	2075	385542.1687	107.8622612	39.59
270_38.D	0.539	0.044	8.16326531	6	1.88E-05	1880	319148.9362	1118.265474	465.57
270_39.D	4.06	0.38	9.35960591	16	2.50E-05	2495	641282.5651	317.7813363	84.83
	238U				A				
Name	Dur	SD	RF	Ns	(unadjusted)	A	rho s	t (Ma)	SD t
278_1.D	19.4	1.3	6.70103093	78	4.58E-05	4578	1703800.786	153.5657166	20.20
278_2.D	37.2	2.5	6.72043011	70	2.75E-05	2745	2550091.075	120.1762479	16.48
278_3.D	25.7	2.1	8.17120623	20	1.92E-05	1921	1041124.414	71.28960649	16.97
278_4.D	39.4	2.1	5.32994924	141	4.72E-05	4724	2984758.679	132.6772372	13.22
278_5.D	26.8	2.5	9.32835821	48	2.74E-05	2741	1751185.699	114.6018531	19.70
278_6.D	11.9	2.4	20.1680672	37	3.32E-05	3321	1114122.252	163.5778264	42.56
278_7.D	49	4.9	10	50	2.88E-05	2884	1733703.19	62.30723395	10.79
278_8.D	35.2	3.4	9.65909091	74	3.29E-05	3287	2251292.972	112.1927961	16.96
278_9.D	14	1.2	8.57142857	21	2.14E-05	2141	980850.0701	122.7981671	28.79
278_10.D	22.6	1.8	7.96460177	32	2.30E-05	2298	1392515.231	108.1196741	20.96
278_12.D	13.9	1.1	7.91366906	25	2.71E-05	2709	922849.7601	116.425689	25.04
278_13.D	39.3	2.8	7.12468193	74	2.48E-05	2481	2982668.279	132.9191774	18.12
278_14.D	8.81	0.6	6.81044268	23	2.93E-05	2933	784180.0205	155.6136858	34.13
278_15.D	39.4	2.7	6.85279188	70	3.68E-05	3676	1904243.743	84.9613808	11.71
278_16.D	35.2	3	8.52272727	60	2.46E-05	2462	2437043.054	121.3630066	18.77

278_17.D	34.5	3	8.69565217	89	2.88E-05	2878	3092425.295	156.6936943	21.48
278_18.D	37.2	2.7	7.25806452	92	2.80E-05	2797	3289238.47	154.5947728	19.64
278_19.D	34.6	3.2	9.24855491	31	2.27E-05	2266	1368049.426	69.58887139	14.06
278_20.D	14.4	1.7	11.8055556	21	2.30E-05	2299	913440.6264	111.2818215	27.61
278_21.D	32.5	3.1	9.53846154	67	2.67E-05	2672	2507485.03	135.1003581	20.94
278_22.D	9.36	0.83	8.86752137	23	1.53E-05	1532	1501305.483	277.7561808	62.94
278_23.D	21	2.7	12.8571429	18	1.40E-05	1403	1282965.075	107.2110244	28.78
278_24.D	17.7	1.4	7.90960452	23	1.98E-05	1983	1159858.8	114.9251726	25.63
278_25.D	37.9	2.8	7.3878628	36	1.65E-05	1651	2180496.669	101.0111991	18.42
278_26.D	16.5	1.5	9.09090909	26	2.56E-05	2564	1014040.562	107.8434879	23.31
278_27.D	16.8	1.8	10.7142857	14	1.92E-05	1922	728407.9084	76.27004361	21.96
278_28.D	16.5	1.4	8.48484848	28	1.57E-05	1573	1780038.144	188.1278892	38.97
278_29.D	13.6	1.5	11.0294118	10	1.38E-05	1376	726744.186	93.87221149	31.44
278_30.D	20.1	1.7	8.45771144	22	1.48E-05	1480	1486486.486	129.5549043	29.72
278_31.D	22.2	1.8	8.10810811	92	3.82E-05	3821	2407746.663	189.1176792	24.98
Name	238U Dur	SD	RF	Ns	A (unadjusted)	A	rho s	t (Ma)	SD t
396_1.D	28.7	2.3	8.01393728	73	2.51E-05	2511	2907208.284	176.8012801	25.08
396_3.D	24.6	1.8	7.31707317	19	1.30E-05	1296	1466049.383	104.6033225	25.19
396_4.D	25.9	1.5	5.79150579	32	1.70E-05	1698	1884570.082	127.4885886	23.72
396_5.D	29.3	2.5	8.53242321	32	1.90E-05	1901	1683324.566	100.8691469	19.80
396_6.D	12.2	1.1	9.01639344	24	1.37E-05	1367	1755669.349	249.7487193	55.73
396_7.D	21	1.8	8.57142857	54	3.26E-05	3263	1654918.786	137.9628446	22.19
396_8.D	29.7	3	10.1010101	51	2.48E-05	2482	2054794.521	121.2776083	20.94
396_9.D	29.6	1.6	5.40540541	54	2.42E-05	2423	2228642.179	131.8740067	19.31
396_10.D	30.1	2.7	8.97009967	39	1.68E-05	1683	2317290.553	134.8109872	24.74
396_11.D	29.8	1.7	5.70469799	77	3.79E-05	3792	2030590.717	119.4637373	15.22
396_12.D	17.6	1.8	10.2272727	44	3.40E-05	3398	1294879.341	128.8925952	23.48
396_13.D	21.8	1.7	7.79816514	60	3.27E-05	3274	1832620.648	147.0662615	22.18
396_14.D	22.3	1.7	7.62331839	59	3.09E-05	3088	1910621.762	149.8554402	22.61
396_15.D	30.5	2.4	7.86885246	96	3.96E-05	3963	2422407.267	139.0323664	17.92
396_16.D	31.6	2.5	7.91139241	62	2.54E-05	2540	2440944.882	135.2592674	20.24
396_17.D	32.8	2.8	8.53658537	75	3.42E-05	3417	2194907.814	117.3394856	16.85

396_18.D	33.4	3.1	9.28143713	101	3.13E-05	3131	3225806.452	168.677772	22.95
396_19.D	30.7	2.5	8.14332248	58	2.71E-05	2705	2144177.449	122.4200126	18.91
396_20.D	26.7	1.8	6.74157303	59	2.65E-05	2646	2229780.801	146.1100913	21.42
396_21.D	22.9	1.4	6.11353712	16	1.30E-05	1301	1229823.213	94.33782798	24.28
396_22.D	20.7	2	9.66183575	57	2.24E-05	2242	2542372.881	213.7514683	35.04
396_23.D	25.2	1.9	7.53968254	30	1.85E-05	1851	1620745.543	112.8155271	22.28
396_24.D	27	1.9	7.03703704	51	2.07E-05	2065	2469733.656	159.8639454	25.05
396_26.D	30.9	2.1	6.7961165	49	2.09E-05	2090	2344497.608	132.8825012	21.02
396_28.D	26.1	1.4	5.36398467	52	2.30E-05	2299	2261852.98	151.5545794	22.53
396_29.D	29	2	6.89655172	81	3.09E-05	3091	2620511.161	157.9490273	20.66
396_30.D	31.8	2.2	6.91823899	66	2.33E-05	2326	2837489.252	155.9919676	22.03
396_31.D	25.9	1.7	6.56370656	49	2.25E-05	2250	2177777.778	147.0989804	23.13
396_32.D	27.5	1.8	6.54545455	25	1.38E-05	1384	1806358.382	115.1980992	24.24
396_33.D	28.8	3	10.4166667	48	2.24E-05	2236	2146690.519	130.5664844	23.24
396_34.D	27	2.7	10	57	2.43E-05	2427	2348578.492	152.1134492	25.25
396_35.D	24.1	1.9	7.88381743	40	2.12E-05	2124	1883239.171	136.8144617	24.17
396_36.D	28.1	2.6	9.25266904	34	2.30E-05	2295	1481481.481	92.62461703	18.05
396_37.D	26.3	1.8	6.84410646	46	1.60E-05	1596	2882205.514	191.063463	31.06
396_38.D	14.7	1.1	7.4829932	34	3.00E-05	3001	1132955.681	134.9590079	25.25
396_39.D	28.1	1.7	6.04982206	43	2.18E-05	2176	1976102.941	123.2551557	20.22
396_40.D	28	2.9	10.3571429	25	1.50E-05	1496	1671122.995	104.7555949	23.59
396_41.D	28.2	2.7	9.57446809	29	1.75E-05	1752	1655251.142	103.0385234	21.53
396_42.D	10.66	0.84	7.87992495	15	2.59E-05	2589	579374.2758	95.46465837	25.77
	238U				A				
Name	Dur	SD	RF	Ns	(unadjusted)	A	rho s	t (Ma)	SD t
446_1.D	17.6	1.3	7.38636364	103	3.12E-05	3124	3297055.058	323.250831	39.81
446_2.D	12.97	0.9	6.93909021	24	1.09E-05	1086	2209944.751	294.6713728	63.53
446_3.D	10.96	0.57	5.20072993	26	1.48E-05	1476	1761517.615	278.3095894	56.47
446_4.D	13.35	0.92	6.89138577	51	2.21E-05	2212	2305605.787	298.5846413	46.60
446_6.D	29.1	2	6.87285223	48	1.76E-05	1760	2727272.727	163.7451578	26.18
446_7.D	14.52	0.88	6.06060606	50	2.58E-05	2581	1937233.63	231.8685255	35.68
446_8.D	16.3	1.2	7.36196319	43	2.04E-05	2043	2104747.92	224.5366976	38.02
446_9.D	17.4	1.4	8.04597701	29	1.63E-05	1626	1783517.835	178.8748138	36.20

446_10.D	16.5	1.1	6.66666667	63	2.71E-05	2713	2322152.599	244.3488178	34.83
446_11.D	12.6	1.2	9.52380952	20	1.59E-05	1588	1259445.844	174.4930812	42.41
446_12.D	9.17	0.74	8.0697928	21	2.00E-05	2003	1048427.359	199.2057193	46.35
446_13.D	12.8	1.5	11.71875	27	1.36E-05	1359	1986754.967	268.9694289	60.60
446_14.D	10.23	0.85	8.30889541	17	9.22E-06	921.8	1844217.835	311.3625977	79.83
446_15.D	15.3	1.3	8.49673203	28	1.42E-05	1416	1977401.13	224.7353868	46.57
446_16.D	19.3	2	10.3626943	29	2.21E-05	2205	1315192.744	119.4708134	25.41
446_17.D	13.9	1.3	9.35251799	27	1.12E-05	1117	2417188.899	300.6014055	64.32
446_18.D	19.3	1.2	6.21761658	53	2.80E-05	2801	1892181.364	171.1931432	25.81
446_20.D	17.5	1.7	9.71428571	28	1.98E-05	1983	1412002.017	141.2186161	30.01
446_21.D	9.92	0.66	6.65322581	28	1.84E-05	1837	1524224.279	266.3151145	53.36
446_22.D	10.65	0.79	7.41784038	30	1.79E-05	1791	1675041.876	272.4744296	53.70
446_24.D	14.9	1.8	12.0805369	16	1.18E-05	1176	1360544.218	159.5878784	44.31
446_25.D	12.6	1.5	11.9047619	18	1.26E-05	1263	1425178.147	197.1071843	52.05
446_26.D	9.4	0.8	8.5106383	5	6.59E-06	658.7	759070.8972	141.3335554	64.34
446_27.D	15.3	1.4	9.1503268	73	2.85E-05	2846	2565003.514	290.0349912	43.09
446_28.D	14.4	1.2	8.33333333	44	2.19E-05	2192	2007299.27	242.0641683	41.70
446_29.D	16	1.3	8.125	96	3.09E-05	3085	3111831.442	335.2844392	43.74
238U									
Name	Dur	SD	RF	Ns	A (unadjusted)	A	rho s	t (Ma)	SD t
598_1.D	20	1.4	7	52	4.87E-05	4873	1067104.453	93.72946717	14.56
598_2.D	22.4	1.8	8.03571429	37	1.88E-05	1875	1973333.333	154.033015	28.19
598_3.D	23.3	1.9	8.15450644	42	2.92E-05	2917	1439835.447	108.4325286	18.92
598_4.D	12.99	0.88	6.77444188	26	2.43E-05	2430	1069958.848	144.1299304	29.91
598_6.D	12.38	0.86	6.94668821	48	2.67E-05	2670	1797752.809	251.9731634	40.36
598_7.D	8.36	0.85	10.1674641	30	2.18E-05	2179	1376778.339	285.024147	59.56
598_8.D	16.4	1.7	10.3658537	20	2.09E-05	2086	958772.7709	102.6290976	25.29
598_9.D	14.5	2.1	14.4827586	45	2.57E-05	2573	1748931.209	209.9774961	43.64
598_10.D	8.29	0.76	9.16767189	37	3.32E-05	3318	1115129.596	233.7404065	44.00
598_11.D	21	1.9	9.04761905	48	2.32E-05	2320	2068965.517	172.0231082	29.30
598_12.D	16	1.4	8.75	31	2.99E-05	2988	1037483.266	113.7325352	22.72
598_13.D	7.6	0.66	8.68421053	35	3.54E-05	3543	987863.3926	226.0000657	42.95
598_14.D	22.3	2.1	9.41704036	58	2.92E-05	2915	1989708.405	155.9839712	25.20

598_15.D	21.9	1.5	6.84931507	20	2.47E-05	2472	809061.4887	65.04364789	15.21
598_16.D	19	1.5	7.89473684	43	3.08E-05	3078	1397011.046	128.8131669	22.12
598_17.D	7.21	0.49	6.7961165	25	3.30E-05	3301	757346.2587	183.2450724	38.71
598_18.D	30	2.6	8.66666667	27	2.35E-05	2354	1146983.857	67.30190036	14.21
598_19.D	17.7	1.3	7.34463277	33	3.27E-05	3265	1010719.755	100.2619395	18.94
598_20.D	13.5	1.4	10.3703704	22	3.42E-05	3417	643839.6254	83.84494213	19.88
598_21.D	14.2	1	7.04225352	33	4.18E-05	4177	790040.6991	97.70707554	18.35
598_22.D	13.8	2.2	15.942029	13	3.75E-05	3749	346759.1358	44.31141849	14.18
598_24.D	6.91	0.58	8.39363242	25	2.62E-05	2616	955657.4924	240.1974361	52.10
598_25.D	6.5	1	15.3846154	36	3.07E-05	3074	1171112.557	311.1867593	70.58
598_26.D	21.4	2.6	12.1495327	43	2.96E-05	2964	1450742.24	118.8575923	23.17
598_27.D	6.56	0.52	7.92682927	28	4.60E-05	4599	608828.0061	162.1723725	33.23
598_28.D	17.4	2.5	14.3678161	20	2.91E-05	2912	686813.1868	69.47162171	18.46
598_29.D	18.7	1.6	8.55614973	29	2.36E-05	2363	1227253.491	115.0986206	23.53
598_30.D	10.8	1.5	13.8888889	57	2.40E-05	2404	2371048.253	377.2315026	72.40
598_31.D	5.33	0.35	6.56660413	33	5.90E-05	5899	559416.8503	183.0991627	34.07
598_32.D	7.37	0.61	8.27679783	11	2.21E-05	2214	496838.3017	118.2007466	36.96
598_33.D	10.4	1.1	10.5769231	13	2.00E-05	1997	650976.4647	109.8215759	32.60
598_34.D	11.8	1.1	9.3220339	29	3.27E-05	3269	887121.4439	131.6795127	27.36
598_35.D	19.3	1.7	8.80829016	32	3.58E-05	3579	894104.4985	81.46000174	16.09
598_36.D	17.4	1.7	9.77011494	23	1.84E-05	1844	1247288.503	125.6145049	28.93
598_37.D	9.25	0.95	10.2702703	19	3.23E-05	3230	588235.2941	111.5594492	28.04
598_38.D	17.5	1.3	7.42857143	27	2.50E-05	2495	1082164.329	108.5063902	22.38
598_39.D	24.7	2.6	10.5263158	54	2.67E-05	2669	2023229.674	143.3412383	24.66
598_40.D	27.5	2.8	10.1818182	51	3.76E-05	3758	1357104.843	86.73930356	15.02
598_41.D	17.7	2.1	11.8644068	34	3.40E-05	3403	999118.4249	99.11990651	20.67
598_42.D	30.1	2.2	7.3089701	28	2.97E-05	2972	942126.5141	55.14980712	11.17

10. APPENDIX B: EXTENDED METHOD

Mineral Separation & Crushing

Mineral separation and crushing of samples was performed by University of Toulouse, France.

Picking

The next procedure after mineral separation in Apatite Fission Track analysis involves the selection of apatite grains from the remaining sample. Utilizing two Olympus SZ61 low magnification (ca. 45X) picking microscopes, apatite grains were discerned visually based on typical apatite features. Features of note included elongated surfaces which ended with stubby/rounded edges, clarity and a shadowing along the edges of the C-Axis of the grain. Dependant on sample size and relative apatite abundance, grains were chosen based on size with larger grains ($>50\mu\text{m}$) being preferred and a lack of inclusions and fractures.

The picking procedure was undertaken using two shallow 10cm diameter picking dishes which were cleaned with ethanol prior to contact with sample materials. The two picking dishes were placed under each microscope, one being used to hold sample materials and one being used to hold a thin-section slide. A thin section slide was prepared using double sided tape which is used to hold the chosen grains in place and placed over a visual reference used to identify the maximum size of the picking/placement area.

A fraction of one of the separated mineral samples is placed into one of the picking dishes which is then viewed under one of the microscopes. Utilizing only a fraction of the sample was important as it assisted in identification and collection of individual apatite grains. Grains were picked from the sample fraction using a fine needle and

arranged in a square raster around the size reference on the double sided tape placed on the thin-section. For each sample used, the number of apatite grains was variable but typically the aim was to form a square raster of minimum 10x10 up to 13x15 or 100 to 195 apatite grains. Due to limited sample separate, for some sample locations this was not possible which resulted in some samples having <50 total grains.

Mounting

Sample mounting was undertaken to embed the apatite separates. This process used a 5:1 ratio of epoxy resin to epoxy hardener. In a small cup on a set of scales, 1g of resin was measured carefully and combined with 0.2g of hardener. This was heated to approx. 40°C and carefully stirred until it became a clear homogenous mixture. Careful stirring was required to avoid introducing bubbles into the mixture. Using a paddle pop stick... The resin mixture was carefully applied to the picking slide, one drop at a time, until all grains were covered. Another cleaned slide was then placed on top of the picking slide to cover and compress the resin mixture. The amount of compression achieved on the resin mixture was limited to exactly one slide thickness, which was achieved by using additional slides as spacers. The resin was then left to dry for 3 days. Once dried, a razor blade was used to remove the double sided tape from the picking slide and cleaned off the resin with ethanol to expose the apatite crystals for further treatment procedures. Slides were then cut to approx. 30mm and cleaned of sharp edges on a grinder to prevent damage to polishing clothes.

Grinding

Grinding was used to remove the top surface (approx. 8µm) of the epoxy resin. This allowed for the internals of the apatite to be revealed for further treatment. Grinding

involved using a 2000 grade sandpaper splashed with water. Slides were then rubbed against the sandpaper in a figure-eight pattern which allowed for an even spread of pressure over the top of the resin which helped in reducing wedging. Initially 10 figure-eight cycles were counted, followed by a series of 5 figure-eight cycles. In-between each cycle, checks were made under a picking microscope to gauge the degree of grinding, keeping in mind the importance of not over-grinding the samples. Over-grinding may cause grains to be lost or become loose in the epoxy. Variable amounts of cycles were used for each individual sample as differing grain and epoxy mount sizes resulted in a different amount of grinding required.

Initially the epoxy had a clear colour, slightly reflective surface and smooth texture.

After grinding the epoxy became cloudy due to being covered in small scratches and the texture became slightly rougher.

Polishing

The first stage of polishing was done using a Struers TegraPol - 11 and the following pre-determined settings were set using a Struers TegraDoser -5. The settings were as follows

Polishing Pad	Surface MD-Dac 3 μ m
Suspension Diapror	3 μ m Diamond suspension 3/7
Process Time	1 Min
Force	10 N
Disc Rotation	50 RPM
5Mp Holder	50 RPM

The first stage was a 3µm polish conducted with a 3µm polishing cloth and 3µm diamond suspension fluid. The length of time spent per sample in the polishing machine was variable between 3 minutes and 10 minutes. The goal of this polish was to return the epoxy resin from a rough cloudy surface to a smooth clear surface. Frequent checks of the samples were made using a Zeiss AXIO Imager M2m microscope. Checks were utilized to identify grain blemishes which could be removed and polishing stopped once a change in the grain surface could no longer be identified.

The second stage and final stage of polishing was a finer 1µm polish. This was achieved using a 1µm polishing cloth and 1µm diamond suspension fluid. Polishing was conducted on a Struers DP-U4 at a low speed with the break set between 1.0 and 1.5 RPMx100 tuned using the upper left knob on the control panel. Samples underwent a first run at 5 mins per sample and were then checked for progress using the Zeiss AXIO Imager M2m. They then underwent a second run at 5 mins per sample and were deemed finished upon a secondary check. Samples were then cleaned using an ethanol bath prior to etching to avoid contamination/dilution of the etching fluid.

Etching

This step was used to exaggerate and reveal the damage tracks in the crystal lattice of the grain. In the case of apatite these can be tracks formed by fission reactions or other means. This step involved taking each sample slide and holding it in a small beaker containing 5M of 20°C nitric-acid (HNO₃) for no more and no less than 20 seconds. Once the slide has been submerged in the acid for 20 seconds it is dropped into a 1L tub of deionised water to dilute the acid and prevent further etching. After etching, samples are checked under the Zeiss AXIO Imager M2m microscope to assure damage tracks have been sufficiently revealed.

Imaging

Imaging of Apatite grains is done using an Autoscan System with the FastTracks software package & a Zeiss AXIO Imager M2m utilizing 1000x magnification. The first step in the imaging process is creating a spatial reference for later identification of grains during the LA-ICP-MS process. Creating the spatial reference is done by attaching three TEM grids to a sample slide and assigning numbers 1 to 3 in FastTracks. The second step is to identify and select apatite grains in the sample; selection of grains is based on quality, which is determined, by a nice clean grain surface and an appropriate countable grain area greater than 30 μ m in width. Once grains are selected the microscope focus is used to identify the grain surface in transmitted and reflective light at 1000x magnification. Once this is completed for a minimum of 20 grains per sample the AutoScan will image through the height of the grain as a series of 16 photos in transmitted light and 3 photos in reflective. Imaging in transmitted light is carried out to reveal the internal sections of the grain while imaging in reflective light is carried out to clearly reveal etch pits on the surface of the grain.

Counting

Surface fission tracks are counted using the TrackWorks software after grains have been imaged. The first step involved in counting involves creating a 'Region of Interest' (ROI) around a selected 'countable' surface of the grain. The ROI defines the area from which track density can be calculated. Once an ROI is established for each grain, the auto-count feature is utilized. Once the process is complete a process of manual counting is undertaken to check the auto-count accuracy. Selection of fission tracks is conducted by viewing the grain through both reflected and transmitted light to identify etch pits and track tails in each type of light respectively. Track numbers identified for each grain are then used in conjunction with the established ROI to calculate track

density for use in an adjusted fission track age equation as described by Hasebe et al., (2004).

In addition to AFT age determination, an estimate of cooling rate can be carried out measuring the length of confined tracks in apatite grains. Confined fission track lengths are measured using the same TrackWorks software but can be conducted on both grains which have been selected for laser and grains which have not. The aim is to measure the lengths of a minimum of 50 confined tracks per sample where possible. Confined tracks are those tracks that are completely contained within the apatite sample and do not breach the ground surface but intersect other tracks or grain fractures. This allows for the etching acid to reach internal parts of the grain normally isolated. Measurement of confined tracks takes into consideration the angle to the grains C-axis and the dip angle to convert an 'apparent length' to a 'true length' and typically range in lengths between 8 μ m and 16 μ m.

LA-ICP-MS

In order to obtain AFT age for each 'Unknown' grain both fission track density and an accurate determination of ^{238}U concentrations are required. An Agilent 7500x LA-ICP-MS coupled to an Nd-YAG ESI NWR213 Laser was used to conduct a multi-element analysis on unknown sample grains and reference standards. Sample slides were cut so that seven unknown slides and two standard slides could fit into the custom sample holder for analysis. Plasma ignition and stabilization occurred after samples were inserted into the laser ablation chamber and tuning by a resident technician was carried out after the laser had stabilized.

Unknown Grains selected during the imaging process are spatially referenced and appropriate grain areas are selected manually using the NewWave software package

located in the University of Adelaide's microscopy centre. Apatite grains are lasered using a 10Hz repetition rate and a laser diameter of 30um (Hasebe et al, 2004). Apatite standards are selected using the NewWave software and are run with the same settings of 10Hz repetition rate and a 30um laser diameter. Pre-ablation, 20 seconds of background is recorded before 30 seconds of ablation with a 20 second post-ablation cooldown. Apatite standards and unknowns are assigned systematically and lasered with no more than ten unknowns per set of standards. Sets of standards are assigned as two NIST 610 standards followed by two MAD standards followed by one Durango standard and one McClure standard with four NIST 610 standards at the very beginning of the run to counter a 'ramp up' period observed in previous experiments. The laser ablation process exports multi-element 'count' data which can then be used to determine elemental concentrations and therefore ages when calculated in accordance with fission track density acquired during the counting process.

Data Reduction

Final counts are acquired and converted into Uranium ppm concentrations using the Iolite software package and inserted into the general age equation defined by Hasebe et al (2004) (*Eq.1*) along with fission track density to determine the Uranium ages. A custom 'Age Calculation' spreadsheet is used to determine the age for all individual grains for both unknown samples and the Durango samples. The data required for the custom spreadsheet includes $^{238}\text{Uppm}$, $^{238}\text{Uppm}$ standard deviation, number of counted tracks per grain and the ROI (cm^2) from which the tracks were counted. Counts and final $^{238}\text{Uppm}$ acquired by the Durango apatite standards are used to define the zeta calibration as described by Hurford and Green., (1986). The zeta calibration is then used

to adjust ages of acquired by unknown apatite grains according to the known 31.2 Myr age of Durango.

Age Equation (Hasebe et al., 2004)

$$\text{Eq.1} \quad t = \frac{1}{\lambda_D} \ln \left(1 + \frac{\lambda_D \rho_s M}{\lambda_f N_A^{238}\text{U} 10^{-6} d R_{sp} k} \right)$$

where $\lambda_D = {}^{238}\text{U}$ total decay constant ($1.55125 \times 10^{-10} \text{a}^{-1}$), $\lambda_f = {}^{238}\text{U}$ spontaneous fission-decay constant ($8.46 \times 10^{-17} \text{a}^{-1}$), $N_A =$ Avogadro's number ($6.02214 \times 10^{23} \text{mol}^{-1}$), $d =$ apatite density (3.19g/cm^3 as in Hasebe et al., 2004), $M =$ the atomic mass of ${}^{238}\text{U}$ (238.0508amu), $k =$ observational parameter = 1 are constants. ${}^{238}\text{U}$ is the measured ${}^{238}\text{U}$ -Uranium concentration (in $\mu\text{g/g}$) in the sample, ρ_s is the spontaneous fission track density (in tracks/ cm^2) and R_{sp} is a registration factor, and corresponds to the range or to half of the measured mean confined fission-track length.

Modelling

Visualisation of acquired ages is determined using Radial Plotter software, which requires age, standard deviation and uranium concentration in PPM. Plots are produced and peak/central ages are determined. Central ages give the best estimation of cooling however, in some samples multiple age populations are present as discussed in the results section of this manuscript. Age populations are determined where possible using the auto-mixture tool present within the RadialPlotter software. The auto-mixture tool utilizes a statistical method defined by Galbraith., (1988) to identify whether or not statistically valid age populations exist within any given sample.

QTQt modelling software was utilized to model the time-temperature (tT) paths of individual samples and sample groups. The data required for modelling includes the sample Age (Ma), Age Standard Deviation, number of counted tracks, ${}^{238}\text{U}$ (ppm),

number of confined track lengths, length of confined tracks (μm) and the angle of the confined track to the grains C-Axis. Constrains were not used for tT modelling in this study. Inverse modelling is conducted using a Markov Chain Monte Carlo approach to determine the most statistically valid result without the need for forward modelling. Various tT paths are generated which include an expected model, maximum likelihood model, mode model and the posterior model. A maximum likelihood chain is output to assess the appropriate number of iterations required to reduce the model complexity. Individual predictions per sample are also utilized to assess how closely the model fits the input data. Numbers of iterations utilized in the MCMC parameters varied per sample group with a Burn-in between 150,000 and 250,000 and a Post-Burn-in between 150,000 and 250,000 depending on the number of samples being modelled. Other MCMC parameters are consistent between samples groups and displayed in **figure xx**.